Final Technical Report

Development of a Low-Cost, Durable Membrane and Membrane Electrode Assembly for Stationary and Mobile Fuel Cell Application

Michel Foure (Primary Contact), Scott Gaboury, Jim Goldbach, David Mountz and Jung Yi
Arkema Inc. (Formerly ATOFINA Chemicals, Inc.)
900 First Ave
King of Prussia, PA 19406-0936
Phone: (610) 878-6790
Fax: (610) 878-6298, E-mail: michel.foure@arkema.com

DOE Technology Development Manager: Amy Manheim
Phone: (202) 586-1507
Fax: (202) 586-9811, Email: amy.manheim@ee.doe.gov
DOE Project Officer: Reg Tyler
Phone: (303) 275-4929
Fax: (303) 275-4753, E-mail: Reginald.tyler@go.doe.gov
Technical Advisor: Tom Benjamin
Phone: (630) 252-1632
Fax: (630) 972-4497, E-mail: benjamin@cmt.anl.gov

Contract Number: DE-FC36-04GO14051

Subcontractors:
Johnson Matthey Fuel Cells, Inc. - 1397 King Road, West Chester, PA 19380
UTC Fuel Cells – 195 Governor Highway, P.O. Box 1149, South Windsor, CT 06074
Georgia Institute of Technology (subcontractor to Arkema) Office of Sponsored Programs, Atlanta, GA 30332-0420
University of Hawaii (subcontractor to UTC Fuel Cells) – 2530 Dole Street, Sakamaki D-200, Honolulu, HI 96822

Start Date: 10-1-2003

Project End Date: 9-30-2006 (extension to 6-30-2007)

Table of Contents

I. Executive Summary

The development of low cost, durable membranes and membranes electrode assemblies (MEAs) remain a critical challenge for the successful introduction of fuel cells into mass markets. It was the goal of the team lead by Arkema, Inc. (formerly Atofina, Inc.) to address these shortages. Thus, this project addresses the following technical barriers from the Fuel cells section of the Hydrogen Fuel Cells and Infrastructure Technologies Program Multi-Year Research, Development and Demonstration Plan:

(A) Durability
(B) Cost

Arkema's approach consisted in using blends of polyvinylidenefluoride (PVDF) and proprietary sulfonated polyelectrolytes.

In the traditional approach to ionomers for proton exchange membranes (PEM), all the features required are "packaged" in one macromolecule. They include: proton conductivity, mechanical properties, long-term endurance, water management, etc. This is the case, for example, for perfluorosulfonic acids (PFSA) containing membranes. However, the cost of these materials is high, largely due to the complexity and the number of steps involved in their synthesis. In addition, they suffer other shortcomings such as mediocre mechanical properties and insufficient durability for some applications.

The strength and originality of Arkema's approach lies in the decoupling of ion conductivity from the other requirements. Kynar® (Arkema trade name for PVDF) provides an exceptional combination of properties that make it ideally suited for a membrane matrix. It exhibits outstanding chemical resistance in highly oxidative environments (such as hydrogen peroxide and bromine), as well as in extreme acidic environments (such as HF, HCl, and H_2SO_4). Due to the exceptional electrochemical stability and mechanical toughness of Kynar PVDF, it is widely used as matrix material in lithium ion batteries.

In a first phase, Arkema demonstrated the feasibility of the concept with the M31 membrane generation. After MEA optimization, it was shown that the beginning-of-life (BOL) performance of M31 MEAs was essentially on a par with that of PFSA MEAs at 60ºC under fully humidified conditions. It was also showed that the M31 MEA could work under dry anode conditions or dry cathode conditions with only a small drop in performance.

On the other hand, long-term durability studies (60ºC, oxygen, 100% relative humidity) showed a high decay rate of 45µV/h over a 2100 hr. test. The performance loss was traced back to sulfur loss. Detailed analytical work showed that the sulfur loss was related about equally to tow distinct mechanisms: polyelectrolyte oligomers leaching and chemical degradation due to the cleavage of a specific bond in the polyelectrolyte.

Arkema then designed several families of polyelectrolyte candidates which – in principle – could not undergo these failure mechanisms. A considerable amount of time and effort was devoted to developing efficient screening techniques at each stage of the polyelectrolyte preparation. Such work culminated in the selection of a new membrane candidate dubbed M41.

M41 offered the same generally good mechanical, ex-situ conductivity and gas barrier properties as M31. In addition, ex-situ accelerated testing suggested a several orders of magnitude improvement in chemical stability. M41 based MEAs showed comparable BOL performance with that of PFSA (80ºC, 100% RH). M41 MEAs were further shown to be able to withstand several hours temperature excursions at 120ºC without appearent damage. Accelerated studies were carried out using the DOE and/or US Fuel Cell Council protocols. M41 MEAs shown sizeable advantages over PFSA MEAs in the Open Circuit Voltage Hold test, Relative Humidity Cycling test and the Voltage Cycling test.

The key technical results are summarized in the following table:

Characteristic	2004 DOE Targets	Arkema 2007 Status	2010 DOE Targets
Operating Temperature	≤80°C	80°C (w/120ºC excursions)	≤120°C
Inlet water vapor partial pressure	50 KPa_{abs}	50 KPa_{abs}	≤1.5 KPa_{abs}
Membrane Conductivity at inlet water vapor partial pressure and: Operating Temperature Room temperature -20°C	 0.10 S/cm 0.07 S/cm 0.01 S/cm	 0.10-0.14 S/cm[g,h] 0.07-0.085 S/cm[h] (not available)	 0.10 S/cm 0.07 S/cm 0.01 S/cm
Oxygen cross-over[a]	5 mA/cm^2	0.8 mA/cm^2 (w/ 25 μm membrane)	2 mA/cm^2
Hydrogen cross-over[a]	5 mA/cm^2	1.0 mA/cm^2 (w/ 25 μm membrane)	2 mA/cm^2
Area Specific Resistance	0.03 ohm cm^2	0.022 ohm cm^2	0.02 ohm cm^2
Cost [b]	65 $\$/m^2$ [c]	≤ 65 $\$/m^2$	40 $\$/m^2$
Durability with cycling At operating temp ≤80°C At operating temp >80°C	 ~2000 hr [d] (not available)[f]	 2100 hr[i] (not available)	 5000 hr [e] 2000 hr
Unassisted start from	-20°C	(not available)	-40°C

(a) Tested in MEA at 1 atm O_2 or H_2 at nominal stack operating temperature.
(b) Based on 2002 dollars and costs projected to high volume production (500,000 stacks per year).
(c) Based on 2004 TIAX Study that will be periodically updated.
(d) Durability is being evaluated. Steady-state durability is 9,000 hours.
(e) Includes typical drive cycles.
(f) High-temperature membranes are still in a development stage and durability data are not available.
(g) At 70ºC.
(h) In liquid water measured by EIS.
(i) Steady state at 0.5 A/cm^2; 60ºC; H_2/O_2, 100% RH, 0 KPag.

The main conclusion is that the MEAs developed by the team showed beginning of life (BOL) performance essentially equivalent to that of PFSA materials such as Nafion®.

In addition, accelerated tests performed according to the US Fuel Cells Council and/or DOE recommended protocols suggest that the Arkema membranes (M41) and MEAs could have better durability. In the Open Circuit Voltage Hold test, (90ºC, 30% relative humidity), M41 achieves 3 to 4 times improved stability over PFSA. M41 also has successfully passed a 20,000 cycle relative humidity (RH) cycling test.

The main known limitation of the M41 family is its ability to function well at low RH. This is a major objective of a new award (Pending Award Number: DE-FG36-07GO17008) to work in this area.

II. Comparison of accomplishments with the original objectives of the project

Objective 1: *Create a new, low-cost, long durability membrane and establish a pilot production facility to make it available to all MEA developers.*

The beginning of life performance of the M41 membrane is essentially equivalent to that of PFSA materials such as Nafion®. A 1000h durability test at 80ºC under static conditions run by Johnson Matthey showed no degradation during the duration of the test. We have begun to run accelerated durability tests per the DOE and/or US Fuel Cell Council protocols. In the OCV Hold Test, M41 shows 3 to 4 times the durability of PFSA 111 (from Ion Power) and Nafion NRE 211 (from DuPont). M41 has also successfully passed a 20,000 Cycles Relative Humidity test (80ºC, 2 min 0% RH, 2 min "150%" RH). PFSA 111 from Ion Power passes this test but Nafion NRE fails around 6,000 to 8,000 cycles.

M41 films have been routinely produced on a pilot line. Their quality is excellent (homogeneous, deflect-free). A pilot equipment for the activation of the film into an active membrane is under construction. Several MEA developers as well as automotive companies have been sampling with M41 membranes.

Objective 2: *Develop a new MEA based on the Arkema membrane and establish a pilot facility to make it available to all fuel cell stack developers.*

MEAs have been developed at the lab scale by Arkema and Johnson Matthey. No MEA has been prepared on a pilot line due to delays encountered in the development of a durable membrane. MEA samples were provided to several MEA developers and automotive companies.

Objective 3: *Demonstrate the practicality of the new membrane and MEA by having a fuel cell stack developer fabricate a 20-cell stack and demonstrate it meets DOE goals over a 4000 hr. test period.*

Stacks have not been built for the reason cited here above. A 400 cm^2 M31 (old generation) MEA was tested at the University of Hawaii using UTC Fuel Cells hardware. A 400 cm^2 M41 membrane is being built by Johnson Matthey for single cell testing.

III. Project Summary

1. Introduction

The development of low-cost, durable membranes and membrane electrode assemblies (MEAs) is a critical challenge for the successful introduction of fuel cells into mass markets. A team led by Arkema and composed of Johnson Matthey Fuel Cells (JMFC), Georgia Tech (GT), UTC Fuel Cells (UTCFC) and the Hawaiian Natural Energy Institute (HNEI) of the University of Hawaii tackled this challenge.

Prior to the inception of the DOE project, Arkema had worked on this topic. First, with the help of UTC Fuel Cells and subsequently also working with Johnson Matthey Fuel Cells (JMFC), we had showed the early feasibility of developing such products.

Arkema had evaluated the Nafion® (and similar perfluorinated ionomers) manufacturing process and concluded that the cost of Nafion would remain high, probably making it very difficult to attain the DOE target for transportation applications. This is due to the complexity of the chemistry and the numbers of steps involved.

2. Approach

Arkema turned to its own fluoropolymers technology to seek more cost-effective solutions, which also could offer several other significant benefits in terms of improved mechanical properties and high temperature performance, for example. Arkema is the world leader in Poly Vinylidene Fluoride (PVDF) of which the trade name is Kynar®. This fluoropolymer exhibits an exceptional combination of properties. Kynar is very stable in extremely acidic media. It is, for instance, used in the chemical industry to carry hydrofluoric acid (HF), hydrochloric acid (HCl) and many other acids. It is also very stable to strong oxidizers such as bromine. It is, for example, used in zinc/bromine batteries. It is also extremely electrochemically stable and has found key uses in lithium ion batteries where the PVDF "sees" a potential around 4V, far exceeding that in fuel cells (<1V). We can also mention its outstanding flame and smoke properties (hence the many applications in the high end of the wire and cable industry) and its recyclability. Kynar is also much cheaper than Nafion.

Arkema proposed to design of novel membrane materials consisting of blends of poly(vinylidenefluoride) and a sulfonated polyelectrolyte.

In the traditional approach to ionomers for proton exchange membranes (PEM), all the features required are "packaged" in one macromolecule. They include: proton conductivity, mechanical properties, long-term endurance, water management, etc. This is the case, for example, for perfluorosulfonic acids (PFSA) containing membranes. However, the cost of these materials is high, largely due to the complexity and the number of steps involved in their synthesis. In addition, they suffer other shortcomings such as mediocre mechanical properties and insufficient durability for some applications.

The strength and originality of Arkema's approach lies in the decoupling of ion conductivity from the other requirements. Kynar provides an exceptional combination of properties that make it ideally suited for a membrane matrix. The sulfonated polyelectrolyte provides the necessary water absorption and protonic conductivity.

3. **Preliminary work**

Prior to the DOE award Arkema, UTCFC and JMFC conducted preliminary tests on novel Kynar-based membranes with promising results. First, we found that the thermal stability of the Kynar/Polyelectrolyte blends was superior to that of Nafion. At 120°C and under a 5 g load, the Atofina membrane maintains its mechanical integrity while Nafion starts to flow at temperatures as low as 70°C. We thus show potential for high-temperature capabilities. This difference in behavior is illustrated in Figure 1. In essence, the Kynar based membrane does not creep at 80ºC or 120ºC.

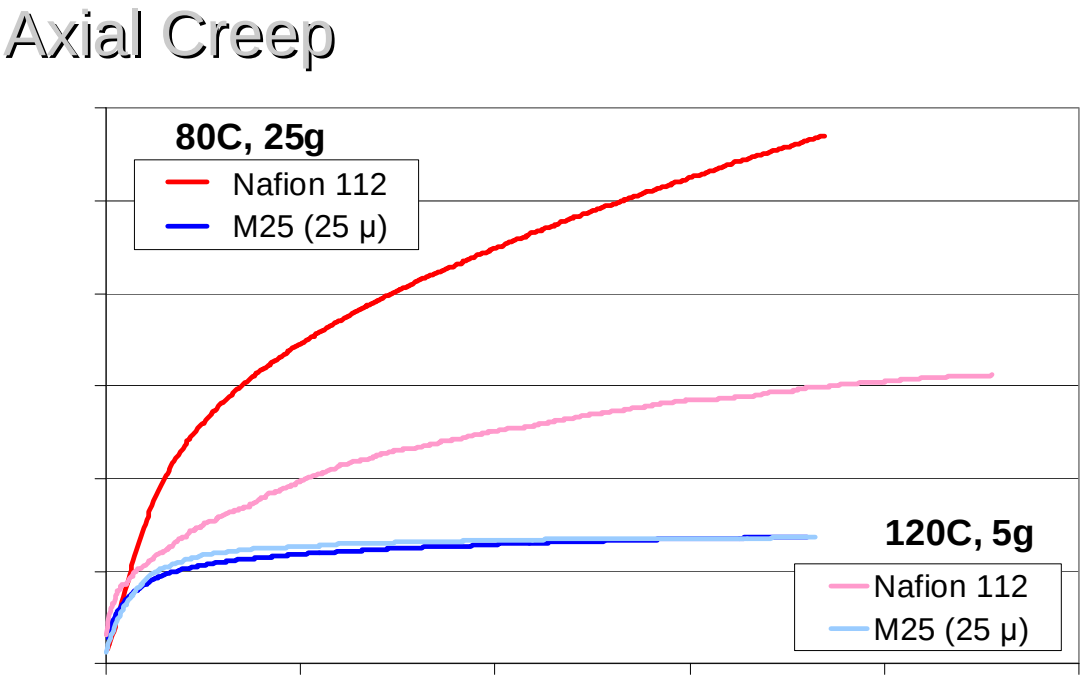

Figure 1: Creep behavior of Nafion and M25 Kynar based membrane at 80ºC and 120ºC.

Table 1 summarizes some key data. Indeed, it indicated that membranes based on PVDF – polyelectrolyte blends showed excellent potential.

Key Properties Measured	Nafion 112	M10	M11	M15	M17	M25
Conductivity at 70°C	130-200	78	**160**	87	55	110
Linear change x,y %	15	**10**	15	20	8	23
Thickness change z, %	15	**6**	8	14	20	20
Water uptake %	37	61	50	47	**21**	64
Hot water test 168 h	-	-	-	2	1	
(% wt loss) 500 h	-	4	1.5	3	1.5	1.5
2000h	1.8	-	-	5	**2**	

Table 1: Properties of early Kynar-Polyelectrolyte Membranes

4. **<u>Proof of Concept: Development of M31 Membrane</u>**

The first task was to prepare polyelectrolyte candidates of various architectural, composition, molecular weight, polydispersity. Two areas of research appeared to be especially important:

- Increasing the polyelectrolyte molecular weight.
- Increasing its equivalent weight (a measure of sulfonic acid groups content).

Below, Figure 2 illustrates how the molecular weight of the polyelectrolyte can be manipulated. The GPC trace shows two different early candidates. One having a molecular weight of 66,000g/mol. and the other 358,000 g/mol. The molecular weight of the ionomer has a profound effect on membrane properties.

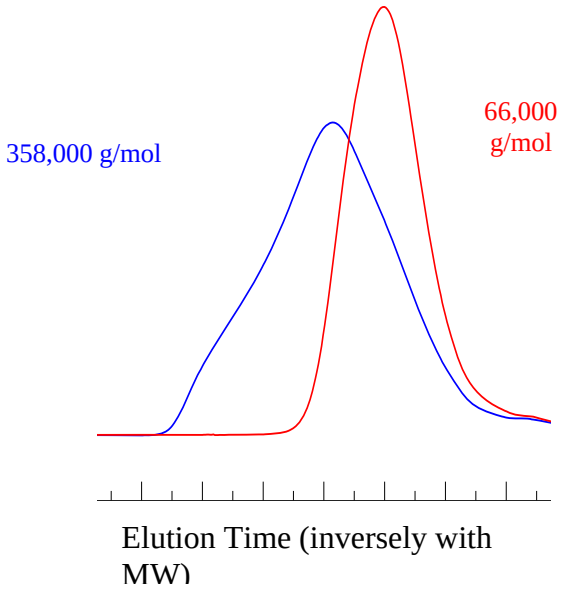

Figure 2: GPC Trace of polyelectrolytes of different molecular weight.

Many of such polymers have been prepared and screened. The choice of the Kynar grade is another important consideration. After preliminary optimization of these parameters, several candidates were selected for membrane scale up. The ex-situ conductivity and swelling characteristics are reported in Table 2.

Property	Nafion®112	M27	M31	M32	M33	M34	M35
X, Y Swell (%)	15	19	27	43	26	24	N/A
Conductivity (mS/cm, 70ºC)	160-200	102	136	184	199	163	137

Table 2: Proof of Concept Membrane Candidates

At this juncture, it is important to underline the criticality of the blending process. It is indeed a considerable challenge to mix PVDF – a highly hydrophobic polymer. The details of the process are proprietary but the schematic is provided in Figure 3. A considerable amount of work was expanded to develop this blending proce3ss and make it very reproducible.

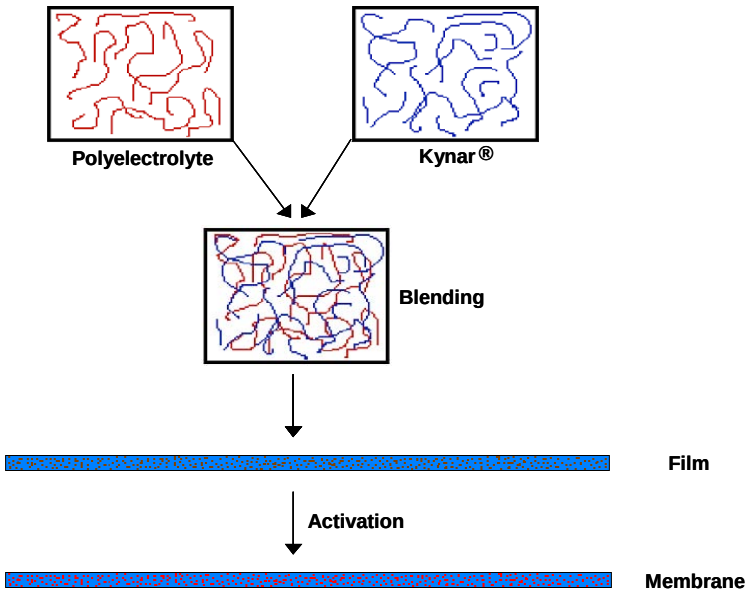

Figure 3: Arkema's blending process for polymer electrolyte membranes for fuel cells.

Strict control of the resulting blend morphology is required to obtain the high proton conductivity necessary for fuel cell applications. Blending hydrophilic and hydrophobic polymers typically yields gross phase separation of the two polymers as shown on the SEM micrograph in Figure 4a. However, the Arkema process allows for Kynar® PVDF and sulfonated polyelectrolytes to be compatibilized, producing a much finer morphology and yielding excellent proton conductivities as shown in Figure 4b.

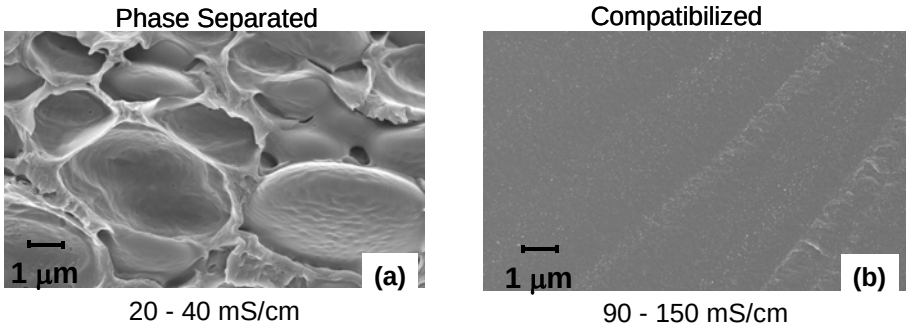

Figure 4: 10k magnification SEM images of (a) uncompatibilized and (b) compatibilized membranes (conductivities are measured at 70ºC, fully hydrated).

In the next step the polymer blend is transformed into a film. Several classical polymer film processes such as extrusion, water-borne casting (from latex) and solvent casting have been studied. The process has been taken several times to a pilot plant level and its excellent reproducibility demonstrated. Most of the trials were carried out to produce films in the 17 to 50µ range. Quality control demonstrated that the film quality was very high through and through. The activation step of the film into a fuel cell membrane also required considerable optimization.

Based on a combination of factors, the M31 chemistry was selected for further testing, MEA optimization and long-term durability studies. The key physical properties are illustrated in Figure 5. The excellent mechanical properties and hydrogen and oxygen barrier properties are noteworthy.

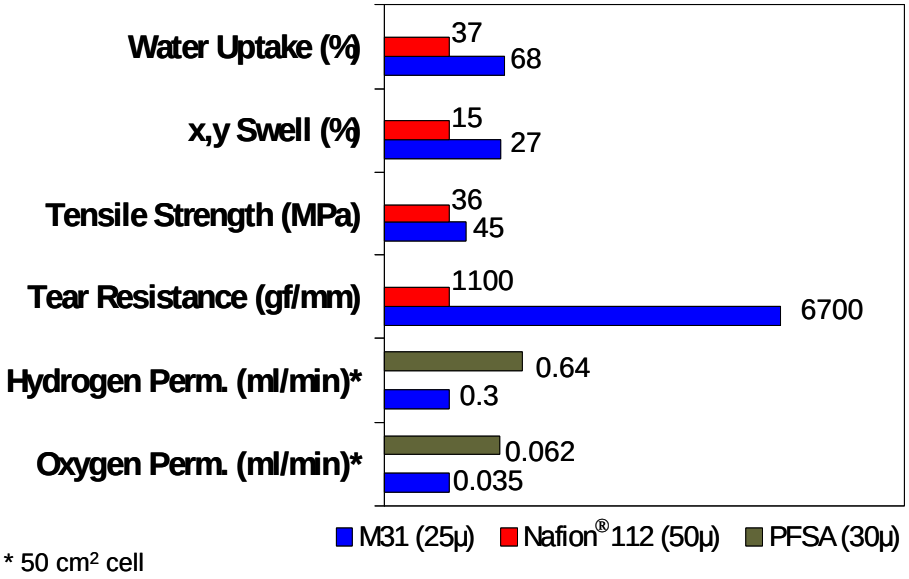

Figure 5: Physical Properties of M31 membranes vs. PFSA membranes.

While the intrinsic conductivity of M31 was not as good as that of Nafion (see Table 2), its excellent mechanical properties and fuel impermeability allowed us to prepare thinner membranes showing better areal resistance than the PFSA control as shown in Figure 6 below.

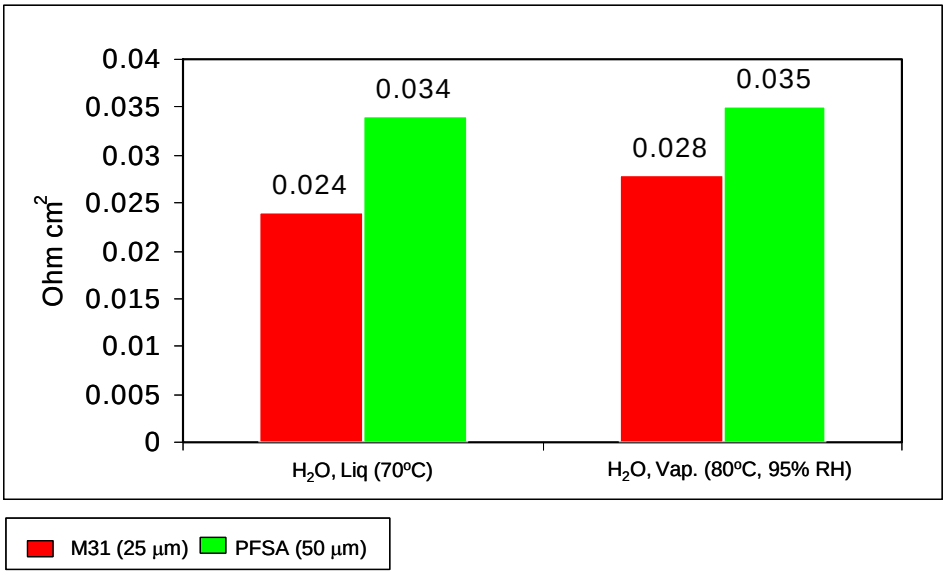

Figure 6: Areal resistance of M31 membrane vs. PFSA membrane.

5. **<u>Proof of Concept: Development of M31-based Membrane Electrode Assemblies</u>**

5.1 Fuel Cell Testing Technique

After reviewing the literature, it became apparent that the procedures of conditioning a MEA and taking a polarization curve varied between fuel cell manufacturers (Gore, JM, GM, Honda, etc.). To verify that our methods provide the same data regardless of conditioning procedure or polarization technique, M31 MEAs were tested by a variety of methods.

a. Conditioning Technique

- Hold at fixed current and record potential – when potential remains steady, MEA is equilibrated.
- Transition MEA between potentials 0.6-0.7 and 0.4-0.5V until current remains steady.

Conclusion: Both conditions provided an equilibrated MEA within the same period: 24-36 hours.

b. Polarization Technique

- Technique 1: Scan the potential (scan rate 0.01V/sec) of the cell from the OCV to 0.3V (or higher potential depending upon the maximum current). Sweep back to the OCV.
- Technique 2: Measure the potential at various currents. Hold the current value for 5 minutes before moving to a higher current.

Conclusion: Figure 7 shows that regardless of how the polarization curve is acquired, the same data is recorded.

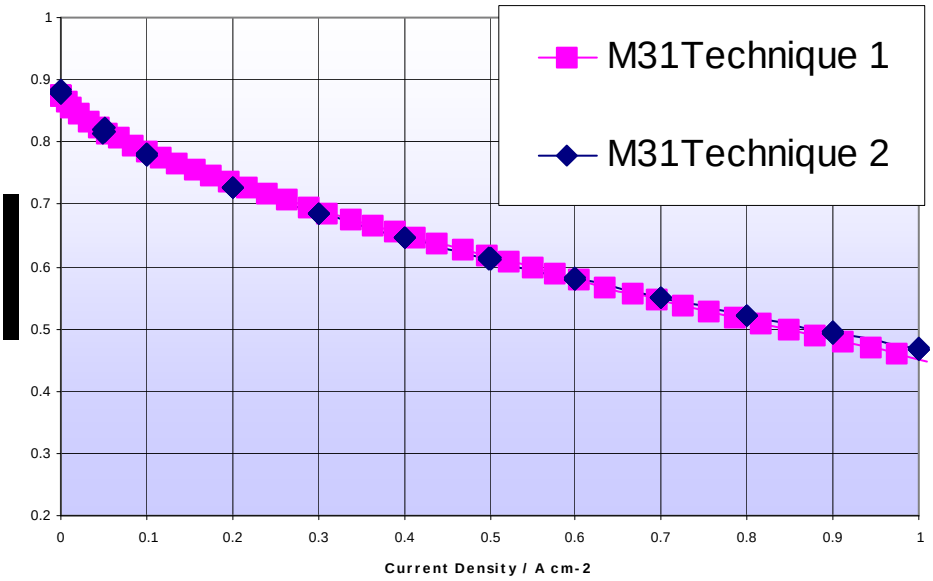

Figure 7: Polarization curves acquired by different techniques.

5.2 M31 MEA Optimization

A considerable effort was expanded to develop high quality membrane electrode assemblies (MEAs). As the Arkema membranes are chemically and physically different from PFSAs, we found that they require specific optimization.

Figure 8 illustrates the progress achieved (with the same membrane) on successive generations of MEAs. Key parameters include assembly parameters (such as temperature, pressure, contact time…) and the composition of the electrode and the gas diffusion layer (GDL).

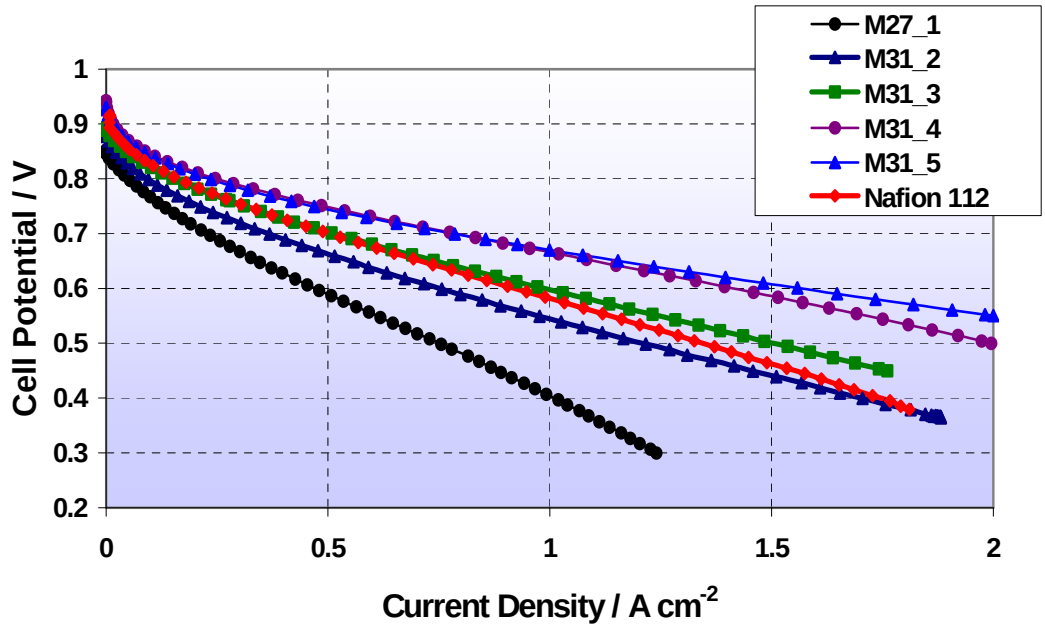

Figure 8: MEA successive optimization with M31 and M27 (60ºC, Oxygen, 100%RH)

Further optimization of the electrode was required to deal with mass transport issues when air is used instead of oxygen at the cathode. Figure 9 below illustrates the dramatic improvement achieved with the proper cathode selection.

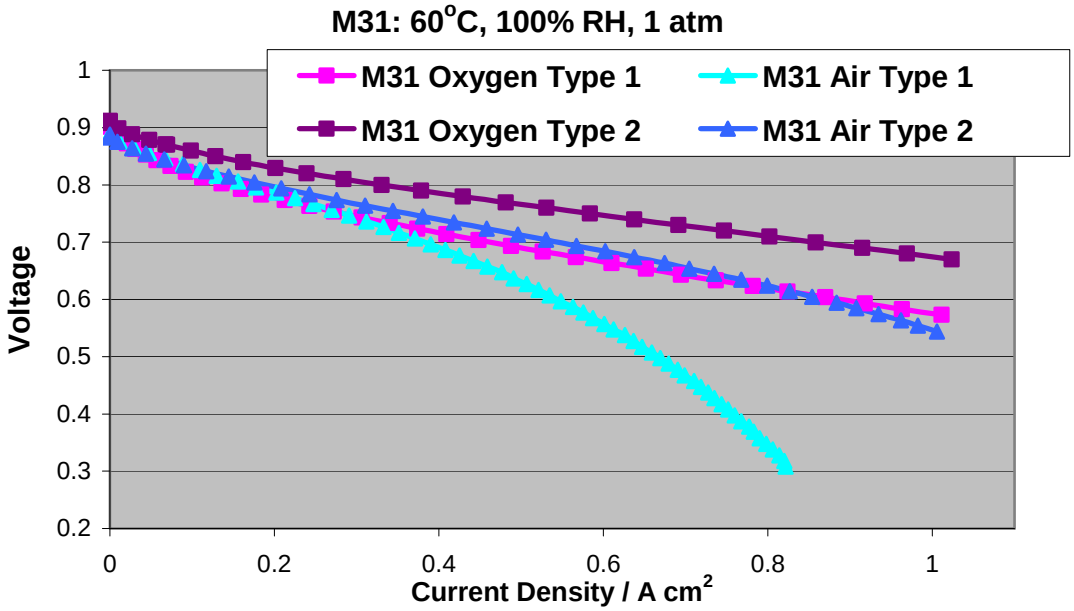

Figure 9: Optimization of electrode for air cathode.

The choice of the electrode and MEA assembly process are thus critical parameters. This is further illustrated in Figure 10. In our hands, the M31 MEA performed on a par with the Johnson Matthey PSFA based commercial MEA (BOL, H_2/O_2, 100% RH 60ºC).

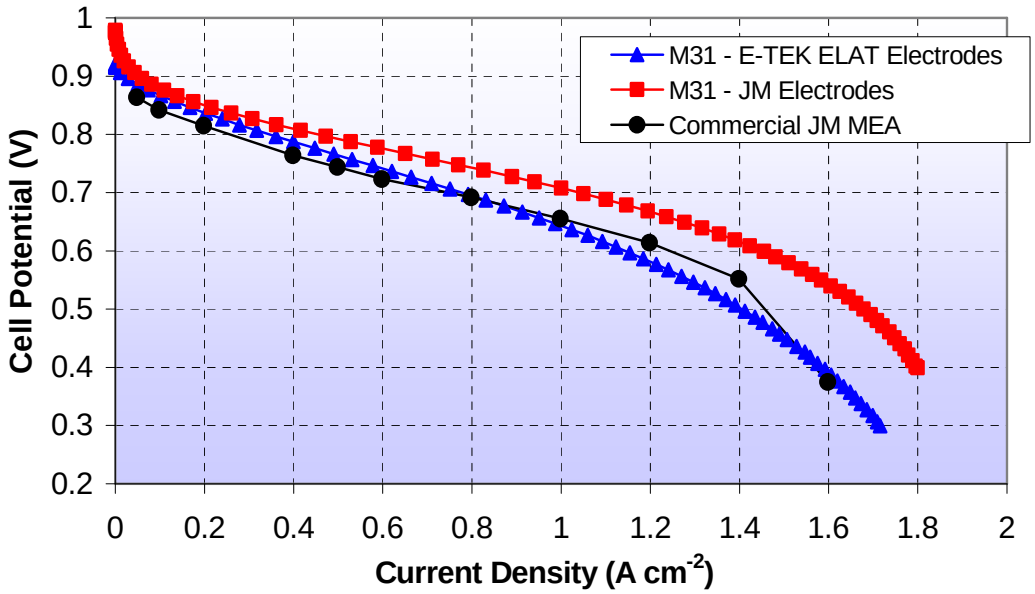

Figure 10: Comparison of M31 MEAs with E-TEK and Johnson Matthey electrodes (60ºC Oxygen, 100%RH).

5.3 Water Management

The Arkema membrane has different water transport properties from that of Nafion. It was observed by JMFC and Arkema that, if the oxygen was not fully saturated with water (100%RH), the MEA performance would drop considerably.

This was attributed to a membrane problem. However, we questioned these conclusions and felt it could be possible to resolve it (at least in part) by addressing the construction of the MEA.

Figure 11 shows the behavior of two differently constructed MEAs using the same M31 membrane when the RH of the cathode was reduced from 100% to 40%. The "standard" MEA (noted "MEA 31-2) became erratic whereas a differently constructed MEA (noted "MEA 31-3" remained stable.

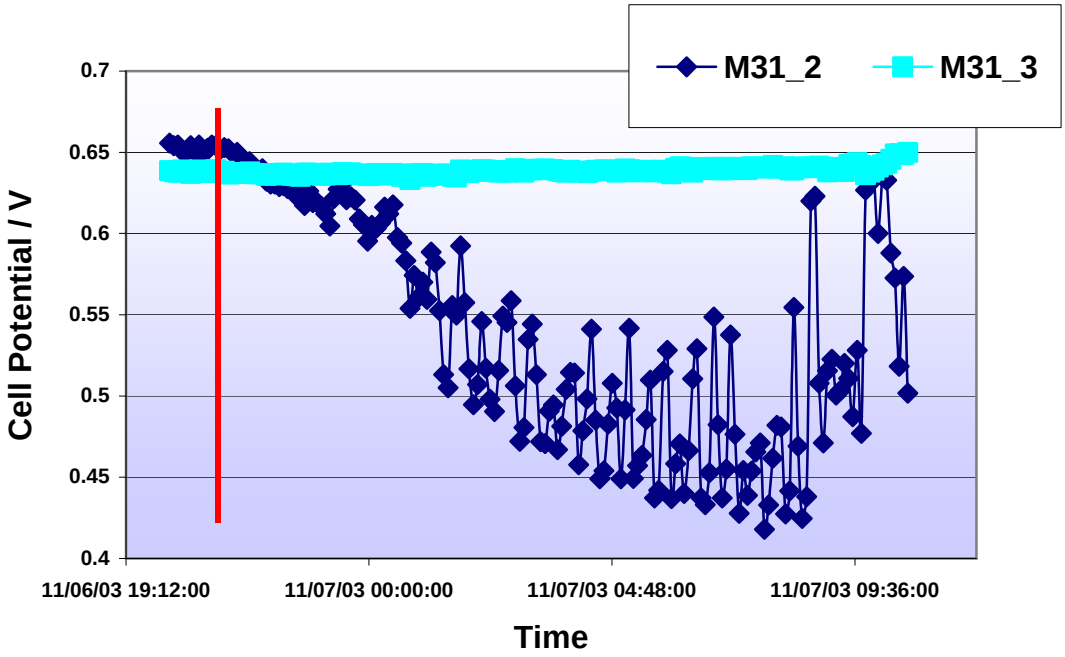

Figure 11: 60ºC, 100% RH Anode, Low RH Cathode, H_2/O_2, 0 psig

Further improvements were made when using a different ELAT electrode from E-TEK as illustrated on Figure 12. While the membrane noted M 31-2 worked well at 100%, it did not work at all at low cathode RH (not shown on the graph). M 31-3 worked adequately at low cathode RH conditions and M 31-4 performed significantly better.

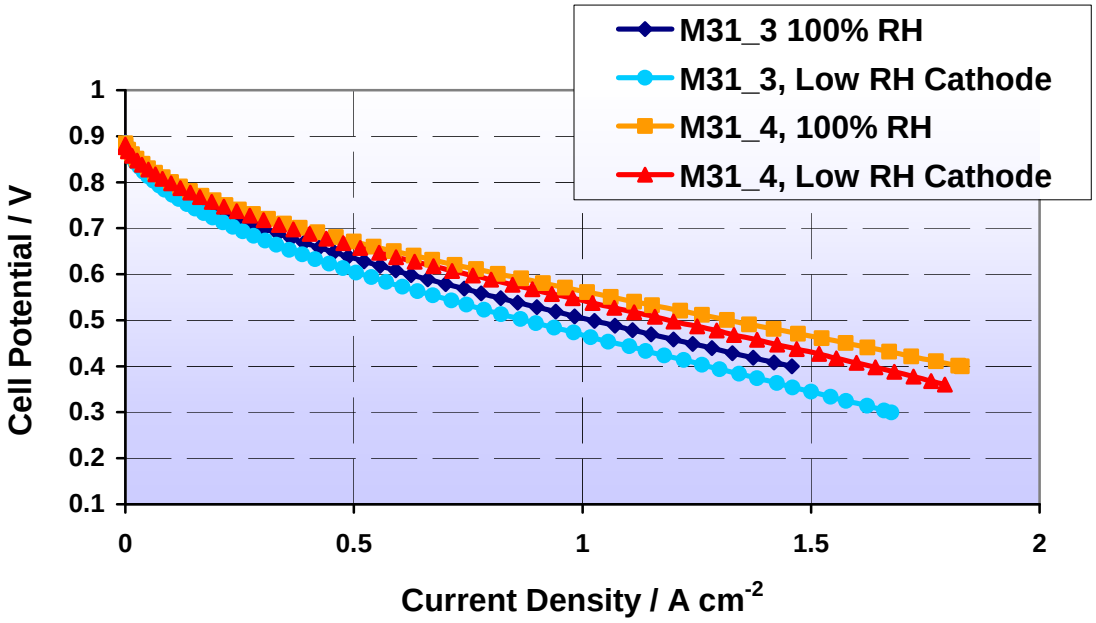

Figure 12: H_2/O_2 100% RH unless otherwise noted, 60ºC, 0 psig

This test was pushed to the extreme and it was shown that, what the proper MEA construction, an M31 MEA could run under fully dried conditions at the cathode as show on Figure 13 below. While a drop in voltage at equal current density is noticed, it appears to be acceptable.

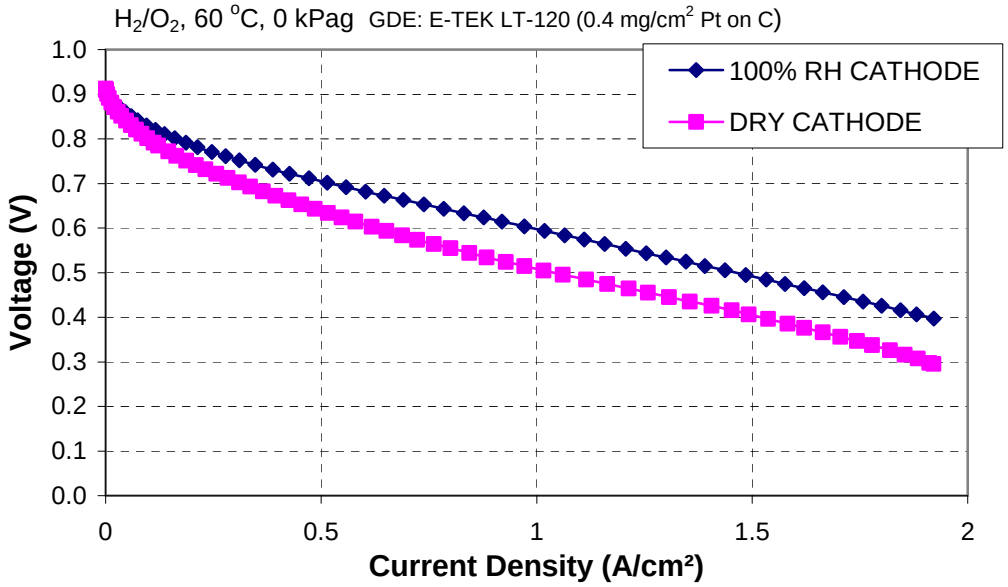

Figure 13: Comparison of M31 based MEA between fully humidified conditions at the cathode and dry conditions.

We carried out a similar experiment under dry anode conditions and found – surprisingly – that with the proper electrode and gas diffusion layer configuration, the M31 performance was very good as seen in Figure 14 below.

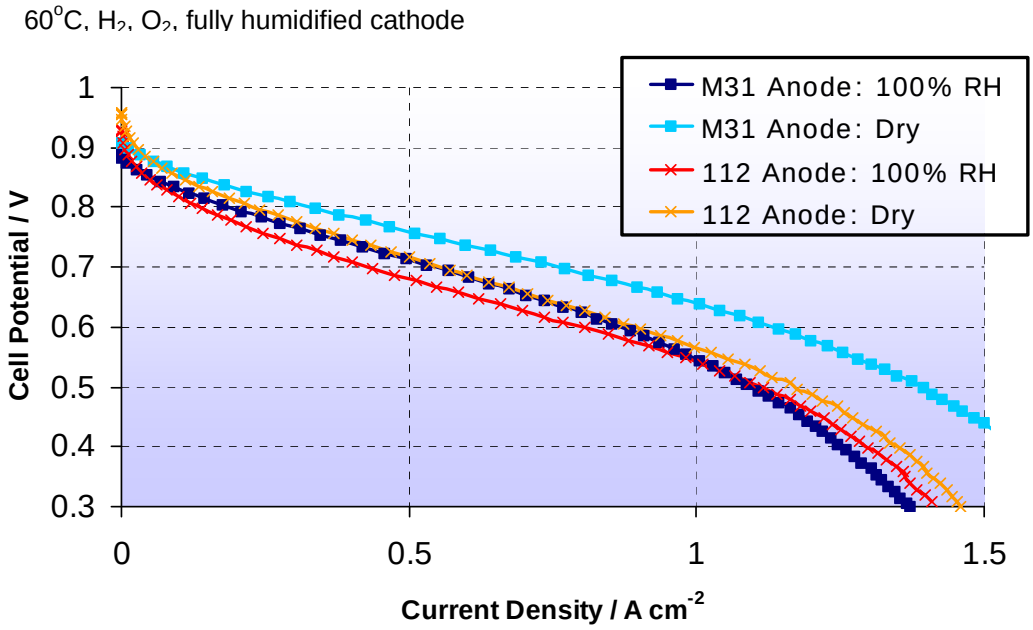

Figure 14: Comparison of M31-based MEA between fully humidified conditions at the anode and dry conditions.

Unfortunately, when both the anode and cathode were dry, the cell did not function.

In conclusion, we found that the M31 membrane offered real promise. Its beginning of life performance was on a par with that of commercial MEAs. It functioned well under oxygen or air and limited MEA optimization work suggested it could work at low relative humdities at the cathode.

6. **Long-term Durability Studies**

Long-term durability tests were intiated at 60ºC under static conditions. An M-27 (a precursor of M31) was tested first. The test was stopped after 1100 hrs. of testing because of test stand problems. The results are shown in Figure 15 below. The M-27 MEA exhibited an overall decay rate of 147µV/h, almost matching the OCV decay rate (145 µV/h). This was of course, unacceptably high (by about 2 orders of magnitude). However, it is noteworthy that ther was a period of ~ 600 hrs. where the decay rate was only 16 µV/h.

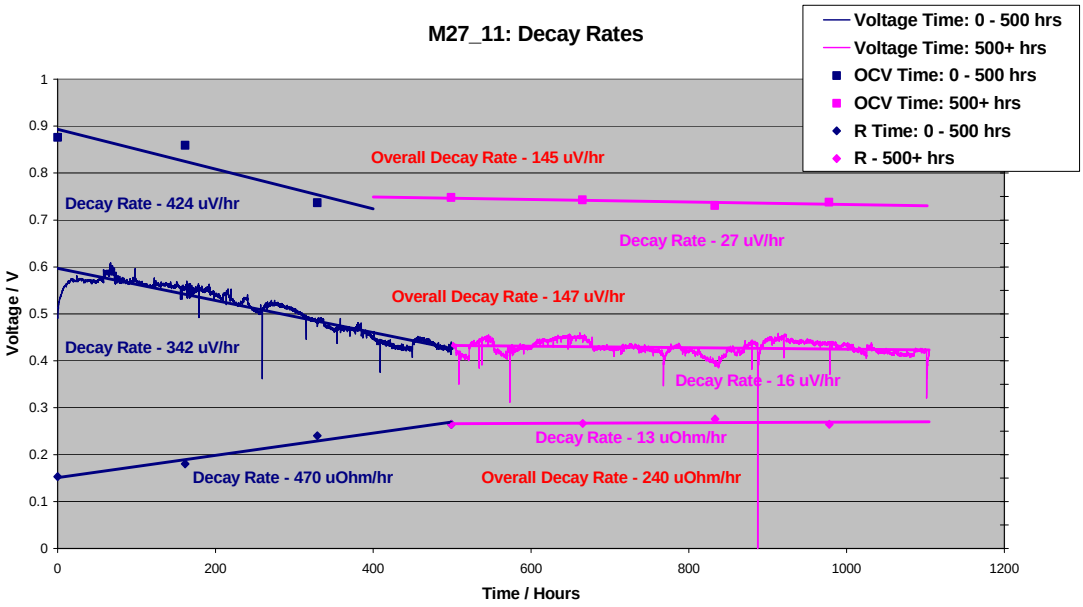

Figure 15: Long Term Durability Test of M-27 MEA at 60ºC.

Similarly, we ran long-term durability tests with M31 based at 60ºC under static conditions. We were able to improve the decay rate from 147 µV/h (M-27) to 75 µV/h (M31-1) and finally 45 µV/h (M31-2). It is noteworthy that these improvements were essentially linked to MEA construction and assembly process optimization. It can further be observed that for M31-2 there was also a period of several hundred hours with very little decay. While the improvement in decay rate was substantial, it is at least one order of magnitude too high for practical applications. The test for M31-2 was stopped at 2150 hrs. (See Figure 16).

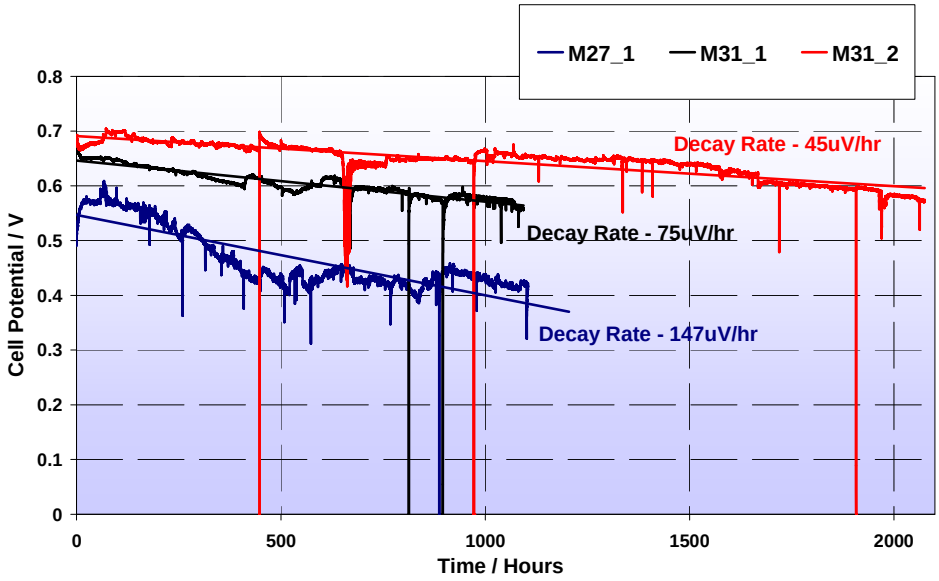

Figure 16: Long-term durability test (60ºC, Oxygen, 100% RH) for various MEAs.

7. **Elucidation of Failure Mechanism**

Membrane durability is one of the primary limitations of PEM systems and continues to be an active area of research. Although PFSA membranes are relatively stable, their performance decays over time due to chemical degradation and material fatigue. Chemical degradation in PFSA polymers is hypothesized to occur when certain key sites (e.g. chain end groups and branched side chains) are attacked by radical species formed in the MEA.[1,2,3,4,5] This leads to gradual, step-wise degradation of the polymer and its material properties. The second mode of performance loss, material fatigue, is produced from stresses that occur during thermal and humidity cycling in the MEA. The combination of chemical degradation and fatigue creates microstructure defects, such as pinholes and fissures, which ultimately causes gas crossover failure.

In the case of the M31 MEA failure in the durability test, post mortem analysis revealed electrode delamination and membrane thinning as can be seen of the SEM images in Figure 17. Electrical shorting was also occurring.

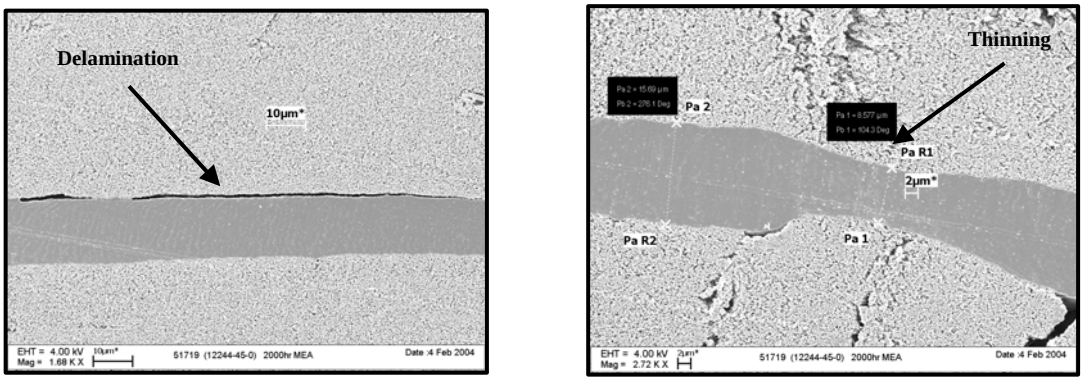

Figure 17: SEM Post-mortem analysis of M31-2 MEA after 2150 hr. durability test.

The membrane thinning observed by scanning electron microscopy was accompanied by a significant loss in sulfur content in the membrane as revealed by the X-Ray Fluorescence (XRF) analysis. Figure 18 shows that this loss was in the range of 40-50% depending where the measurement was taken on the membrane.

(1) LaConti, A.; Hamdan, M.; McDonald, R. Mechanisms of Membrane Degradation. In Handbook of Fuel Cells – Fundamentals Technology and Applications. Vielstich, W.; Lamm, A.; Gasteiger, H. *eds.* (2003) England: Wiley, Chapter 49.

(2) Pianca, M.; Barchiesi, E.; Espoto, G.; Radice, S. *J. Fluorine Chem.* **1999**, *95*, 71-84.

(3) Curtin, D.; Lousenberg, R.; Henry, T.; Tangeman, P.; Tisack, M. *J. Power Sources* **2004**, *131*, 41-48.

(4) Healy, J. *et. al. Fuel Cells* **2004**, *5(2)*, 302-308.

(5) Schiraldi, D.; Zhou, C.; Zawodzinski, T. *Prepr. Pap. – Am. Chem. Soc., Div. Fuel Chem.* **2005**, *50(2)*, 519-520.

- Cross-sectional XRF shows decreased sulfur concentration across the membrane thickness

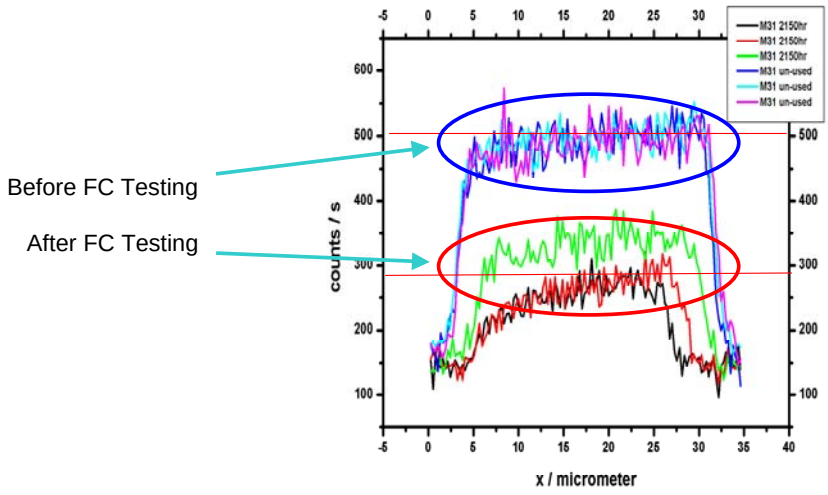

Figure 18: X-Ray Fluorescence analysis of M31-2 MEA after durability test.

Since the only source of sulfur in the membrane was the sulfonic acid groups in the polyelectrolyte, it was thus obvious that the polyelectrolyte was degrading.

In order to understand this failure mechanism, it was necessary to determine what compounds were leaching out of the membrane. This led us to undertake a very comprehensive analytical effort to tackle this issue. The task was very difficult for several reasons. First, the concentration of species involved are minute. Secondly, the analytes are eluted in water – a solvent presenting difficult challenges. Thirdly, no "off-the shelf" method did exist in our company. We found that a combination of ion chromatography and gel permeation chromatograph (GPC) provided the most powerful insights.

Effluent analysis by ion chromatography showed a large amount of sulfur (mostly as sulfate ions) while the sulfur loss was negligible in the JMFC PFSA commercial MEA. Conversely, it was also noted that the fluoride losses were much lower for the Arkema membrane vs. the PFSA membrane as seen in Table 3.

Effluent	F (ppm)	S (ppm)
M31 80°C (Johnson-Matthey in cell)	0.16	6.42
PFSA 80°C (Johnson-Matthey in cell)	0.91	<0.1
M31 80°C (Arkema *ex-situ*)	0.1	6.54

Table 3: Fluorine and Sulfur content in Water (Measurements performed by ion-chromatography).

The analysis of very low levels of oligomers (low molecular weight polymers) in water is a particularly difficult problem. We enlisted the help of Prof. Wayne Reed, Chairman of the Physics Department at Tulane University and a world authority in the field of GPC in water. With his help, we were able to demonstrate the presence of oligomers in the fuel cell water effluent as shown in Figure 19. The red trace in the gel permeation chromatogram shows the presence of low molecular ionomers.

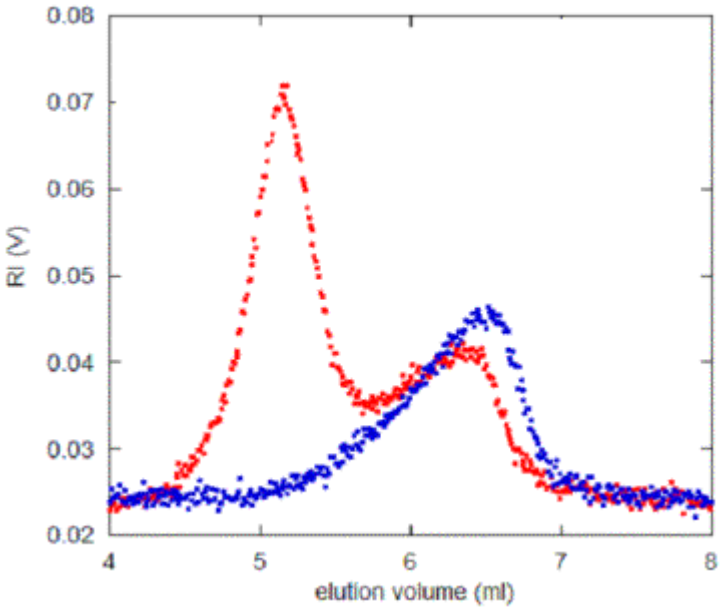

Figure 19: GPC Analysis on fuel cell effluent (Prof. Wayne Reed, Tulane University).

In parallel, we developed a hot water extraction test. While not a perfect match for fuel cell test, it showed the same general trends and was in good agreement with the results obtained from the fuel cell test leachate.

The key conclusions from this work was that the sulfur loss observed in M31 membranes was related to two distinct mechanisms:

- oligomer leaching
- chemical degradation due to the cleavage of a specific bond in the M31 polyelectrolyte

In addition, each mechanism accounted roughly to half of the sulfur losses. These mechanisms are visually represented in the cartoon of Figure 20.

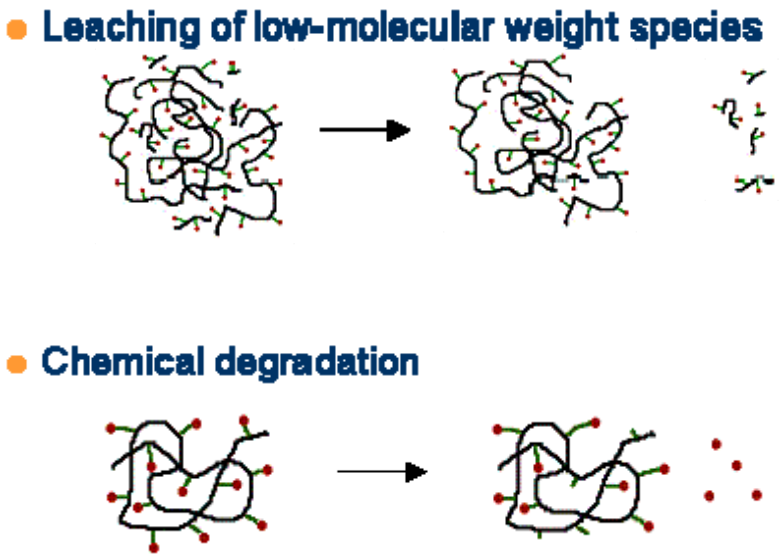

Figure 20: Representation of sulfur loss mechanisms in the M31 membrane.

8. **Development of the next generation membrane**

The leaching of oligomers can be relatively easily mitigated. As there is a high flux of water in a fuel cell environment, it is necessary to somehow immobilize the ionomer in the PVDF matrix. In principle this can be achieved by increasing its molecular weight or by cross-linking it. Indeed, we demonstrated that increasing the polyelectrolyte molecular weight nearly eliminated oligomer leaching. Figure 21 shows GPC traces of the polyelectrolytes that were used to demonstrate this effect.

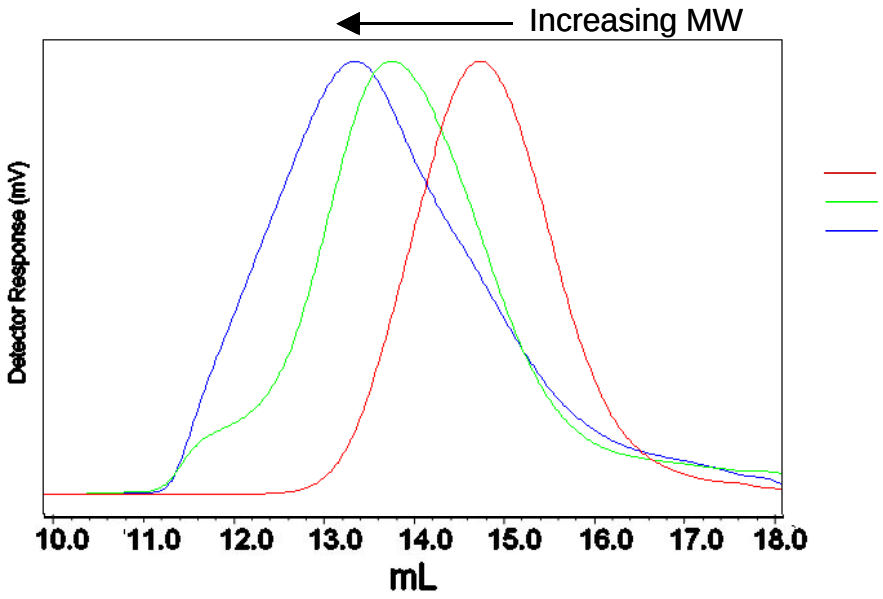

Figure 21: Gel Permeation Chromatogram of polyelectrolyte featuring the same composition and architecture ionomer but increasing molecular weights.

When formulated into membranes with PVDF, the resulting sulfur loss was reduced by approximately 50% compared to M31.

Regarding the chemical leaching, we found out it was associated to the cleavage of specific bond in the chain linking the sulfonic acid group to the polymer backbone as represented in the following cartoon. The solution would therefore consist in redesigning the side chain and entirely eliminating a weak bond linking the SO_3H bearing moiety to the polyelectrolyte backbone.

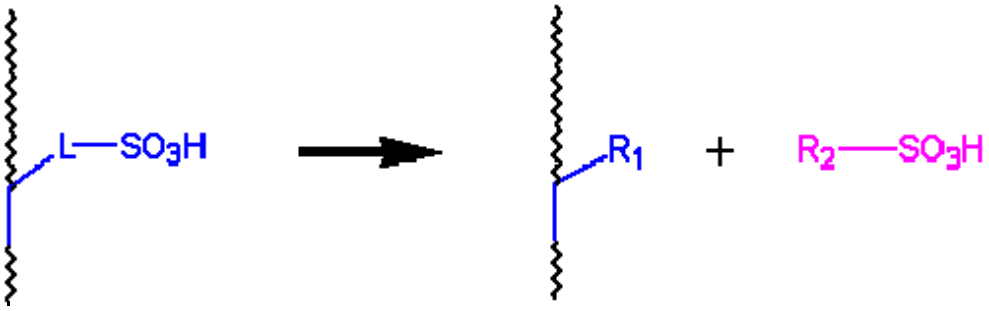

8.1 Design of early screening tests

The project work flow for polyelectrolyte development is illustrated in Figure 22 below.

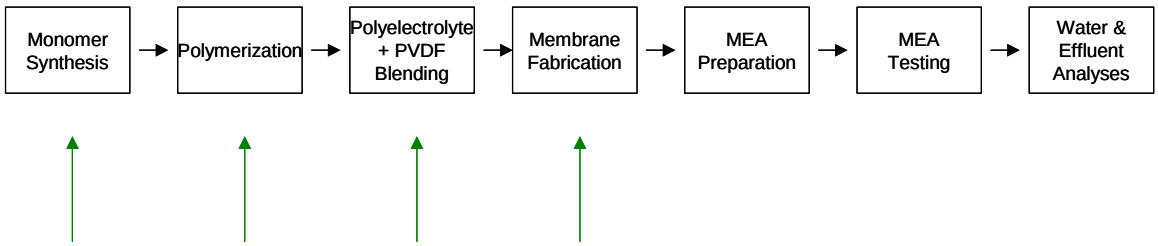

Figure 22: Project workflow for polymer polyelectrolyte membrane development. The green arrows indicate the steps for which accelerated tests were developed.

There is a 7-step process from monomer synthesis to analysis for membrane degradation in a fuel cell test. This was obviously not compatible with rapid development and the project time line. In order to quickly identify promising leads, a series of four accelerated tests were designed in the first four steps. While the details of these steps are proprietary, the general principal and conclusions will be discussed below.

8.1.1 Monomer screening

Arkema designed an accelerated NMR test to assess the stability of the polyelectrolyte building blocks: the monomer themselves. Figure 23 illustrates that, when subjected to this accelerated test, the M31 sulfonated monomer degraded, yielding in the process the same metobolites as in the fuel cell test. The red arrows shows the presence of degradation products.

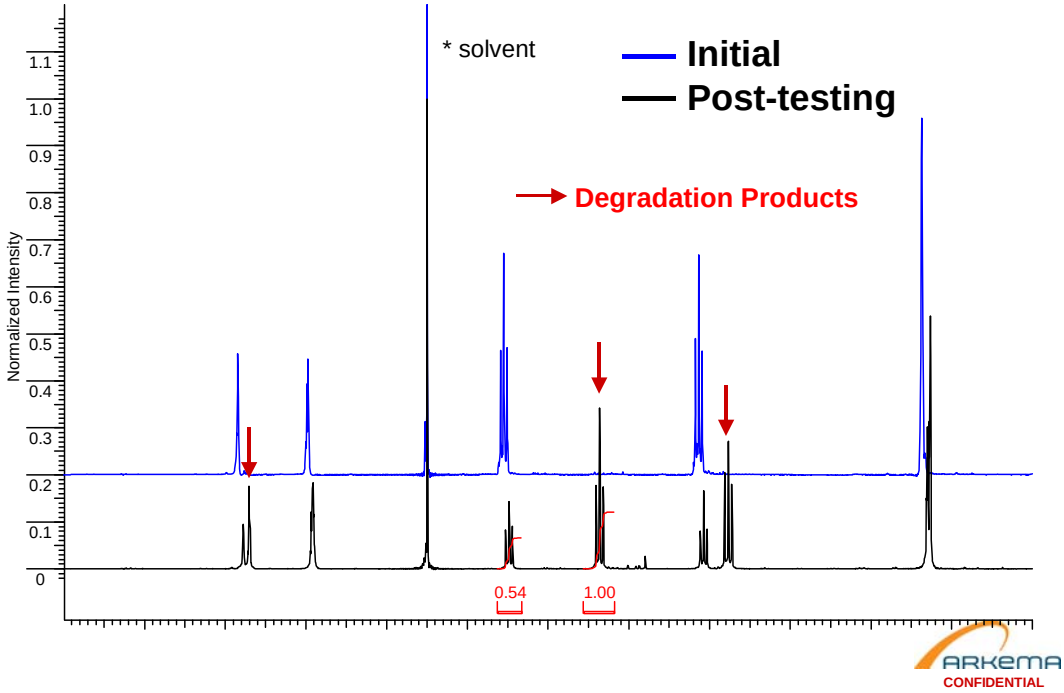

Figure 23: M31 Sulfonated Monomer Chemical Stability: ^{1}H NMR

NMR and ion chromatography analysis were also applied to the leachate obtained in this test and fuel cell effluent experiments. The same by-products were also identified confirming the validity of this accelerated test, at least on a qualitative basis.

8.1.2 Polyelectrolyte Screening

The monomer screening test provides very useful information: monomers failing this test will not yield a stable membrane/MEA. However, the monomer test can also provide false positives. As we were developing this accelerated testing methodology, we used AMPS (2-acrylamido-2-methylpropane sulfonate) and Poly-AMPS. As can be seen in Figure 24, AMPS passed the monomer screening test but Poly-AMPS did not as shown on Figure 25.

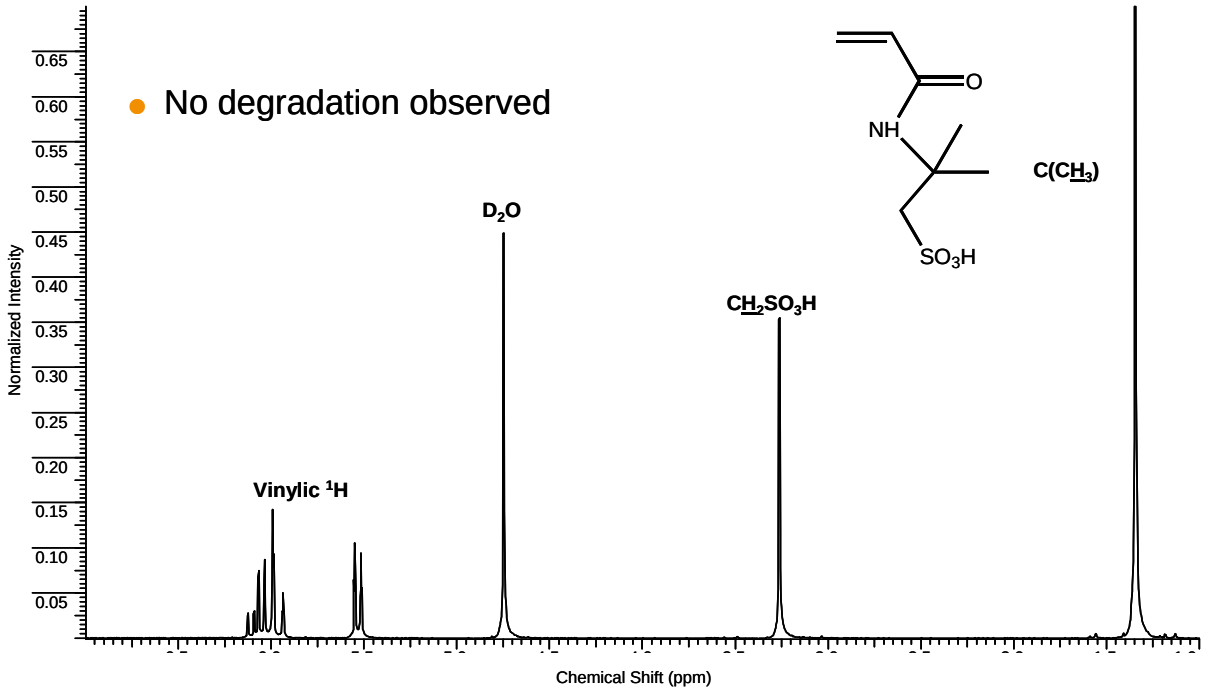

Figure 24: Accelerated testing of AMPS monomers

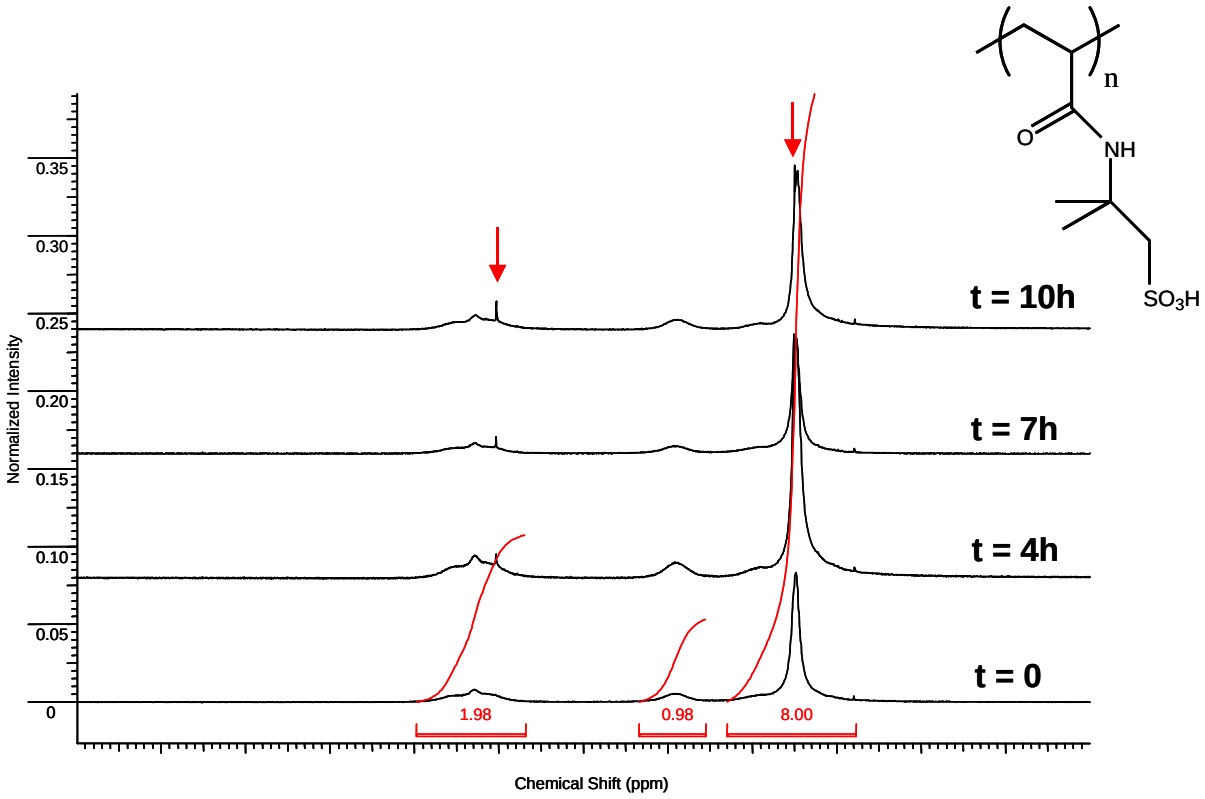

Figure 25: Accelerated testing of Poly-AMPS

In this particular case, the degradation product was unambiguously shown to be dimethyltaurine (DMT) as shown in Figure 26. The sample was spiked with an authentic sample of DMT conclusively confirming the identity of the degradation product.

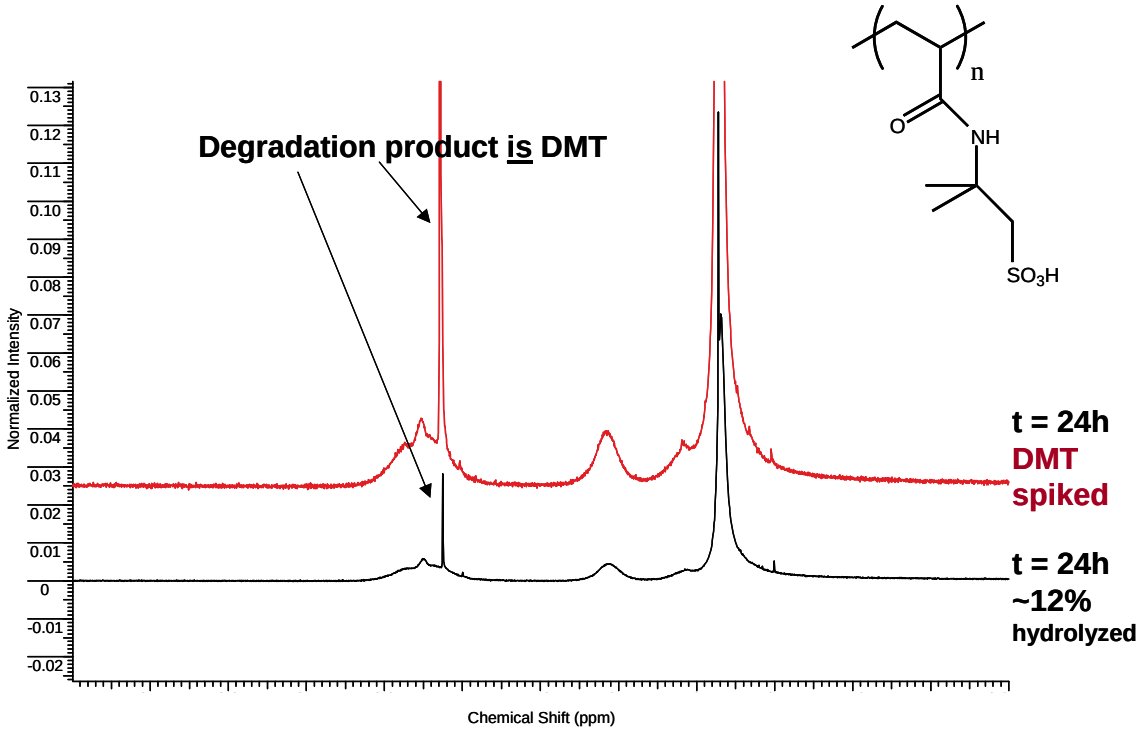

Figure 26: Accelerated degradation of Poly AMPS

8.1.3 Polyelectrolyte – PVDF Blending Process

All the work done on the M31 membrane and its predecessors were done with polyelectrolytes having a related composition and architecture. The polyelectrolyte/PVDF blending process had been optimized for these families of ionomers.

As new potential polyelectrolyte candidates were developed, a central question arose: could these new materials be blended with PVDF and if yes, how much optimization would be needed? Small scale screening tests were developed and three criteria were deemed to be particularly important:

- visual aspect
- mechanical strength
- proton conductivity

Simple visual examination could readily reveal poor mixing (such as haziness). A mechanical property is another important practical consideration. Poor mixing is also usually related to mediocre mechanical strength. Proton conductivity is obviously critical for membrane development.

In addition to the M31 polyelectrolyte, we examined a series of model ionomers of very different chemistries. We found out that, with minimal optimization, these polyelectrolytes could be blended with Kynar PVDF as illustrated in Figure 27.

Polyelectrolyte	Conductivity (mS/cm)*	Structure
• Family A	130-180	Proprietary
• Family B	120-140	Proprietary
• Poly(acrylic acid)	-	
• Sulfonated Polystyrene	50-90	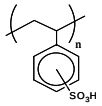
• PolyAMPS	90-140	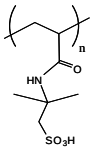

* 70°C in Water

Figure 27: Blending of Kynar PVDF with various polyelectrolytes

8.1.4 Membrane Durability Screening

In the same spirit of the tests developed for monomers and polyelectrolyte screening, we also developed an accelerated test to probe the membrane stability (ex-situ of a fuel cell). We previously showed that it is not possible to directly extrapolate the stability of the polyelectrolyte from that of its monomer building blocks. This is also true – although to a lesser extent – in the case of the membrane compared to its own constituents. In the case of the membrane durability test, the main response parameter of interest here is the sulfur loss (directly correlating with the sulfonic acid groups losses) as a function of test time.

8.2 Selection of the next membrane generation

To summarize thus far, the rate and mechanism of degradation are dependent upon the polyelectrolyte composition. Therefore, the rate of degradation can be controlled by the chemistry employed to synthesize the polyelectrolyte. The targeted general structure for the polyelectrolyte can be represented as follows:

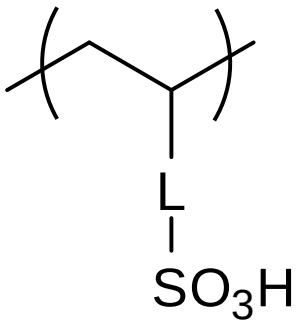

where L is a linking group between the polyelectrolyte backbone and the sulfonic acid group. L must be chosen so that the previously identified degradation mechanism in M31 cannot occur.

A great deal of time and effort was expanded to identify possible chemistries as well as suitable architecture, molecular weight and polydispersities for polyelectrolyte candidates. All this work is, however, highly proprietary.

Table 4 illustrates the kind of tedious work required for optimizing the synthesis of polyelectrolyte candidates.

Code	Initiator Charge 1 (mol %)	Initiator Charge 2 (mol %)	Ave M_w (× 10)	M_p (× 10^{-3})	PDI	Conversion (mol %)
12487-153-2	0.30	0.15	110	90	2.5	> 98
12487-162-1	0.20	0.10	145	120	3.0	> 98
12487-162-2	0.10	0.05	166	140	2.8	96
12487-162-3	0.10	0.20	181	150	3.4	> 98
12487-163-4	0.05	0.20	200	185	4.0	> 99
12487-163-5	0.01	0.20	200	172	4.0	96
12487-163-1	-	0.20	195	130	3.5	97
12487-150-4	-	-	310	280	3.8	75

Table 4: Example of optimization of polyelectrolyte molecular weight and polydispersity as a function of initiator charge.

Four different families of polyelectrolytes identified as potential targets (besides the M31 polyelectrolyte, referred as Family A). They are noted Families B, C, D and E. Essentially each family represented new chemistries that had to be demonstrated on a small scale then sufficiently optimized to provide reproducible, high quality materials in sufficient quantity to produce membranes and MEAs for evaluation purpose.

Due to the robust nature of our blending process, we have successfully developed several new families of polyelectrolytes that are resistant to degradation and can be incorporated into membranes that have similar physical properties to our early Kynar based membranes.

Ex-situ tests have been developed to rapidly screen the degradation properties of these new polyelectrolyte families designed for enhanced stability, as shown in Figure 28. The plot illustrates that the M31 polyelectrolyte and polyelectrolyte B had very high sulfur losses, while polyelectrolytes C and D show much lower rates of degradation. The most promising of these candidates is polyelectrolyte D, which shows no statistically significant increase in degradation products over 2500 hours of testing. The membranes produced with polyelectrolyte D are hereby referred to as M40 family.

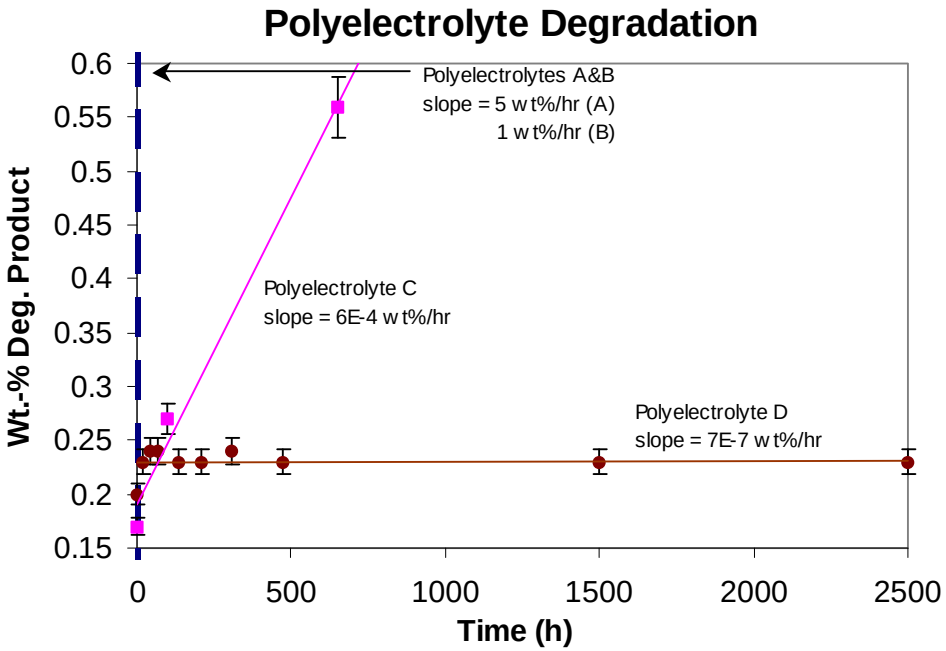

Figure 28: Sulfur loss data for different polyelectrolytes at 80ºC in ex-situ test

Polyelectrolyte D was converted to the corresponding membrane using the process discussed in section 4. Figure 29 shows a direct comparison of the membrane sulfur loss in the Arkema developed ex-situ test for Nafion, M31 and M40.

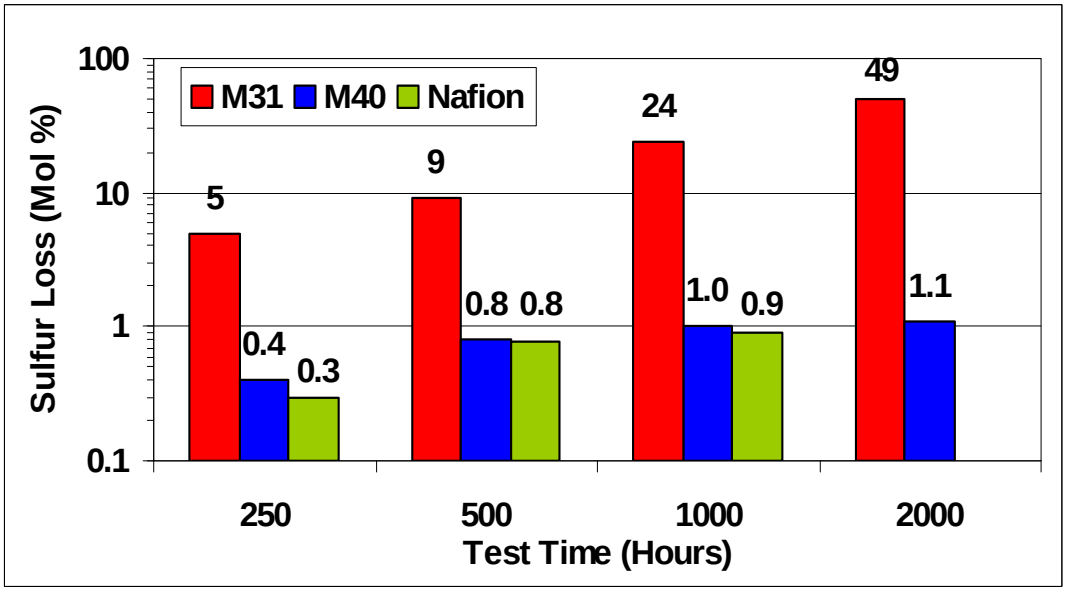

Figure 29: Ex-situ membrane sulfur loss test

Several variations of the M40 family membranes were examined. Most of the data presented from now on in this report will focus on a particular membrane referred to as M41.

Similarly, to M40, M41 also exhibits very low sulfur loss test in ex-situ test (as it uses a very similar composition and architecture to that of M40) as shown on Figure 30.

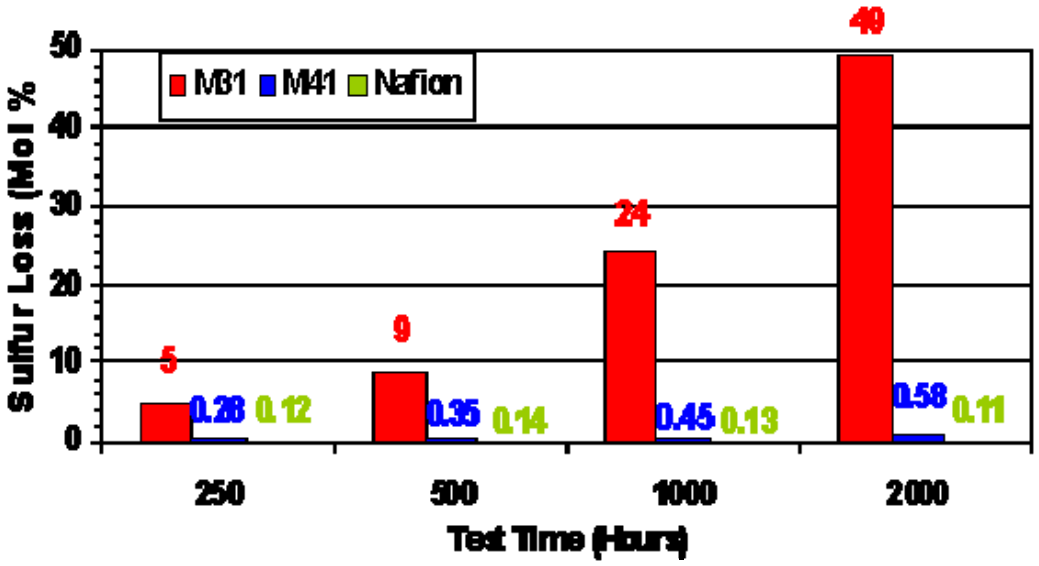

Figure 30: Ex-situ M41 membrane sulfur loss test

8.3. Characterization of M40, M41 Membranes

The key physical properties of the M41 membrane are summarized in Table 5 below. M41 generally exhibits equal or better mechanical properties than Nafion 111.

	Nafion®111	M41
Dry Thickness (μm)	25	25
Equivalent Weight	1100	800
Density (g/cm^3)	1.8	1.5
Water Uptake (%)	37	60
X,Y Swell (%)	15	20
Thickness Swell (%)	14	10-15
Tensile Stress Break (MPa)	19	27
Elongation (%)	103	95
Tear Strength(lb$_f$/in)	404	934
Tear Propagation (lb$_f$)	0.004	0.018

Table 5: M41 membrane physical properties

The gas barrier properties of M40 and M41 were evaluated. This is an important consideration as fuel cross-over has been suspected to be at the origin of hydrogen peroxide formulation initiating chemical degradation of the membrane electrode materials. At equal thickness, M40 exhibits a hydrogen impermeability 4 to 5 times better than that of PFSA. This is illustrated by Figure 31 below showing the hydrogen cross-over measured by the classical electrochemical method.

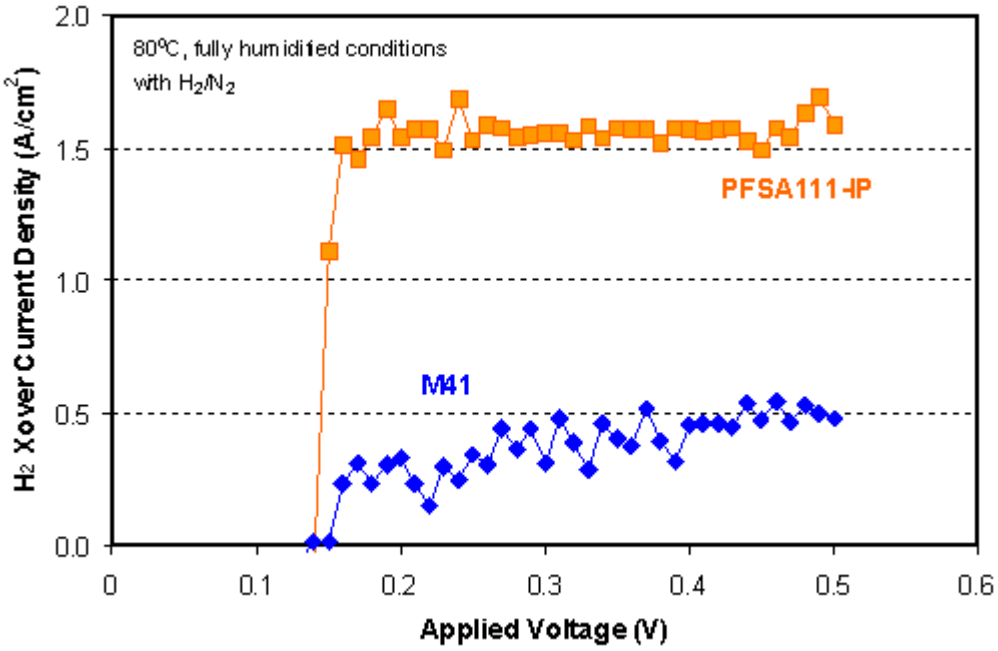

Figure 31: Hydrogen cross-over: Nafion® 112 vs M40.

Further measurements were carried out by Johnson Matthey Fuel Cells and they show the same trends as show in Table 6.

Membrane/MEA	**H_2 Permeation** (electrochemical) mL/min
Commercial PFSA	1.44
Arkema M31	**0.27**
Arkema M40	**0.25**

Table 6: Hydrogen Cross-over: Commercial PFSA vs. M31 and M40 membranes.

M41 exhibits very similar cross-over properties to that of M40.

The proton conductivity was measured using the 4-point probe method (in water at 70°C). The initial results were as follows:

- M40 110 mS/cm
- M41 120 – 130 mS/cm
- Nafion 162 mS/cm

We measured the conductivities at various temperature and found they were equal to M31 for M40 and slightly better for M41 as can be seen on the plot of Figure 32.

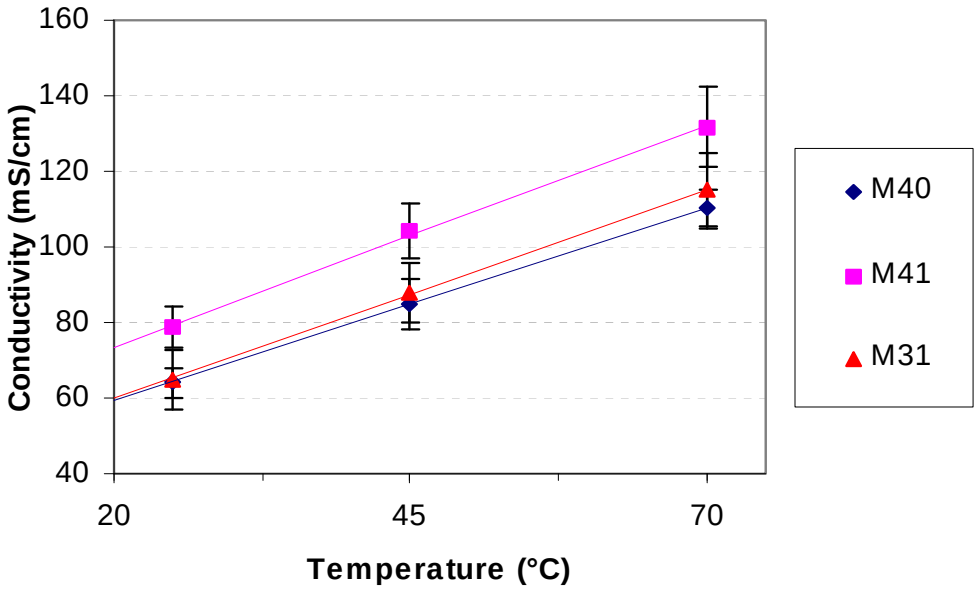

Figure 32: Ex-situ conductivity measurements at various temperatures.

However, we have observed that ex-situ conductivities are influenced by the process conditions for both the film casting and the film activation process. This is illustrated in Figure 33 below. By optimizing these processes, we have measured conductivities exceeding 150mS/cm. They also approach the conductivities we measure for Nafion® in the same conditions in our laboratory (160-165mS/cm).

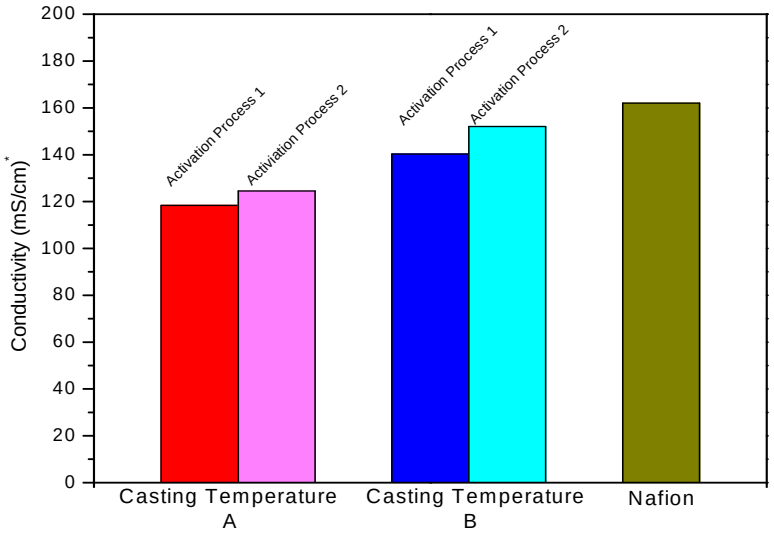

*Completed hydrated membrane at 70°C

Figure 33: Optimization of M41 conductivity.

As already shown on Figure 4, the membrane conductivity is profoundly affected its morphology. Similarly for M41, we found that the membrane fabrication process conditions affect the morphology and the conductivity as illustrated on Figure 33. the high-resolution TEM work was carried out at Oak Ridge National Laboratory by Karren More and her team. Gaining insights in the relationships between the membrane architecture, its fabrication process and morphology is believed to be important for future progress.

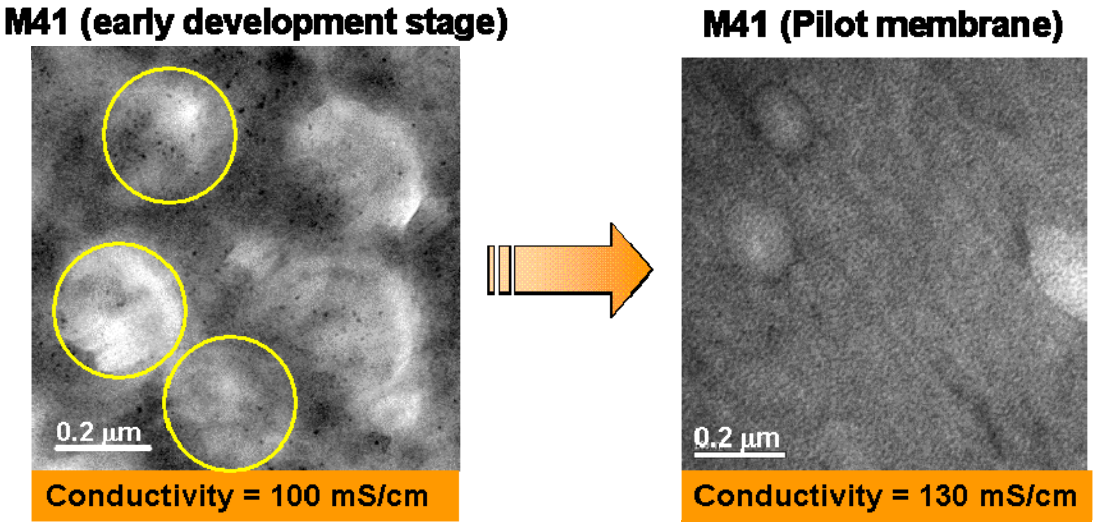

Figure 33: Morphology characterization and control.

8.4 MEA Characterization

Early development stage versions of M40 were assembled to prepare MEAs using JMFC electrodes (0.4mg/cm^2 Pt on C). The same assembly process was used as the one previously developed for M31. Without any optimization it was shown that the performance of M40 was close to that obtained with M31 at 60°C as shown in Figure 34.

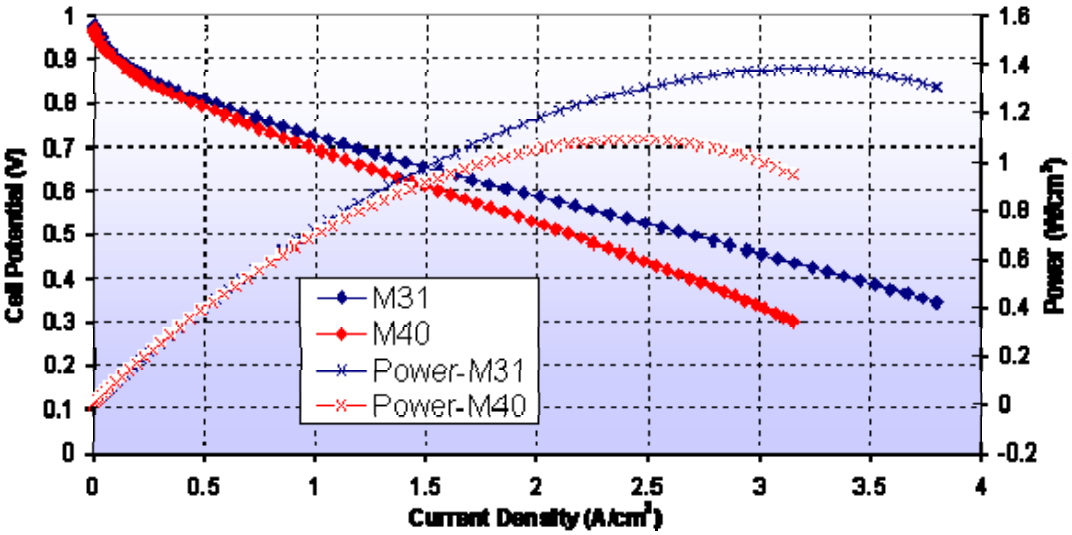

Figure 34: Testing of an early M40 MEA at 60°C.

While the proof of concept evaluation was carried out on M31 at 60°C it was clear that the application required the ability to function at higher temperatures. In the next step, the new generation membranes were evaluated at 80°C. As can be seen on Figure 35, the M31 beginning-of-life (BOL) performance is quite acceptable at this temperature but drops rapidly within 24 hours. (This can be traced back to the failure mechanism previously described for M31). On the other hand, the M40 performance remained stable under the same conditions.

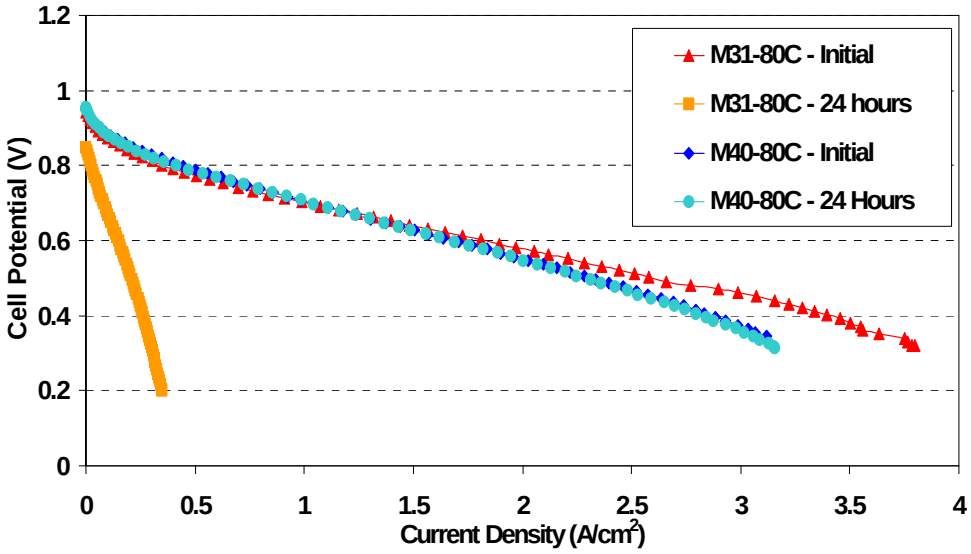

Figure 35: M31 and M40 Performance at 80°C.

After a minimum of optimization work we demonstrated the ability to produce M40 MEAs as good as Nafion 112 as seen on Figure 36.

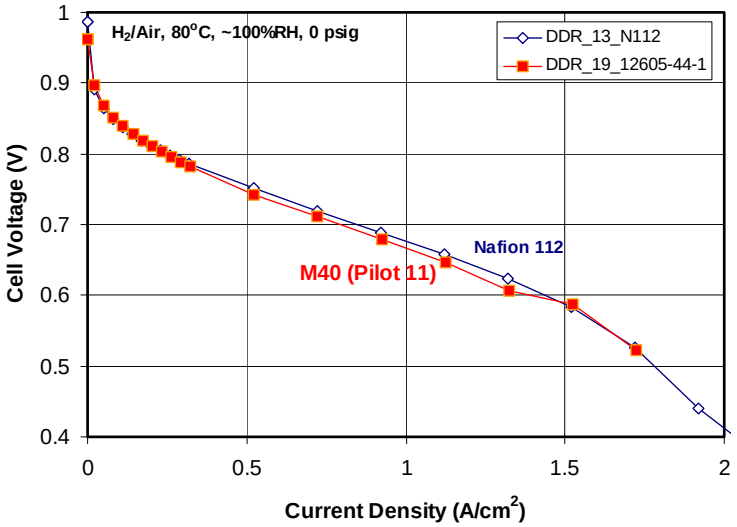

Figure 36: MEA Performance – M40 vs. Nafion® 112 at 80°C, 100% RH.

8.4.1 Membrane – Electrode Interface Characterization

It is important to quantify the performance of membrane from the overall in-cell polarization results. The membrane performance is indicated by the ohmic losses combined the loss due to electrical resistance through the electron conductive layers and the loss due to the flow of ions in the membrane and electrodes. The ohmic losses in fuel cell can be quantified by the hydrogen pump experiments and current interruption techniques. The principle of the hydrogen pump set up is illustrated in Figure 37.

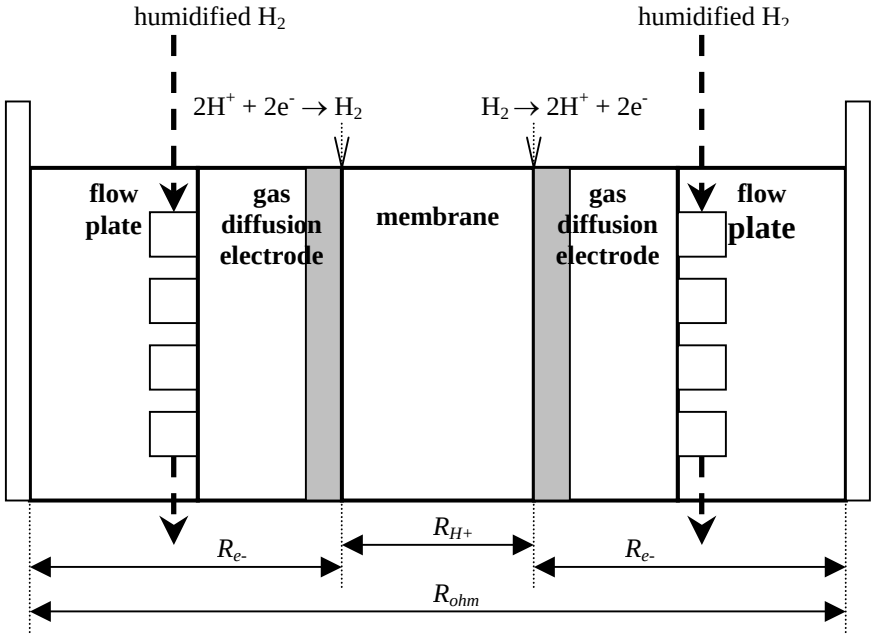

Figure 37: Schematic of the hydrogen pump set up.

Hydrogen pump experiments were performed to assess the membrane resistances through the conducting layers of the fuel cell setup. By flowing humidified H_2 on the anode and the cathode and applying a current load across the cell, polarization due to the ohmic resistances (membrane plus electronic resistances) present in the cell can be measured. Since the theoretical limiting current density of hydrogen electrode estimated from a typical fuel cell configuration is several orders of magnitude higher than the current densities applied in this test, the hydrogen transport resistances can be ignored assuming the hydrogen oxidation and reduction reactions take place right at the membrane/electrode interface for both electrodes. This assumption is supported by the fact that a linear dependency of the cell voltage and current densities was observed when applying hydrogen pump test in our cells as demonstrated in Figure 38, which shows a typical hydrogen pump polarization results at for different temperatures. Depending on the difference in the average hydrogen concentrations and the catalytic properties of each electrode, the value of the intercept in the graph is determined. The slope of the voltage versus current curve represents the total ohmic resistance (R_{ohm}) for at given test conditions (see Figure 37). The experimentally measured ohmic resistance (R_{ohm}) is the sum of the electronic resistance (R_{e^-}), which includes the contact resistance within the solid layers, and the protonic resistance through the membrane (R_{H^+}). Therefore, the total resistance obtained from the slope of the polarization curve can be used to compare the membrane conductivity between cells at the same temperature. The same information can be obtained by doing current interruption measurements. The detail description of the techniques can be found in the literature[6].

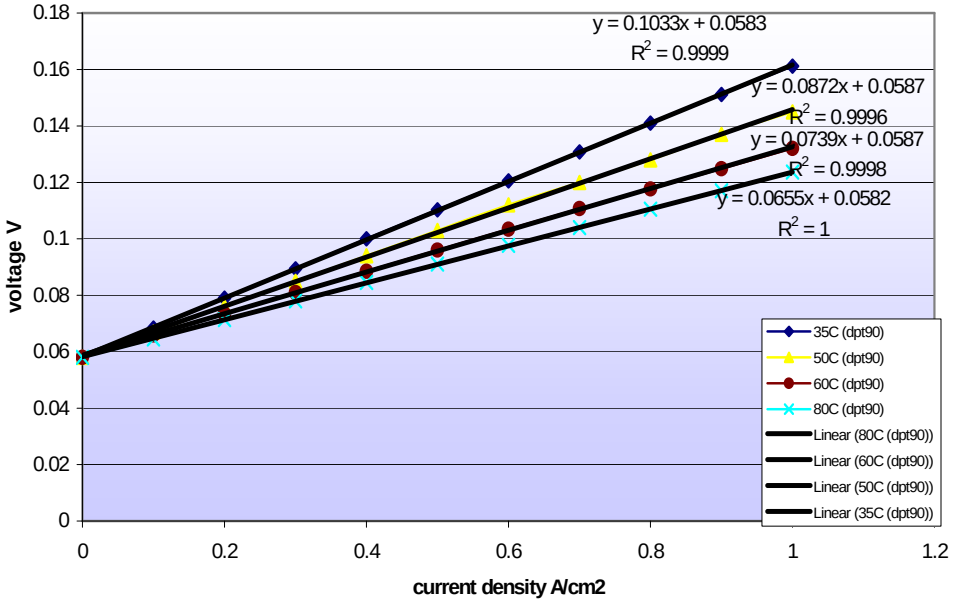

Figure 38. Polarization curves obtained from hydrogen pump tests at various temperatures.

[6] James Larminie and Andrew Dicks, *Fuel Cell Explained*, Weley, 2003.

A PFSA111- (Ion Power) membrane was used. Here the cell voltage is defined to the anode potential minus cathode potential. While measuring the corresponding cell voltage, a current load was applied to the cell starting from 0 to 1.0 A/cm^2 with an increment of 100mA/cm^2 every five minutes. For a given current density, the steady-state values of the cell voltage are reported in Figure 38.

The absolute magnitude of the membrane conductivity can be estimated applying this test to several different temperatures. The electrical conductivity of carbon materials is practically constant within the operation range of PEM fuel cells. Therefore, it is reasonable to assume that the changes in the ohmic resistance (R_{ohm}) with temperature (T) as measured by the hydrogen pump is due to the temperature dependency of the proton conductivity (σ_m) of the membrane as shown in Equation (1).

$$\sigma_m(T) = \frac{t_m}{R_{ohm}(T) - R_{e-}} \tag{1}$$

Where, t_m is the thickness of the membrane (cm) and R_{e-} is the electron transport resistance (Ω-cm^2). Also, σ_m can also be expressed in an Arrhenius form as described in Equation (2).

$$\sigma_m(T) = \sigma_m^0 \cdot \exp\left(-\frac{E_m}{R \cdot T}\right) \tag{2}$$

Where, σ_m^0 is the Arrhenius constant for the proton conductivity, R is the molar gas constant, and E_m is the apparent activation energy of proton transport through the membrane. Based on *ex-situ* proton conductivity measurements reported in a literature, the activation energy (E_m) of PFSA membrane is about 15.57 kJ/mol (for both vapor saturated and liquid saturated conditions)[7]. By combining Equations (1) and (2), the total ohmic resistance can be decoupled to estimate the magnitude of the proton transport resistance through the membrane.

[7] S. Cleghorn, J. Kolde, and W. Liu, *Handbook of Fuel Cells-Fundamentals, Technology and Applications,* Vol. 3, 3, 566, W. Veilstich, A. Lamm, and H. A. Gasteiger (Eds), John Wiley & Sons, Ltd, Chichester (2003).

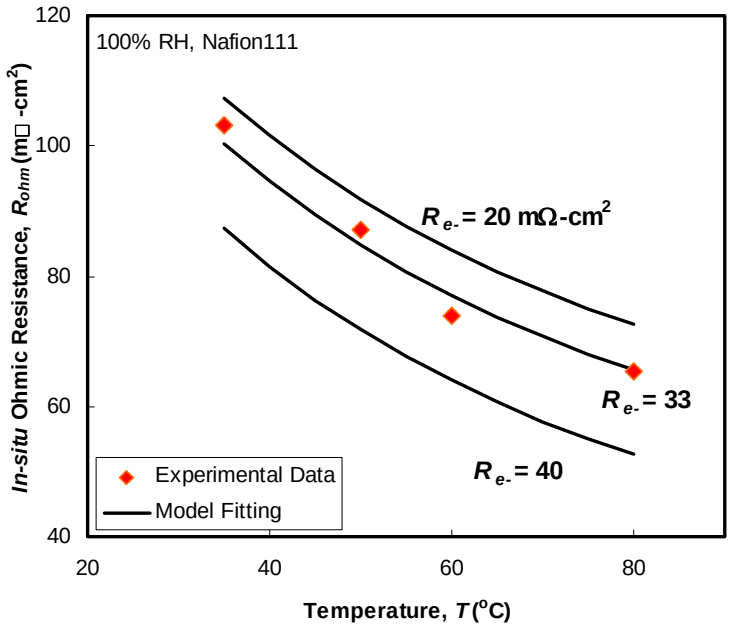

Figure 39. Demonstration of the parameter estimation steps to estimate the electronic resistance from hydrogen pump tests.

With the assumption that the limiting step of the proton transport through the membrane is identical for both *ex-situ* conductivity test and *in-situ* hydrogen pump test, the known activation energy, $E_{m,}$ from the *ex-situ* data can be applied to analyze the hydrogen pump results. The total ohmic resistance (R_{ohm}) measured from the hydrogen pump is plotted as a function of temperature (shown as red diamonds in Figure 39). Then the value of the electronic resistance (R_{e-}) is applied to have the same slope with the experimental data. When the 33 mohm-cm^2 is used for R_{e-}, the estimated membrane conductivity data from the hydrogen pump tests gives the same trend to the experimental results. Therefore, the estimated electronic resistance value becomes 33 mOhm-cm^2 for the fuel cell setup with the gas diffusion electrode used in this test. Then the membrane resistance at various temperatures can be calculated (membrane resistance = total ohmic resistance – 33 mOhm-cm^2).

As shown in this demonstration, the hydrogen pump technique constitutes an important *in-situ* diagnostic tool to evaluate the membrane and electronic resistance of the fuel cell. Moreover, the hydrogen pump technique can also be employed to determine the hydration status of a PEFC membrane under various operating conditions by comparing the obtained membrane conductivity data with *ex-situ* data at varying humidity conditions. This can provide important insights regarding the fuel cell water management and its sensitivity to the hydration condition of the membrane during operation.

Another way to estimate the membrane resistance in fuel cells is by comparing the ohmic resistance of membrane electrode assemblies (MEAs) with various membrane thicknesses. For this analysis a 25 μ and a 50 μ thick PFSA based membranes are used, and the measured ohmic resistances of the MEAs are compared to the areal resistances of the membranes measured by *ex-situ* conductivity in water at 70 ^{o}C. The results obtained both by the hydrogen pump tests and the current interruption techniques are shown in Figure 40.

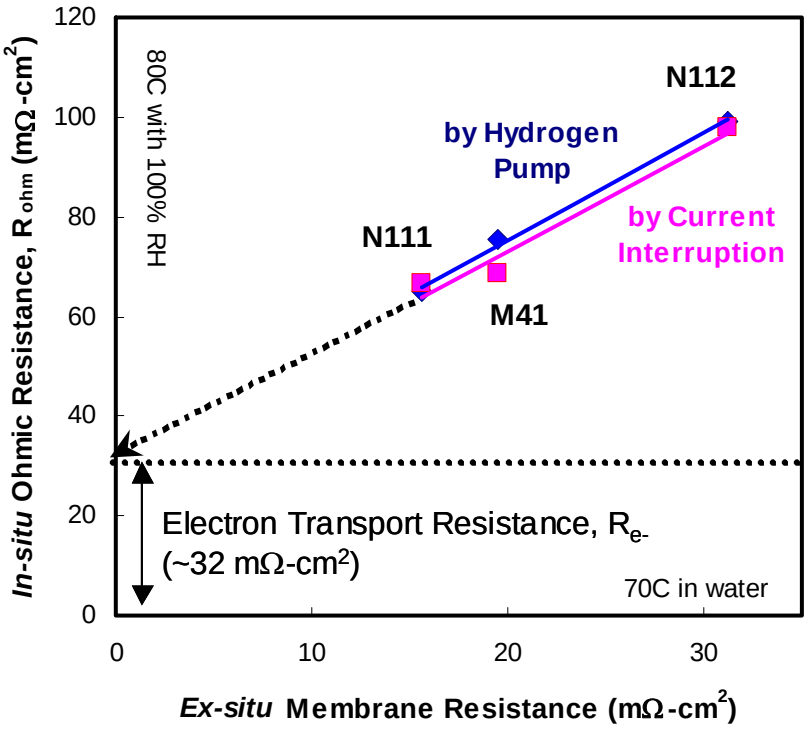

Figure 40. Effects of membrane thickness on the correlation between ex-situ membrane resistance and in-situ ohmic resistance.

Interestingly the intercept in the graph, which represents the electron transport resistance (R_{e-}) of the cell, was 32 mOhm-cm^2 practically identical to the electronic resistance estimated by the temperature study discussed above. This demonstrates that the proton transport resistance of membrane and the electron transport resistance of the cell can be successfully decoupled to quantitatively diagnose the membrane performance in operating fuel cells.

Figure 40 also shows the ohmic resistances of M41 membrane compared to the PFSA based membranes. As shown in the figure, the results are in line with the correlation obtained with PFSA membranes. This demonstrates that the sufficient interfacial contact has made between M41 membrane and the electrode without causing any additional performance losses in operating fuel cells.

8.4.2. Excursions at Higher Temperatures

M40 based MEA performance was tested after a one-hour excursion at 120ºC. As can be seen on Figure 41, the polarization curve measured at 80ºC after a one-hour temperature excursion at 120ºC was essentially unchanged.

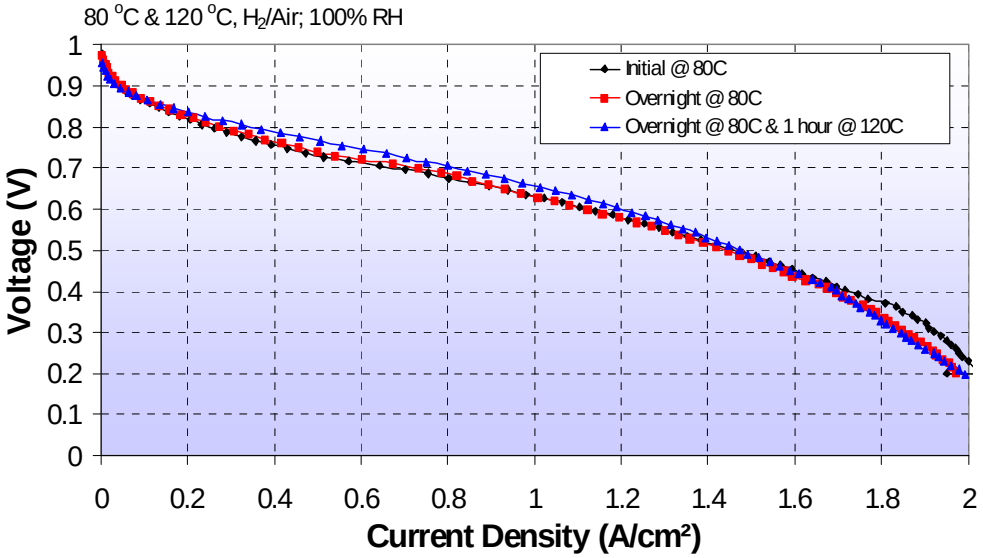

Figure 41: M40 Performance after excursion at 120ºC

The performance was further measured at 120ºC (see green squares on Figure 42). Because of equipment limitations, the relative humidity could not be properly measured at 120ºC but it was estimated to be around 20 to 25%. As can be seen, the performance remained quite good until 0.6 V before dropping significantly at lower voltages.

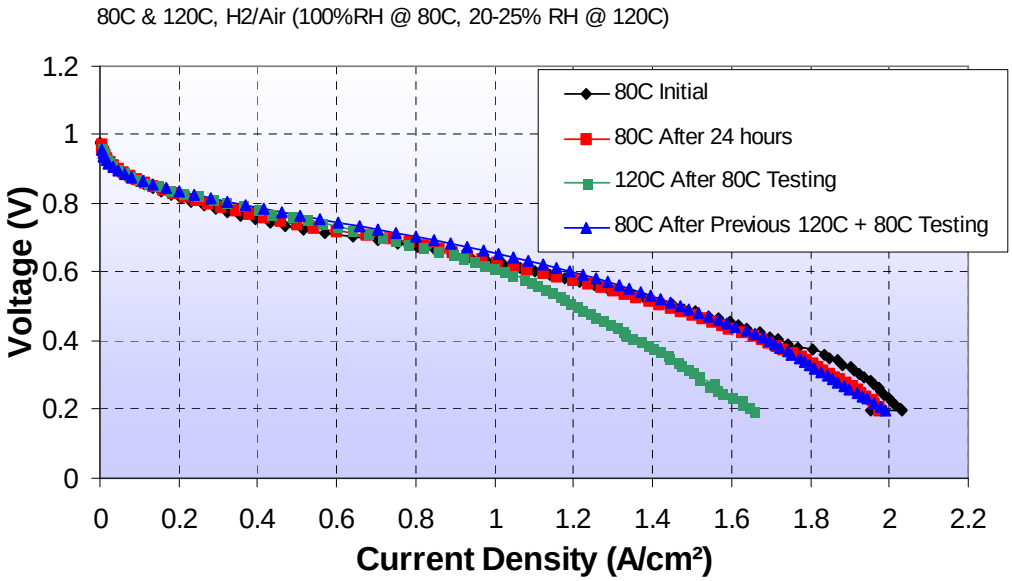

Figure 42: M40 Performance at 80ºC and 120ºC

While Arkema considered these results to be very preliminary, they show a considerable improvement vs. the previous generation (M31). They also suggest that the membrane/MEA could survive at least for short periods of time at elevated temperature.

A somewhat more detailed study was carried out with more advanced M41 membrane. M41 based MEAs were submitted to temperature excursions at 120ºC (130ºC dew point temperature) at 3 bars according the temperature cycle illustrated in Figure 43.

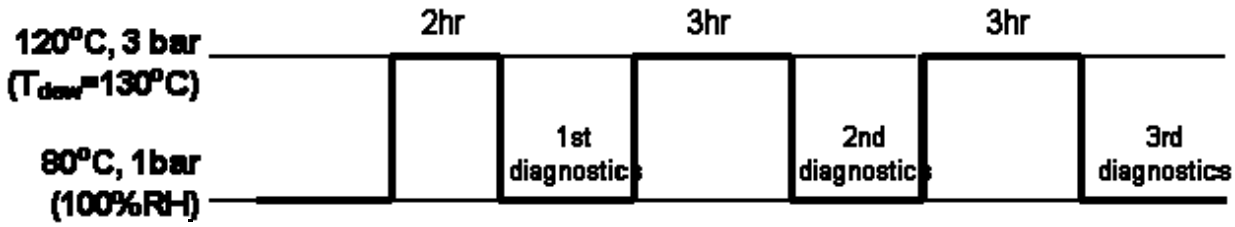

Figure 43: Short-term high-temperature test procedure.

Diagnostics were performed at 80ºC immediately after the high temperature excursion. The key results are plotted on Figure 44 below.

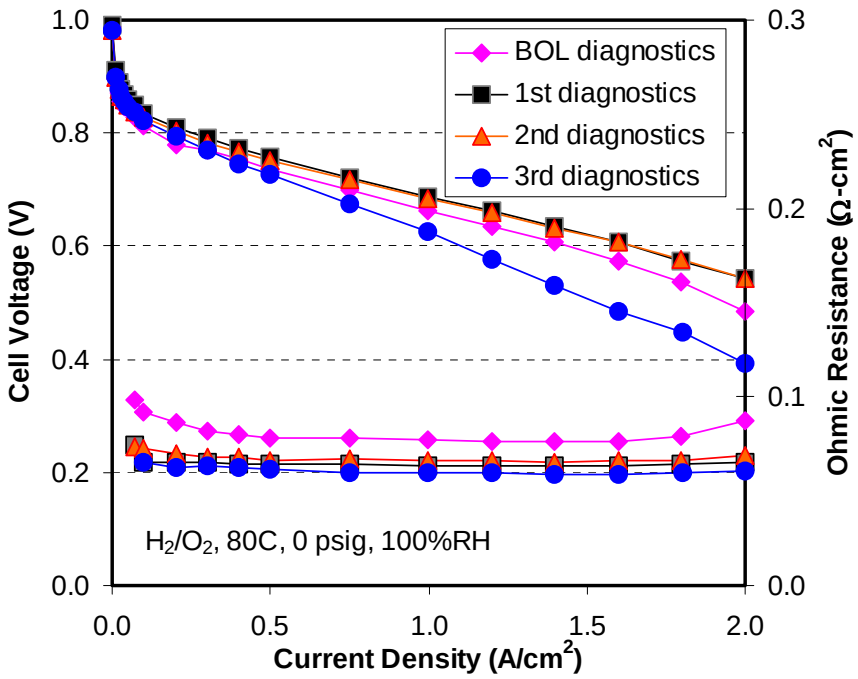

Figure 44: Polarization curves of the M41 membrane cell before, during and after the high temperature test.

As can be seen, there is no significant change in the oxygen polarization performance up to 5 hours at 120ºC. However, after 8 hours at 120ºC, a substantial decrease in performance is observed. The fact that there are no significant changes in ohmic resistance and no increase in hydrogen cross over, current density (see Figure 45) suggests that the membrane is still functioning properly. On the other hand, the increase in "oxygen gain" (the difference in oxygen vs. air performance) as shown on Figure 45 accompanied by a 20% loss electrochemical area (ECA) suggest instead that the electrode is degrading during this test.

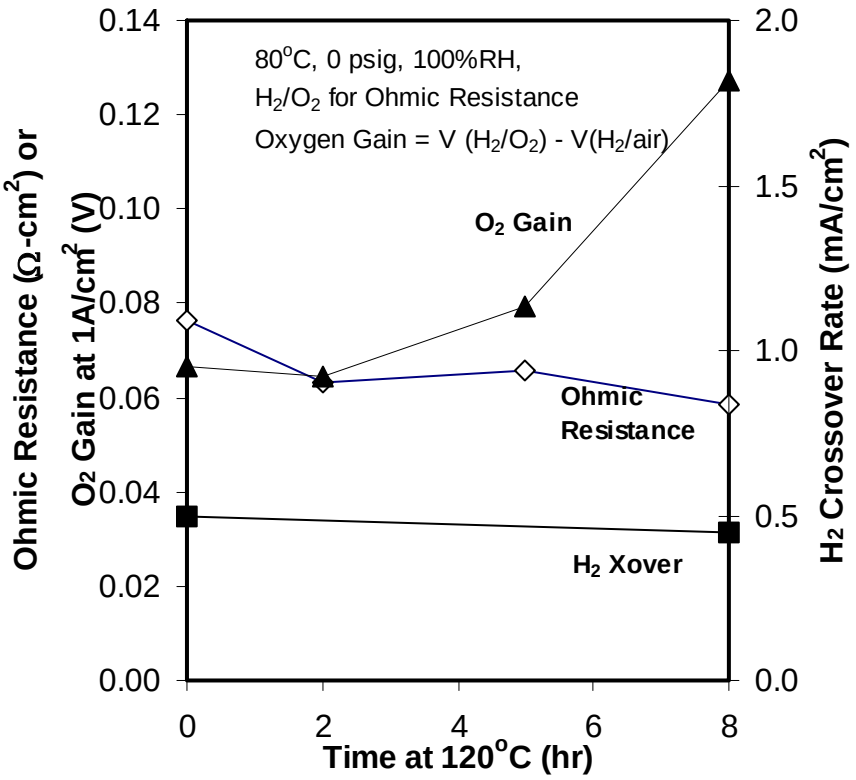

Figure 45: Changes of performance of the M41 cell during the high temperature test.

8.5 Durability Studies

8.5.1 Steady State Durability

A steady state test was carried out by Johnson Matthey Fuel Cells for a period of 950h. To probe for stability of the M-41 membrane, in-situ durability testing has been conducted in a 50cm^2 screener cell. The test protocol is described below (similar to testing for M-31 membrane):

- Steady state durability at 500 mA/cm^2 for MEA#W15467-1 (HiSPEC® 4200 cathode layer)
- MEA conditioned overnight or until stable voltage @ 500 mA/cm^2 with full humidification at 80 °C, stoic. 1.5/2.0 H2/air 100kpag pressure.
- Hold at 500 mA/cm^2 at 80 °C, H_2/air at 100/100 kPa, 100/100 %Rh A/C, 1.5/2.0 stoichiometry.
- BOL/EOL performance testing under H2/air, oxygen.
- Membrane failure detected by voltage decay rate and OCV decay rate.

- Total of 1000 hours of testing with BOL/EOL performance.

Ca. 950hrs of steady state durability testing (Figure 46, 500mA/cm^2, 80 °C 100%RHa/c 100kpag) has been completed at JMFC for M41 MEA with the modified HiSPEC® 4200 cathode (W15467-1). Performance testing has shown that MEAs made with the modified HiSPEC® 4200 cathode layer have helped in partially resolving the flooding issues compared to the JM standard layer.

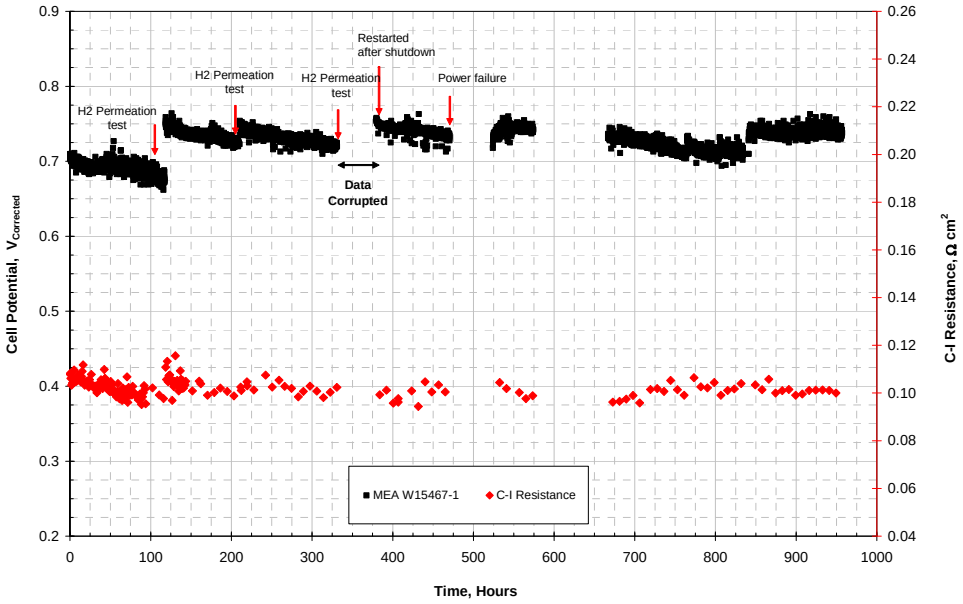

Figure 46: Steady state durability testing for the M41 MEA W15467-1 with modified HiSPEC® 4200 layer. (80°C, H_2/Air, 100/100 kPa abs., 100/100% RH, 1.5/2.0 stoichiometry at 500 mA/cm^2.)

It may be seen that no measurable decay in cell potential occurs over the test period for the MEA containing the M41 membrane. This positive result marks a clear improvement in the M41 membrane relative to the M31 case – for which a decay rate of approximately 485µV/hr was measured in June 2004 when tested under the same durability protocol. (The high CI resistance shown in both Figure 46 and 47 below are attributable to MEA test stand issues.)

Within the 500mA/cm^2 hold durability test, the OCV of the MEA was periodically assessed; the results are shown in Figure 47.

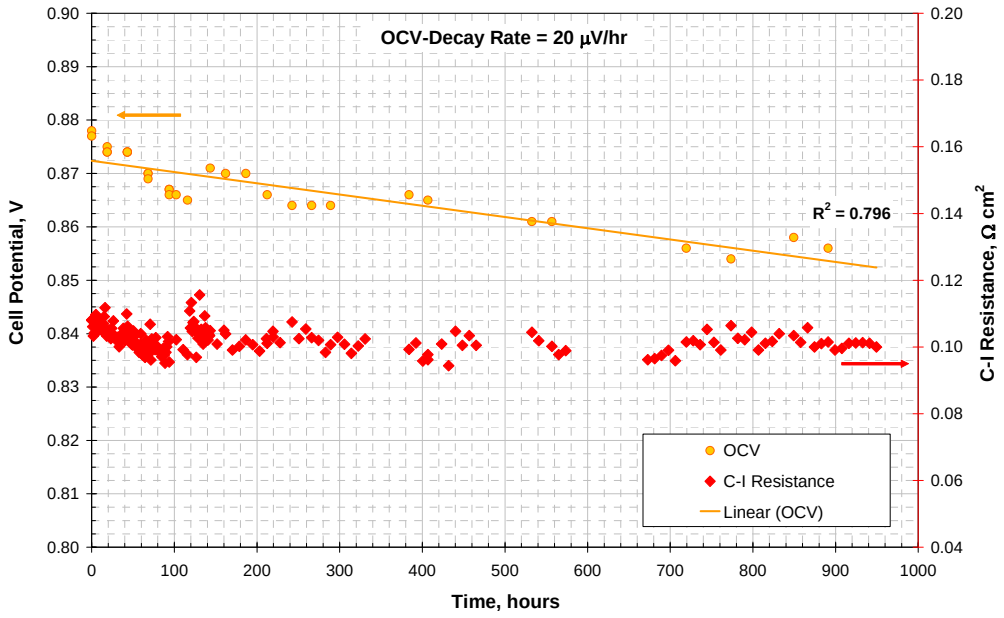

Figure 47: Change in OCV for MEA W15467-1 during steady state durability test. (80°C, H_2/Air, 100/100 kPa abs., 100/100% RH, 1.5/2.0 stoichiometry at 500 mA/cm^2.)

Over the 950-hour test time, a steady decrease in the OCV was observed with a low, average decay rate of 20µV/hr. For PFSA membranes, such a decrease in OCV is indicative of membrane thinning – increased levels of hydrogen pass through the membrane resulting in a mixed potential occurring on the cathode. It is possible that this process is also occurring in this steady-state test for M41.

The effect of the ~ 20mV in (1000 hours) loss on the operating MEA i.e. when a current is drawn, would be sufficiently small that no change in performance could be detected in the experimental noise of the data of Figure 46.

8.5.2 Accelerated Stability Studies

The accelerated tests performed at Arkema on M41 MEAs are aligned with the tests protocols defined thus far by DOE and the US Fuel Cell Council[8)].

8.5.2.1 Open Circuit Voltage (OCV) Hold Test

The chemical stability of the membrane and MEA is an important consideration. LaConti *et al.* proposed a mechanism of formation of hydrogen peroxide through the following sequence [9) 10)]:

[8)]US DOE Cell Component Accelerated Stress Test Protocols for PEM Fuel Cell, 2007.
[9)]LaConti, A.B. In ACS *Polymer Division Topical Workshop on Perfluorinated Ionomer Membranes*, Lake Buena Vista, FL, 1982.
[10)]LaConti, A.B.; Fragala, A.R.; Boyack, J.R. In Proceeding of the Symposium on Electrode Materials and Process for Energy Conversion and Storage; McInyre, J.D.E., Will, S.S.,G., Eds.; The Electrochemical Society, Inc.: Princeton, NJ 1977.

$$H_2 + Pt \rightarrow Pt - H \text{ (anode)}$$
$$Pt - H + O_2 \text{ (diffused from cathode)} \rightarrow HOO^{\bullet}$$
$$HOO^{\bullet} + Pt - H \rightarrow H_2O_2$$

Studies ex-situ of a fuel cell showed that PFSA membranes are very sensitive to peroxide and radical degradation. A recent review by R. Borup *et al.* provides a good overview on the subject. Initially, the Fenton test was often used as a first screening test. The reaction of hydrogen peroxide with a metal such as iron is well known to form the very reactive hydroxyl ($^{\bullet}OH$) and hydroperoxy ($HOO^{\bullet}$) radicals:

$$H_2O_2 + M^{2+} \rightarrow M^{3+} + OH^- + {}^{\bullet}OH$$
$${}^{\bullet}OH + H_2O_2 \rightarrow H_2O + HOO^{\bullet}$$

The development of the Open Circuit Voltage (OCV) Hold Test represents a useful contribution to a more realistic test, i.e. a test more representative of actual fuel cell conditions. Incidentally, UTC Power researchers showed that there was a very poor correlation between Fenton's test and OCV results in the case of hydrocarbon membranes[11)].

The protocol used by Arkema follows the DOE and US Fuel Cell Council test specifications. The test is run at 90°C and 30% RH on both the anode and cathode sides. Failure is determined by hydrogen cross over. The cell fails when the H_2 cross over currently exceeds 10mA/cm2 (for a 25cm^2 cell). Figure 48 features the data obtained with various M41 MEAs as well as Nafion NRE 211 (DuPont) and PFSA 111 from Ion Power. It can be seen that M41 clearly outperforms PFSA's in this test.

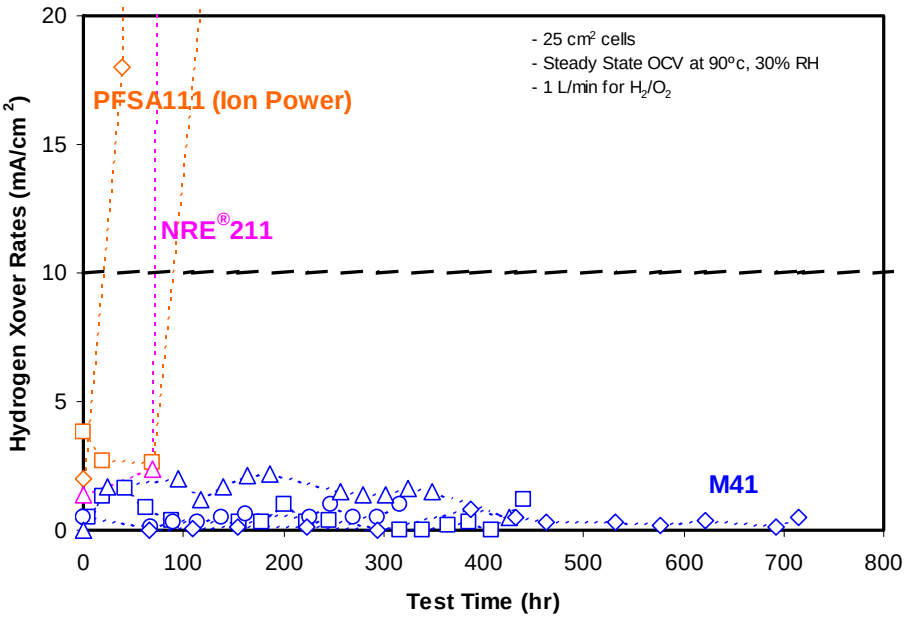

Figure 48: OCV Durability Test (Gas cross over)

[11)]Lesia Protsailio. *Development of High Temperature Membranes and Improved Cathodes.* 2006 DOE Hydrogen Program Review. Arlington, VA.

Figure 49 below shows the OCV plot. We found out that the result is affected by the electrical shorting of the MEA. Shorting actually decreases the OCV durability for both M41 and PFSA membranes. Our working hypothesis is that shorting may be induced by the surface roughness of the gas diffusion layer.

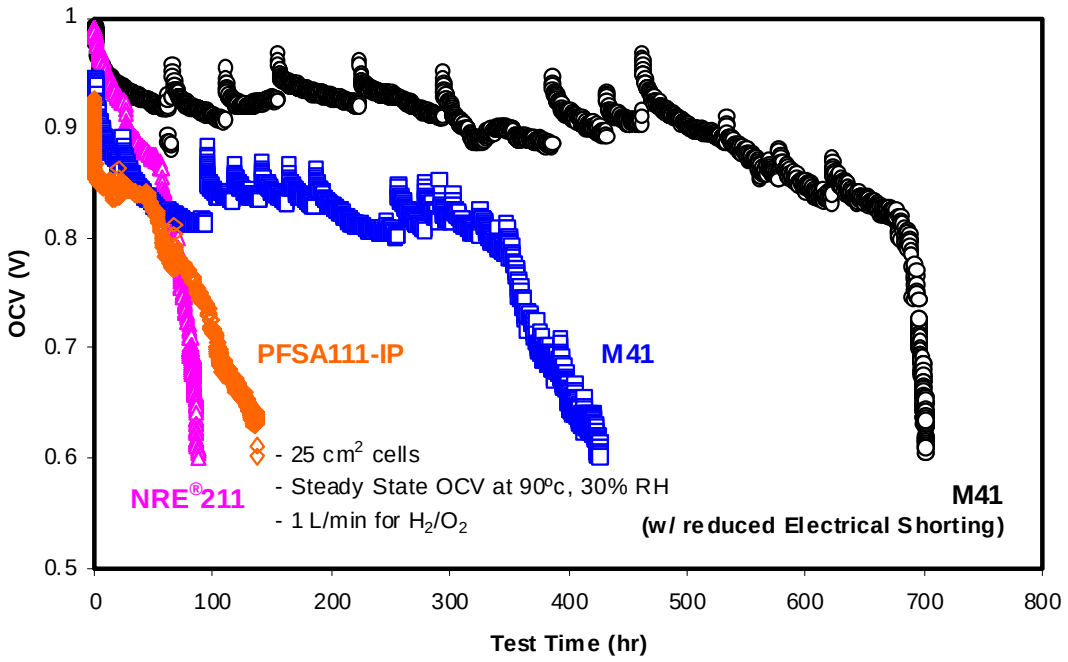

Figure 49: OCV Durability Test. Effect of Electrical Shorting

In order to better understand the degradation process during the OCV Hold Test, water effluents were analyzed by ion chromatography (IC). Fluoride and sulfate concentrations were measured in triplicate for better accuracy, and the results were compared to a typical fluoride and sulfate release rates of M41 membrane cells. This Nafion cell showed the highest fluoride emission rate among all tested to-date and is similar to the literature data. In addition, low sulfate release rates were observed for both M41 and Nafion membranes. This data further confirms the excellent chemical stability of M41 under these testing conditions. (See Figure 50)

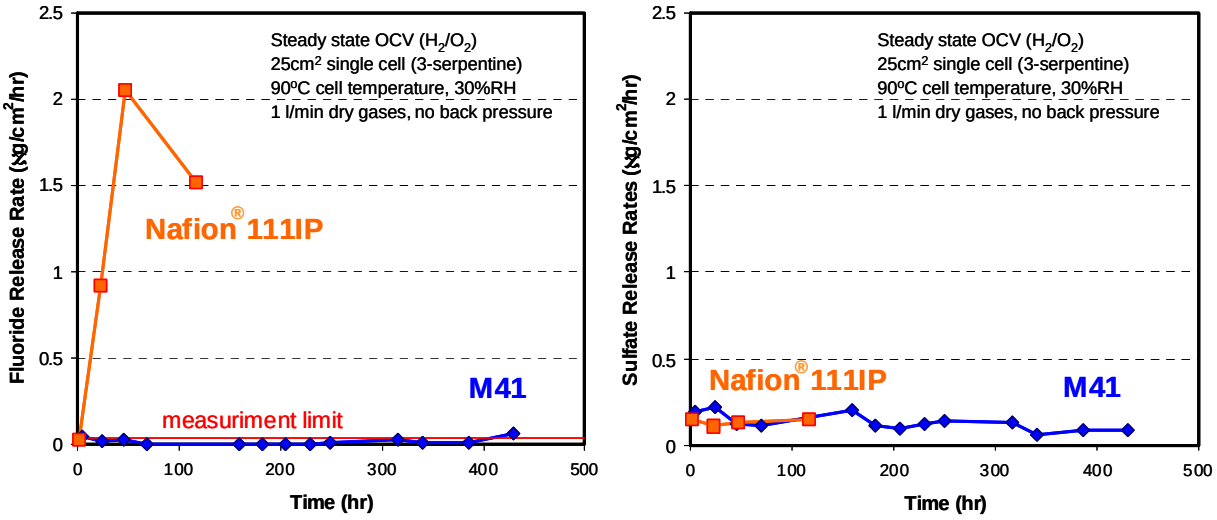

Figure 50: OCV Durability – Fluoride and Sulfate Release

Polarization curves at normal operating conditions were compared for the Nafion MEA before and after OCV durability testing. Much lower OCV values are shown in the end-of-life polarization curve due to high crossover and shorting. Electrode degradation is also observed with H_2/air performance. However, no significant degradation of membrane resistance (ohmic resistance) was observed although IC results are indicative of fluorine and sulfur losses. This would indicate that localized pinhole-type failure is occurring rather than gradual thinning of membrane.

A polarization curve at normal operating conditions were taken after the OCV durability test. As seen in Figure 51, the OCV has decreased. However, no significant degradation of membrane resistance (ohmic resistance) was observed.

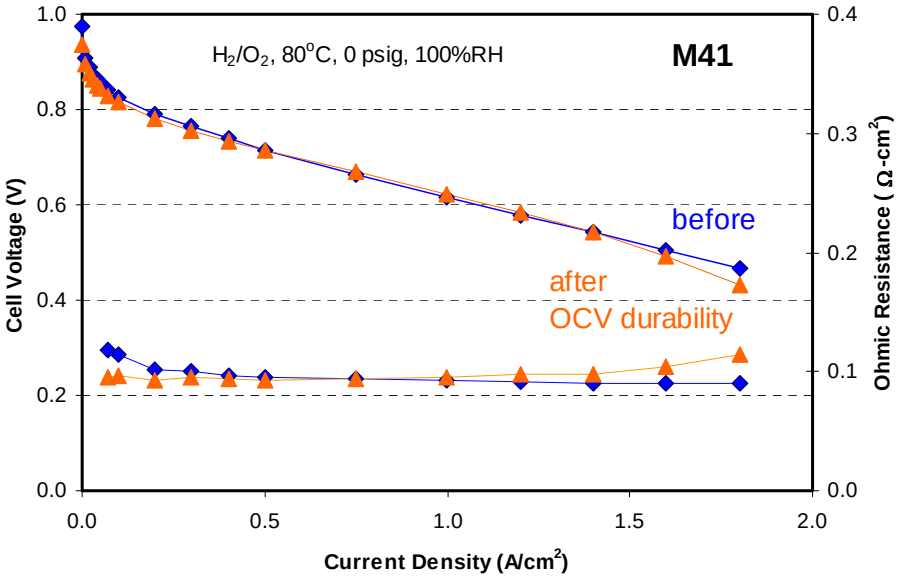

Figure 51: Polarization curves before and after OCV Hold Test.

8.5.2.2 *Relative Humidity Durability Test*

The relative humidity cycling test is a purely mechanical test. It relates to the relative humidity associated with transitions between high and low power in a fuel cell. It can be seen as a fatigue test as the membrane swells when exposed to high RH conditions and shrinks at low RH. The test is further accelerated as the conditions oscillate between the two extremes: fully dry and saturation.

Several sets of RH cycling tests have been completed using a Bekktech stand. We are using the DOE protocol (draft) cycle: 2 min. @ 0% RH followed by 2 min. @ "150%" RH [8]. However, because of equipment limitations we are currently using 25 cm^2 (instead of 50 cm^2 specified in the test protocol). Failure is determined as the point when hydrogen cross over exceeds 5 ml/min. The DOE target is >20,000 cycles.

With the permission of GM[12], we are reproducing their first results. (See figure 52 below.) It shows that PFSA 111 from Ion Power (noted Nafion® N111-IP) passes the test while Nafion® NR-111 (from DuPont) fails around 5,000 cycles. M41 membrane (noted Arkema 12605-121C) failed around 3,000 cycles in the equipment at GM.

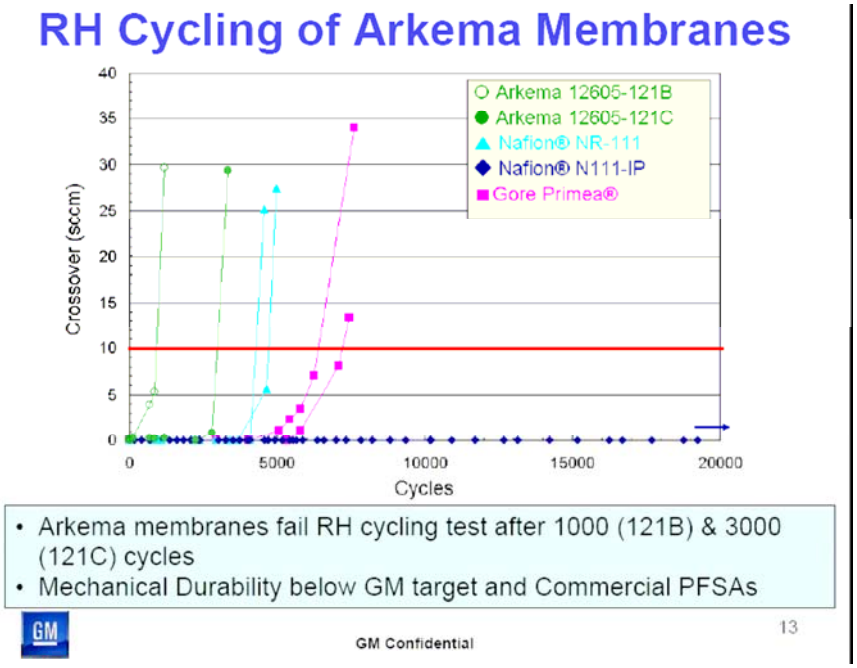

Figure 52: GM Relative Humidity Cycling Test

In our hands, we were indeed able to reproduce the fact that the PFSA 111 membrane from Ion Power passed the test while the Nafion NRE 211 membrane failed around 6,000-8,000 cycles.

---

[12]C. Gittleman e-mail to M. Foure – July 19, 2007.

On the other hand, the M41 MEA built at Arkema reproducibly passed the 20,000 cycles test: in one case, the experiment was voluntarily stopped at 20,000 cycles and in another, the test was pursued to failure which occurred at 26,000 cycles as shown on Figure 53 below.

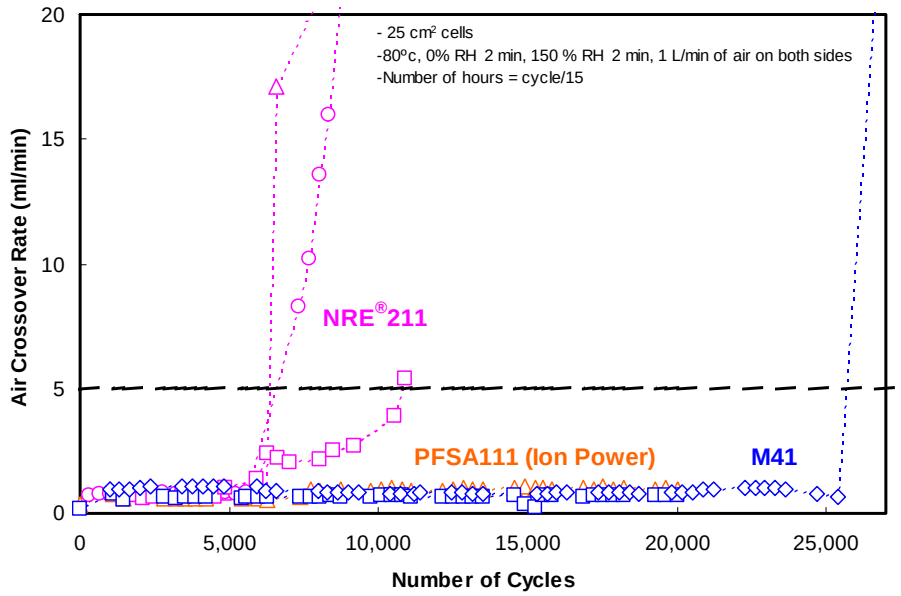

Figure 53: Arkema Relative Humidity Cycle Test (PFSA 111 from Ion Power, Nafion NRE 211 and M41)

These results are obviously different from those obtained by GM with M41. We are investigating two plausible explanations:

- The M41 MEA tested by GM was built by GM. However, we know that the Arkema membranes require a very different assembly process than PFSA membranes. Thus, it is possible that the M41 MEA tested by GM was damaged during its preparation.
- The other differences have to do with the MEA size and bipolar plates flow channel. GM used a 50 cm^2 cell with single flow channels while Arkema uses 25 cm^2 MEAs with triple flow channels.

To clarify this point, Arkema will reproduce the GM data with their exact configuration.

8.5.2.3. Voltage Cycling Test

A fuel cell will undergo many rapid fluctuations in load over the course of its life time. This is particularly true in the case of automotive applications. The fuel cell potential will typically vary between 0.6 and 1.0V. The voltage cycling test is aiming at assessing the durability of the MEA under such conditions. While a standardized protocol is still being developed, we used the following conditions:

- 25cm^2 cell
- 90ºC, 50% RH

- 1 min. @ OCV followed by 1 min. @ 0.4V.

Cell voltage, current density and hydrogen crossover are monitored as a function of time (i.e number of cycles).

A typical plot is shown in Figure 54 below. It shows that the M41 Mea outperforms the PFSA 111 MEA by a factor ~ 4 to 5.

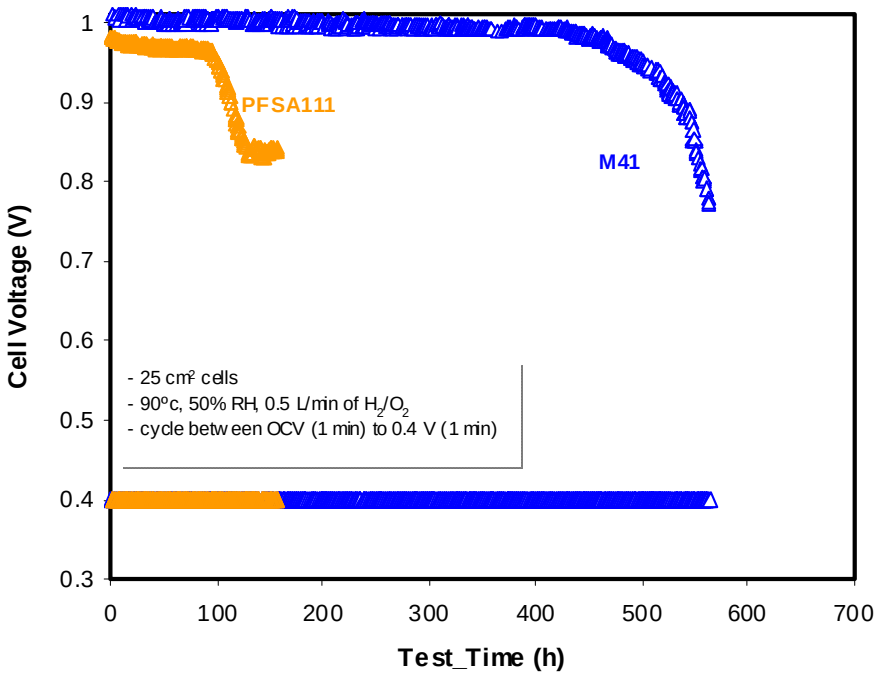

Figure 54: Voltage Cycling Test

However, if we examine Figure 54 where the current density provided by cell is plotted (right hand scale), we can see that the current drawn from the M41 MEA is about ¼ of that of the PFSA 11 MEA under these conditions. This is related to the fact that relative humidity is kept at 50% and the M41 MEA performance is suffering. Taking this observation into consideration, one might ask whether the M41 durability in this test is an artifact since the current density is limited. Overall, if we integrate the quantity of coulombs over the duration of the test, we can see that they are about the same for both MEA constructions.

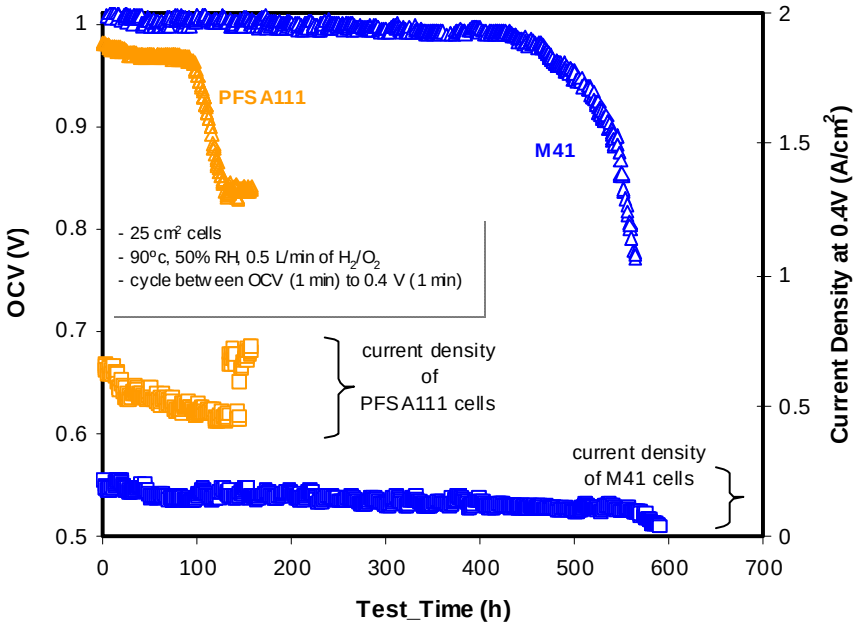

Figure 55: Voltage Cycling Test

In order to attempt to resolve this issue, we imposed to the current density at 0.1 A/cm^2 in the case of the PFSA111 cell. In this case, the PFSA111 cell oscillates between OCV and about 0.7V (see figure 55), but both cells operate at ~0.1 A/cm^2 within the experimental limitations of the test stand. As can be seen on Figure 56, this does not change the overall results of the test: M41 still appears to have a durability 4 to 5 times greater than PFSA111 in this test.

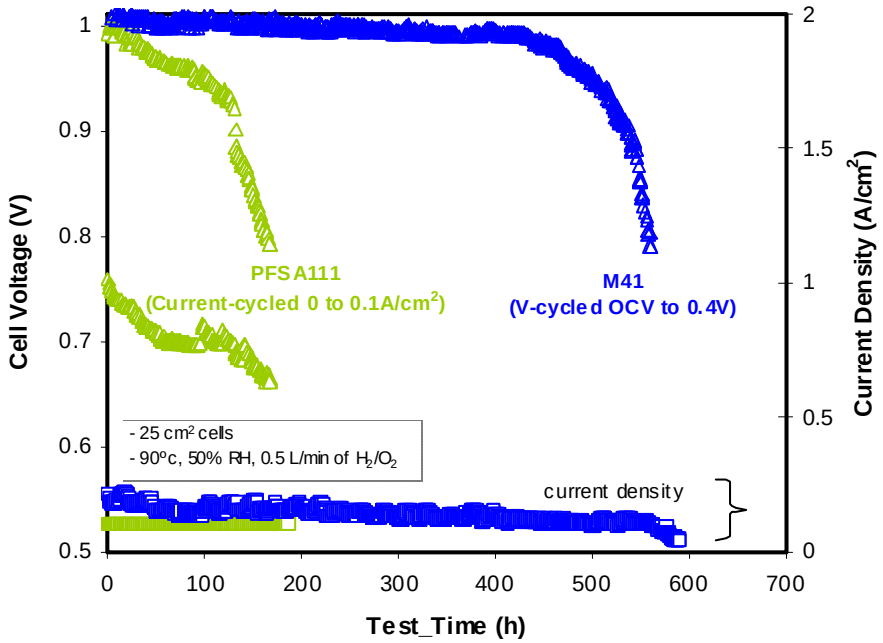

Figure 56: Voltage Cycling Test: Comparison of M41 and PFSA111 with similar current density ranges.

Finally, we plotted the hydrogen crossover rates at a function of time of time for the various experiments that we ran (3 PFSA111 cells and 3 M41 cells). The plot shows are same trends. The failure (H_2 crossover rate of 10 mA/cm^2 by definition) time appears to be ~ 4 to 5 times greater for M41 than for PFSA111.

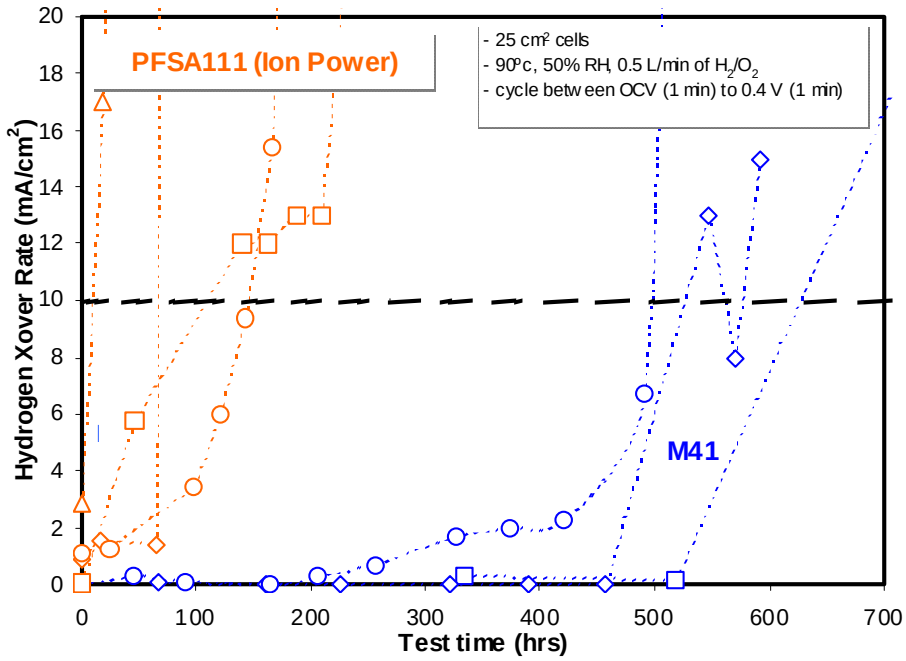

Figure 57: Voltage Cycle Durability: hydrogen crossover.

IV. Georgia Tech Final Report

EXECUTIVE SUMMARY

Activities may be summarized as falling within two categories : (1) Technology development for rapid or high-throughput measurement and (2) screening of formulations for PEMs. In measurement technology, the Georgia Tech team developed two new high-throughput screens, an ionic conductivity measurement and a water permeation measurement with expansion capability for water + gas (e.g., fuel) permeation. In a third technology area, we developed a methodology for gradient-blending of the complex PEM formulations. Using this newly developed instrumentation, we screened a large matrix of composition combinations for 2 types of polyelectrolyte (sulfoethylmethacrylate-type) blended with 5 types of Kynar resin. This set included 10 combinations of structure multiplied by 8 combinations of composition PE/Kynar each, and a temperature-dependent annealing study performed for 4 of the compositions. In addition, detailed measurements of conductivity as a function of humidity were performed for 5 selected systems. The results indicated the wide breadth of conductivities possible from these approximately 2000 combinations of conditions (including duplicates and controls for statistical repeatability), and identified optimal conductivity compositions.

Overall this was a successful project, in that the originally planned series of blends was screened reproducibly. In addition, two new measurement technologies have been produced, and the existing composition-gradient procedure was expanded considerably. In the course of the project, important limitations of high-throughput screening were also identified, especially with respect to conductivity screening and permeation screening. These will be detailed below.

DETAILED REPORT

1. Technology Development

The purpose of high-throughput screening must be kept in mind, since the objectives are often quite different than conventional 'detailed' scientific measurements. In general, the goal of HTS is to identify trends and outliers efficiently, while accepting some sacrifice of accuracy. In addition, miniaturization of samples and instrumentation is often beneficial, in order to reduce the burden of sample preparation for the HTS tests. Hence, a side-benefit of HTS is usually reduced usage of preparatory solvents and materials (on a per sample basis). One can consider HTS methods as falling within two broad categories:

- Series Measurement Techniques, such as our conductivity and mechanical tests
  - small "per-spot" measurement times (minutes)
  - 1 complex, expensive sensor

- Parallel Measurement Techniques, such as our permeability test
  - long measurement times (hours, days)
  - many inexpensive sensors

1.1 High-Throughput Conductivity Screen.

Detailed descriptions of this instrument's development have been presented in previous quarterly reports.

1.2 High-Throughput Permeation Screen.

Detailed descriptions of this instrument have also been given previously.

1.3 Gradient Combinatorial Libraries for Complex Mixtures

Our original gradient coating process was based on creating a time-dependent linear composition gradient in a batch mixer, sampling this gradient mixture and depositing it on a substrate for knife-edge coating. For a number of reasons, but primarily the viscosity difference between Kynar and PE solutions, this process was not successful for PEM fabrication. About ½-way through the project, the Ga Tech team decided to develop a new type of composition gradient mixing process, termed direct gradient coating. The three key experimental developments were (1) the use of pumps that allow continuous linear increment or decrement in flowrate to feed each component solution, (2) switching from batch to a continuous-flow dynamic mixing apparatus, which mixes the input streams to produce an outlet stream that varies continuously in composition. (3) A new type of coating blade, termed a ***chambered blade***, was fabricated to spread the time-varying stream evenly over the knife-edge for coating. This blade, pictured below, has channel widths designed to equalize pressure drop (viscous losses) as the flow branches out. (This is actually a design from nature as it borrows the concept from the naturally-occurring branching of blood vessels in animals.)

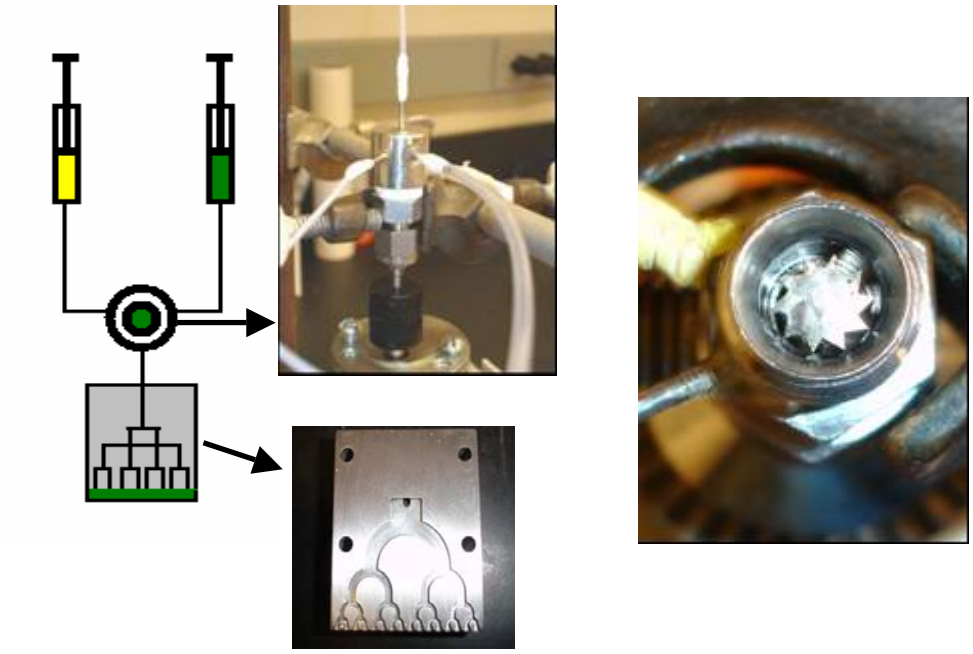

The new apparatus presented new challenges due to the continuously varying input stream flowrates and the static volume within the mixer, which produces an "averaging" effect due to the finite residence time. Hence, input flowrates cannot be programmed intuitively based upon an ideal zero-volume approach. The result is illustrated in the figure below. The desired result was a gradient in PE composition from 20 % to 80 % by mass. Clearly the result was far from this target. This challenge was solved by developing a model of the transient mixing process, and using the model to predict the input ramped flowrate profiles needed to produce the desired gradient. An example of

this is given in the figure below (bottom) for a ‘simplified’ blend system (PMMA + PEO cast from 1 % mass CHCl3 solution).

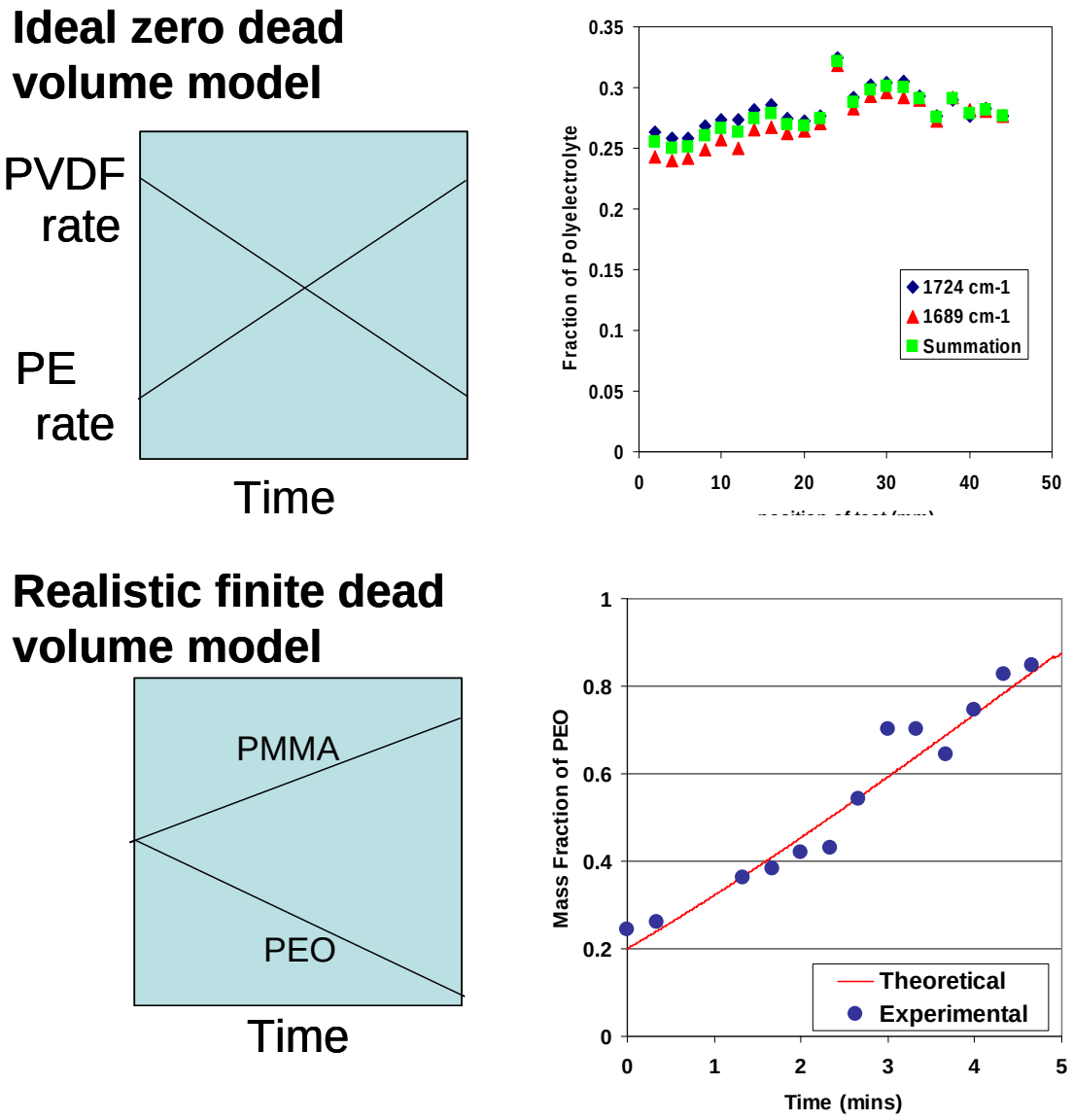

Composition gradients for Kynar-PE (top) with flowrate based on a zero dead volume mixer and for PMMA-PEO (bottom) using a realistic finite dead volume (310 μL) model.

Finally, gradient coating of PE-Kynar formulations in N-methylpyrrolidone lead to linear gradients with the desired slope. However, the intercept (starting) value is too high. The figure below provides data to illustrate this concept. The target gradient from 0.2 to 0.8 mass fraction PE is shown as a line. A linear composition spread is observed, but the mass fraction of the PE was always observed to be higher (~0.4) than the expected mass fraction of 0.2. In addition there is considerable scatter in the compositions. We believe both of these undesirable effects are due to the viscosity differences between the two feed solutions. The mixer is initially charged with 80:20 ratio

of the Kynar-PE. There is likely some breakthrough of low viscosity PE solution (~10 cP relative to >100cP for Kynar solution) into the outlet stream, bypassing the mixing zone.

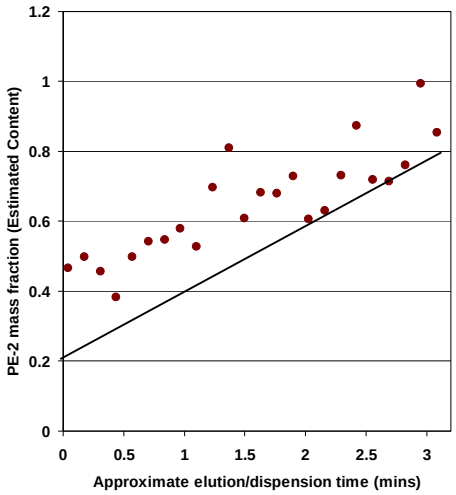

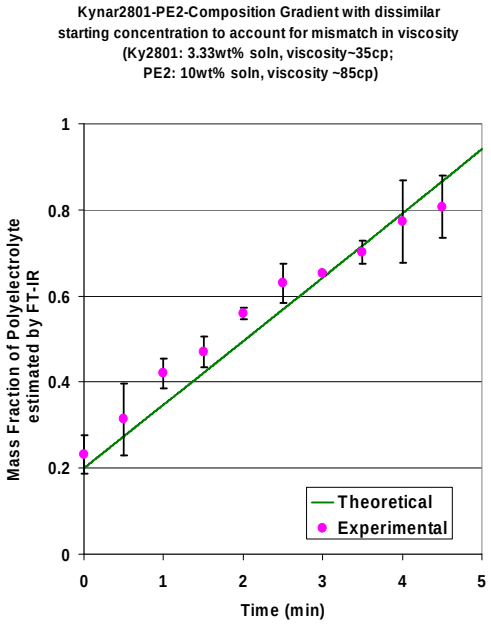

2. Screening Results

2.1 Overview of MATRIX

The table on the following page illustrates all conditions at which screening measurements were performed. This is presented as a summary guide to data available in the database that has been created to contain all results from this study. Temperatures in the table refer to annealing temperatures for conductivity studies.

PEM Matrix		POLYELECTROLYTE			
		PE-1		PE-2	
KYNAR	Kynar - 2801 (KY - 1)	25 °C	20% - 25 °C	25 °C	20% - 25 °C
		50 °C	25% - 25 °C	50 °C	25% - 25 °C
		70 °C	30% - 25 °C	70 °C	30% - 25 °C
		90 °C	35% - 25 °C	90 °C	35% - 25 °C
		115 °C	40% - 25 °C	115 °C	40% - 25 °C
		135 °C	45% - 25 °C	135 °C	45% - 25 °C
			50% - 25 °C		50% - 25 °C
			55% - 25 °C		55% - 25 °C
			60% - 25 °C		60% - 25 °C
	Kynar - 500 (KY - 2)	25 °C	20% - 25 °C	25 °C	20% - 25 °C
		50 °C	25% - 25 °C	50 °C	25% - 25 °C
		70 °C	30% - 25 °C	70 °C	30% - 25 °C
		90 °C	35% - 25 °C	90 °C	35% - 25 °C
		115 °C	40% - 25 °C	115 °C	40% - 25 °C
		135 °C	45% - 25 °C	135 °C	45% - 25 °C
			50% - 25 °C		50% - 25 °C
			55% - 25 °C		55% - 25 °C
			60% - 25 °C		60% - 25 °C
	Kynar - 2851 (KY - 3)	25 °C	20% - 25 °C	25 °C	20% - 25 °C
		50 °C	25% - 25 °C	50 °C	25% - 25 °C
		70 °C	30% - 25 °C	70 °C	30% - 25 °C
		90 °C	35% - 25 °C	90 °C	35% - 25 °C
		115 °C	40% - 25 °C	115 °C	40% - 25 °C
		135 °C	45% - 25 °C	135 °C	45% - 25 °C
			50% - 25 °C		50% - 25 °C
			55% - 25 °C		55% - 25 °C
			60% - 25 °C		60% - 25 °C
	Kynar - 731 (KY - 4)	25 °C	20% - 25 °C	25 °C	20% - 25 °C
		50 °C	25% - 25 °C	50 °C	25% - 25 °C
		70 °C	30% - 25 °C	70 °C	30% - 25 °C
		90 °C	35% - 25 °C	90 °C	35% - 25 °C
		115 °C	40% - 25 °C	115 °C	40% - 25 °C
		135 °C	45% - 25 °C	135 °C	45% - 25 °C
			50% - 25 °C		50% - 25 °C
			55% - 25 °C		55% - 25 °C
			60% - 25 °C		60% - 25 °C
	Kynar - 2821 (KY - 5)	25 °C	20% - 25 °C	25 °C	20% - 25 °C
		50 °C	25% - 25 °C	50 °C	25% - 25 °C
		70 °C	30% - 25 °C	70 °C	30% - 25 °C
		90 °C	35% - 25 °C	90 °C	35% - 25 °C
		115 °C	40% - 25 °C	115 °C	40% - 25 °C
		135 °C	45% - 25 °C	135 °C	45% - 25 °C
			50% - 25 °C		50% - 25 °C
			55% - 25 °C		55% - 25 °C
			60% - 25 °C		60% - 25 °C

2.2 Conductivity

2.2.1 Composition dependence. Below, the primary composition-dependence of conductivity is presented as a function of Kynar type and PE mass fraction for both PE1 and PE2. In all cases, conductivity increases as expected with PE fraction. In addition PE2 yields higher s values for a broader range of Kynar types and compositions, as expected due to its structure (has lowest equivalent weight). An interesting local maximum is observed in a number of the samples close to 35 % PE. This is close to the optimal PE content discovered by KOP.

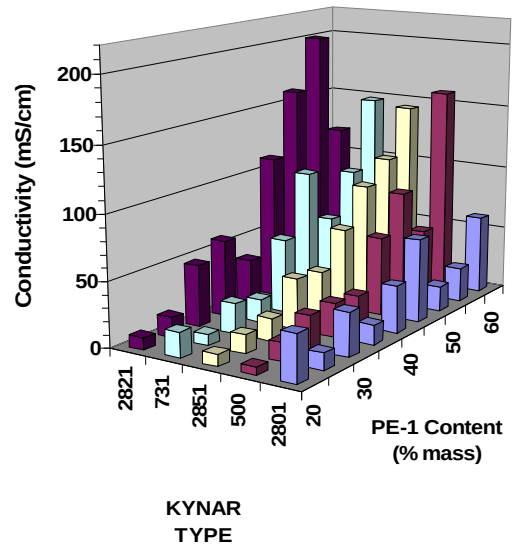

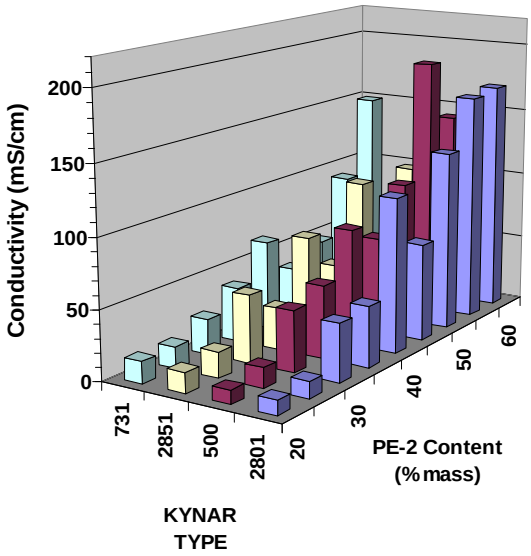

2.2.2 Annealing dependence. The figure below presents an overview of the effect of a two-hour anneal on PEM formulations blended with PE2. There is an initial decrease in conductivity with increasing anneal T (the conductivity is measured at room T). A minimum occurs near 90 ºC, followed by an increase again. Further increases in T up to 135 ºC do not increase conductivity further. These results, while of academic interest, indicate that there is little to be gained by adding an annealing step. On the other hand, the results also indicate potential structural rearrangements with temperature during fuel cell operation.

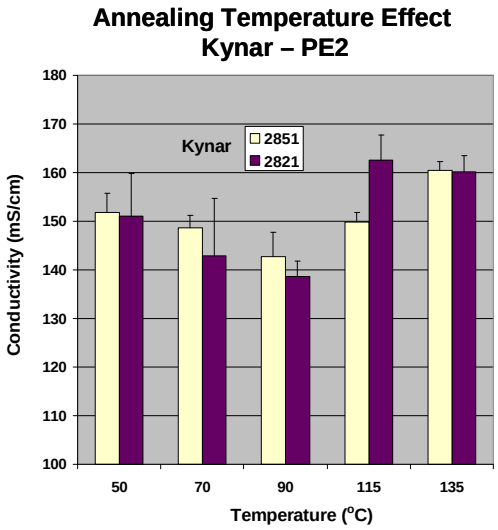

2.2.3 Humidity dependence. The figure below presents typical results obtained for a humidity-exposure series of measurements. The entire conductivity apparatus is enclosed in an acrylic cabinet, and relative humidity is ramped in steps, each followed by 30 minute equilibration period and a conductivity measurement. Conductivity is measured on the same position for each humidity.

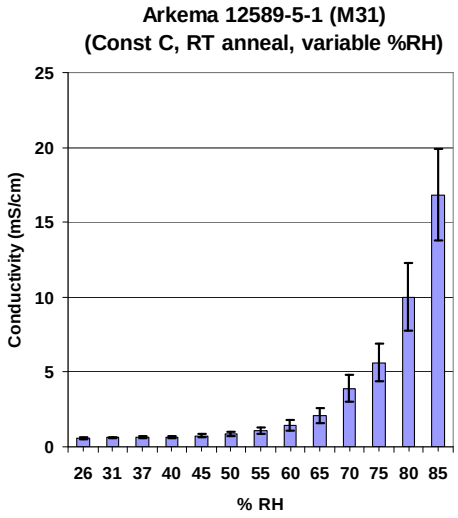

2.3 Permeability

The parallel-cell permeation screening system (pictured below) has been instrumented for a 4x4 array of sensors. One of the most significant findings is that water diffusivities in membranes can be measured using either vapor (steam) or liquid sources. There is good reason, however, to utilize liquid water in order to increase the throughput and repeatability of the screening.

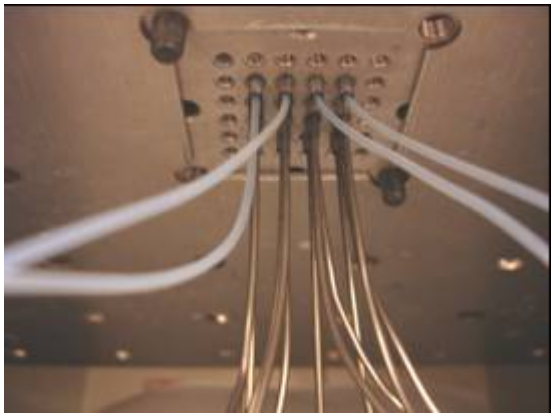

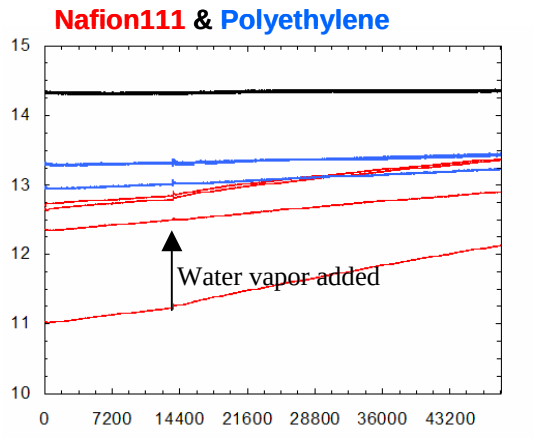

At the left, the figure illustrates raw data (time, s) versus pressure (psig) for water vapor at room temperature diffusing through Nafion111 and polyethylene. Note the clear distinction between the slopes of the red (Nafion) vs. blue (polyethylene) lines, especially after the addition of water vapor to a nominally dry atmosphere.

The next figure below shows the response of two different Kynar-PE blends to the addition of water droplets. A quick pressure drop (thought to be due to capillary action as the water penetrates the membrane) is followed by the vaporization of water from the membrane surface to fill the chamber at the liquid's saturation pressure. In both figures the black line represents the oven's overall pressure.

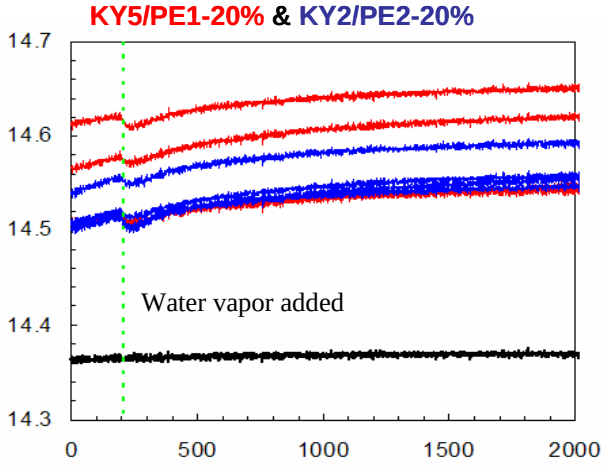

Below the two figures show typical vapor (left) and liquid (right) data transformed from pressure to M(t) / M_∞ (mass sorbed at time t / mass sorbed at long times). As one can see, the curves give essentially equivalent results. The initial slope is taken as the 'short-time' diffusivity, which is about 5 x 10^{-9} cm^2/s in this case.

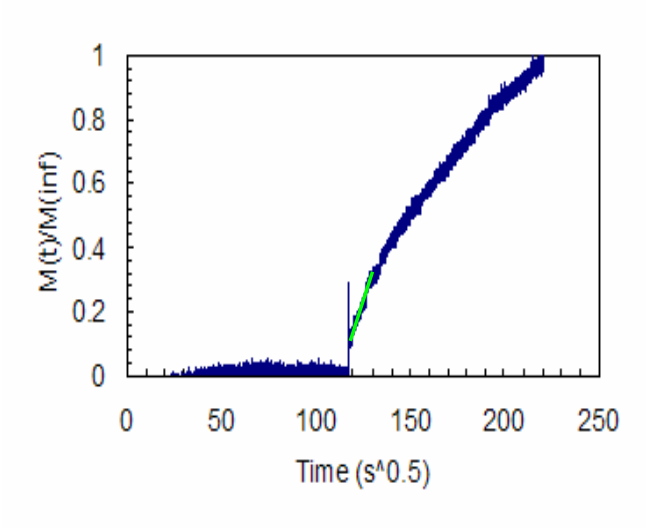

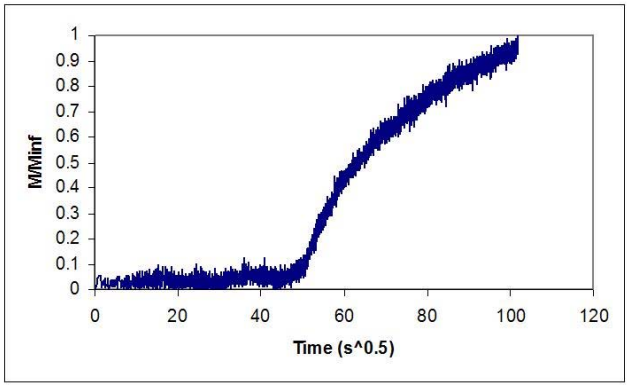

2.3.3 Mechanical

Mechanical data, recorded with the HTMECH, was collected for most of the matrix of samples. Overall, it was necessary to condition the membranes in a humid environment or by placing droplets of water on the HTMECH sample grid, prior to obtaining a satisfactory stress-strain profile. Otherwise the membranes were too brittle to obtain a result readable by our strain gauge. The stress strain data was largely unremarkable, exhibiting behavior typical of semi-interpenetrating network polymers.

V. Johnson Matthey Final Report

Task 2

Johnson Matthey Fuel Cell's role in this project was to develop a high performance membrane electrode assembly (MEA) utilizing Arkema's newly developed Kynar-based Semi Interpenetrated Network (SIPN) membranes. In order to realize the full potential of these materials, continuous optimization of both the MEA fabrication parameters and its constituents (e.g. catalysts and electrode architectures) was performed over the course of the three year project.

Within Task 2.1; "MEA Fabrication Development", a series of ex-situ membrane tests were conducted to provide an initial understanding of how the properties of the Kynar membranes compared to more conventional PEM materials. Specifically, mechanical methods such as Tensile Strength Testing, Thermo-Mechanical Analysis and Tear Resistance were employed for some of the initial membrane materials to obtain an understanding of the conditions that could be employed during MEA lamination. Once the general differences between these new materials and more conventional perfluorosulfonic acid (PFSA) membranes were understood, these tests were not continued. In addition, membranes were also subjected to Fenton's test to assess their chemical stability prior to use in operational test cells.

Under Task 2.2; "MEA Screening", MEAs containing Arkema membranes were assessed, correlating cell performance with MEA configuration variables. A high proportion of the MEA testing focused on the use of the M31 membrane for which parameters such as cell temperature and humidity were varied to obtain fuel cell performance and to understand the inherent properties of the membrane and their influence on cell behaviour (Task 2.2.1.) An extensive effort was then given to the optimization of the MEA electrodes, modifying the electrode layer structure, electrode fabrication method and choice of fuel cell catalyst such that the properties of the anode, cathode and membrane were more suitably matched. In particular, much attention was given to controlling the water management of the operating MEA. The learning obtained from these developments was applied to new variants of the Kynar SIPN membranes as they became available through the course of the program.

The in-situ stability of two membrane materials was assessed (Task 2.2.3) in steady state and accelerated open circuit voltage (OCV) durability protocols (>500 hours) which showed significant improvement in durability performance for the membranes developed through the course of this program. Additional diagnostic membrane testing (gas and water permeance) was finally conducted to help fully account for the MEA performances observed (Task 2.2.4).

Task 2.1: MEA Fabrication Development

The functionality of the proton exchange membrane comprises a variety of inter-related properties including mechanical strength, proton conduction, water uptake and permeability, gas impermeability and chemical stability. A series of ex-situ techniques was applied to measure these mechanical and chemical properties.

Task 2.1.1: Ex-Situ Mechanical Testing

Tensile Strength Testing
Tensile testing is used to determine the strength, ductility and stiffness of a material. The ultimate tensile strength and elongation of the membrane can be approached locally during fuel cell operation due to expansion and contraction during humidity cycles, thus tensile data was used to quantify the differences between membranes of varying composition and the effect of alternative processing methods. The material properties of the membrane are also important during processing and MEA manufacture.

Samples of membrane were cut from the machine and transverse directions of the roll and allowed to equilibrate for at least 24h at 23 ±1°C and 50 ±5% Rh prior to measurement of the membrane thickness and mechanical testing. The samples were tested at a strain rate of 50 mm/min (5 samples/direction). From the resulting tensile curves it was possible to determine the Ultimate Tensile Stress (UTS), Elongation and the Young's Modulus (E-mod), which is defined as the ratio of stress to strain when the material is behaving elastically.

The tensile stress data from some of the Arkema membranes assessed over the course of this project are shown in Figure 2.1, with data from a commercial PFSA membrane included for reference. Data shown as solid lines are from the transverse direction (horizontal) of the membrane and the corresponding data from the machine direction (vertical) are shown as dotted lines. This technique is capable of highlighting differences in mechanical properties between the machine and transverse directions of the membrane thereby indicating how the polymer chains are aligned. Within the datasets from the Arkema membranes, little difference is observed between the transverse and machine directions which suggest the membranes are isotropic in nature – typical of solution cast membranes. This behavior is clearly quite different from that exhibited by the commercial PFSA material in which the membrane properties vary significantly between the membrane orientation directions.

For all of the Arkema membranes, the initial elastic region of the tensile curve is steep in comparison to the commercial PFSA and leads to a distinct yield point (5 – 10% extension). After the yield point is exceeded, the tensile stress decreases by approximately 30% (strain softening) to a ductile plateau region in which the elongation continues to rise but the stress remains constant. This region, where extension occurs at constant stress ('cold drawing'), is attributed to molecular re-orientation. The presence of polyvinylidene fluoride (PVDF) in the Arkema membranes may facilitate slippage by disrupting a proportion of the hydrogen bonds. This ultimately results in increased stiffness and hence an increasing gradient of the stress-strain curve. Although initially linear, the tensile curve then continues to rise until the point of membrane failure.

In contrast, the tensile curve of the commercial PFSA membrane rises more slowly and does not suffer the same decrease in tensile strength after the yield point. The commercial membrane also does not exhibit a plateau region probably owing to the presence of the sulphonic acid side groups, whose presence reduces the potential for molecular re-orientation due to their physical size and intermolecular hydrogen bonding.

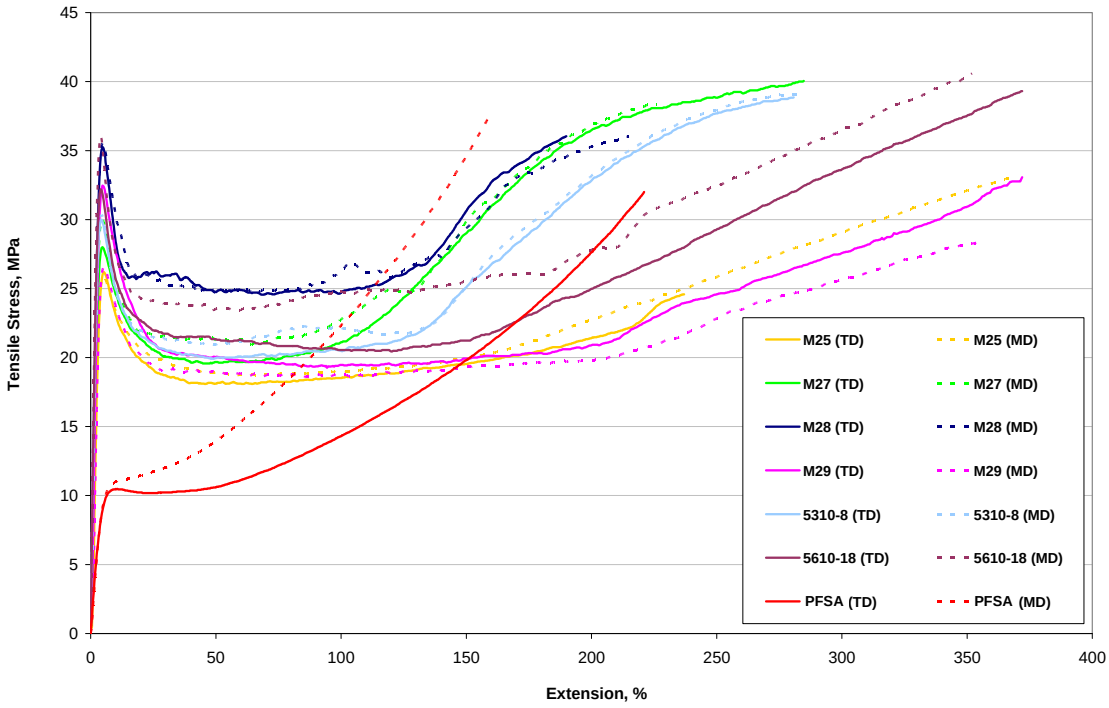

Figure 2.1: Tensile Stress Data of Arkema Membranes vs Commercial 30µm PFSA Membrane
(TD = Transverse direction, MD = Machine Direction)

Table 2.1: Summary of Tensile Strength Data

Sample	Direction	UTS (MPa) Average	UE (%) Average	E-mod (MPa) Average
M25	MD	30	324	930
M25	TD	30	348	956
M27	MD	37	211	1129
M27	TD	38	250	1059
M28	MD	37	197	1280
M28	TD	35	185	1209
M29	MD	28	266	862
M29	TD	32	347	1062
5310-8	MD	37	241	1234
5310-8	TD	35	226	1250
M31 (5610-18)	MD	37	320	1350
M31 (5610-18)	TD	36	340	1232
M31 (2)	MD	27	279	1009
M31 (2)	TD	29	328	975
M36	MD	32	243	292
M36	TD	34	259	278
M38	MD	31	254	400
M38	TD	33	315	464
Commercial PFSA	MD	36	152	233
Commercial PFSA	TD	28	200	234

The results of tensile strength tests for Arkema membranes analysed are summarized in Table 2.1. All Arkema membranes show significantly higher Young's modulus (E-mod) (av. 850-1359 MPa) compared to the commercial PFSA (Av. 250 MPa) indicating higher stiffness in the elastic region. The E-mod is probably dominated by the PVDF component of the membrane (Kynar PVDF has an E-mod of approx 1700MPa). It should be noted that the UTS (Ultimate Tensile Strength) and UE (Ultimate Elongation) results differ from Arkema's own data that showed UTS values of 51MPa and 33MPa for M27 and M25 *cf.* JMFC's 37 and 30MPa respectively. From the results presented it is suggested that the differences observed are a function of the strain rate used. All JMFC results were recorded at a cross-head speed of 50 mm/min, to allow comparison with a wide range of previously tested materials, whereas Arkema used a cross head speed of 1000 mm/min. Clearly, the strain rates experienced in service are likely to be quite low, as they are induced by humidity and temperature changes.

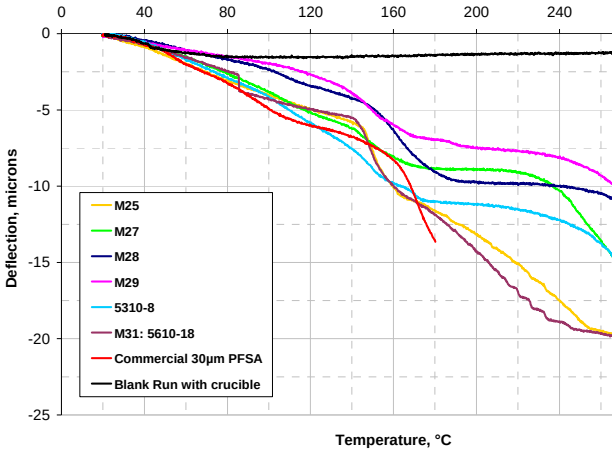

Thermo-Mechanical Analysis

The thermo-mechanical flow properties of membranes and polymers incorporated into the fuel cell were identified as important characteristics as they influence MEA fabrication conditions, thermal stability and operational durability of the MEA. Thermo-Mechanical Analysis (TMA) was used to differentiate between membranes fabricated with various ionomers and processed under different conditions. From the resulting

deflection/temperature curves, it was possible to infer potential lamination conditions, providing guidance into MEA fabrication for these novel membranes.

Using a thermo-mechanical analyzer, the sample was placed under a fixed, 80g load, and the position of a 5mm diameter hemispherical probe was monitored whilst the sample temperature was ramped from ambient to 300°C at 10°C/min under an inert gas (N_2 or He) blanket.

The TMA data from the Arkema membranes assessed using this protocol are shown in Figure 2.2 and summarized in Table 2.2. Curves derived using the TMA appear to separate the Arkema membranes into two groups. M27, M28, M29 and 5310-8 show a broad temperature range over which the membrane thins (~100°C to 170°C), followed by a plateau region extending to 220 to 240°C where there is little or no thickness change until a second softening point is observed.

M25 and M31 membranes show a sharp decrease in thickness between ~140°C and 170°C, followed by a gradual thinning of the film with increasing temperature; no plateau region was observed in either case which suggests more intricate mixing of the membrane components. The commercial PFSA is observed to soften at ~130°C with the onset of flow commencing at ~156°C; no end point was reached as the run was terminated at 180°C.

Table 2.2: Summary of data from TMA test of Arkema and commercial membranes

	Initial Thinning		Plateau		Second Thinning	
Sample	**Softening Point °C**	**Onset of Flow °C**	**Start °C**	**End °C**	**Softening Point °C**	**Onset of Flow °C**
M25	143	146	-	-	-	-
M27	142	142	173	217	217	233
M28	143	149	193	245	245	265
M29	112	134	166	237	237	249
5310-8	142	142	175	220	220	243
M31: 5610-18	141	144	-	-	-	-
Commercial PFSA	138	**160**	-	-	-	-

Since the temperature for the onset of flow for Arkema membranes is 15-25°C lower than that from the PFSA material, some modifications to the conventional MEA lamination conditions were judged necessary to prevent membrane flow into the catalyst layer and over-thinning of the membrane during fabrication.

Tear Resistance

The tear resistance of a membrane is of importance both during manufacture and fuel cell operation. If a membrane has a low tear resistance then small defects, either inherent in the membrane or generated during the MEA assembly process, can propagate, which can then lead to premature cell failure.

Table 2.3: Results of tear resistance test of Arkema and commercial membranes

Sample	Average Force (N/mm)
M27	4.39
M29	12.72
M31: 5610-18	5.92
M31 (2)	5.92
M36	4.40
M38	6.94
Commercial PFSA	**0.67**

Trouser-shaped samples of membrane were cut from the machine and transverse directions of the roll and allowed to equilibrate for at least 24 hours at 23 ±1°C and 50 ±5% Rh prior to testing. The samples were tested under ambient conditions at a strain rate of 200mm/min. From the resulting tensile curves the force required to propagate the tear was determined, which is typically expressed as Force (N)/mm membrane. The results of the tear resistance tests are shown in Table 2.3

The reference commercial PFSA membrane has a tear resistance of <1N/mm under standard conditions of temperature and humidity. All Arkema membranes show significantly higher tear resistances (4-12N/mm), which can probably be attributed to the PVDF content of the membrane; PVDF has a quoted tear resistance of 18.5N/mm. The higher tear resistance of the Arkema membranes is an important and advantageous feature in both MEA preparation and, particularly, in operation.

Task 2.1.2 Ex-Situ Chemical Stability

Peroxide Testing

Table 2.4: Chemical Stability Testing of Arkema & Commercial PFSA Membranes: Observations Following Fenton's Test

Membrane	Weight Loss	Visual Observations
Commercial PFSA 1	10%	Slightly wrinkled at edges
Commercial PFSA 1p	16%	Blistered, wrinkled, distorted
Commercial 2	7%	No visible change
Prototype A	14%	Wrinkled
Prototype B	17%	Samples broke up during immersion
M31: 5610-18	99%	Only residue remaining
M36 M38 M40:12605-27	> 99%	Complete dissolution of membrane

The chemical degradation of the PEM membrane in an operational fuel cell can result in the formation of pinholes within the membrane that allow excessive crossover of the reactants. Damage to this site is exacerbated by the exothermic combination of fuel and oxidant and ultimately leads to cell failure. It is generally accepted that attack by peroxide decomposition species, which are generated at low levels during fuel cell operation, is the primary chemical degradation mode of the membrane.[6] However, chemical PEM degradation generally occurs over a relatively slow rate during fuel cell operation (1000's of hours). Consequently, accelerated ex-situ test protocols have been developed to simulate chemical membrane degradation.

In the Fenton' test strips of membrane were cut, weighed and measured prior to placing in a solution of 5% v/v H_2O_2 / 5ppm Fe^{2+} solution. The samples were heated at 80°C for 96hrs – the peroxide solution was refreshed every 24 hours. The membranes were removed, rinsed, dried and left overnight under ambient conditions before being re-weighed, visually inspected and assessed for weight loss and change in mechanical properties.

The results of the application of a Fenton's test to the earlier Arkema membranes and commercial PFSA materials are summarised in Table 2.4. Observations show that all of the Arkema membranes

[6] "Mechanisms of Membrane Degradation", La Conti *et. al*., Handbook of Fuel Cells – Fundamental Technology and Applications, Ed. W. Vielstich, H. Gasteiger & A. Lamm, Vol 3: Fuel Cell Technology and Applications Part 1, Pub. John Wiley & Sons, Ltd., 2003

assessed are significantly less robust under this test protocol than other commercial and prototype materials.

It should be noted that use of the Fenton's test makes two assumptions; firstly that there will be sufficient transition metal ion contamination (e.g. Fe^{2+}) within the membrane to catalyse the decomposition of hydrogen peroxide to the hydroxyl (•OH) or peroxyl (HO_2•) radical, which attack the membrane; secondly, that there is sufficient oxygen crossover through the membrane to generate hydrogen peroxide at the anode. In the absence of these features, peroxide will not be generated, or only in miniscule amounts, and the membrane will not be attacked.

Increasingly, the use of Fenton's test as an accelerated protocol to assess membrane degradation is being questioned. Recent fuel cell literature shows evidence for the direct formation of peroxyl radicals from the reaction of hydrogen and oxygen over platinum (either in the catalyst layer or as deposited in the membrane) without prior formation of H_2O_2. Since the gas cross-over rates for hydrocarbon membranes are typically lower that in conventional PFSA materials, it is thought that this degradation mechanism will be suppressed in the membranes considered herein. Further, stable performance over 4000hr has been reported for membranes that did not survive Fenton's test[7] and replacement test protocols have been suggested.[8,9]

Ex-Situ Membrane Testing: Conclusions

- The Arkema membranes are significantly more tear resistant than the commercial PFSA membrane and have higher E-mod values.
- The initial softening point of the Arkema membranes is similar to that of the commercial PFSA membrane.
- Mechanical deformation of the Arkema membranes varies, but is generally lower than that of the commercial PFSA membrane tested.
- Arkema membranes are less robust than commercial membranes during accelerated peroxide chemical stability testing. The significance of this finding needs to be evaluated by in-cell durability tests and oxygen crossover measurements.

Task 2.2: MEA Screening

Although there are many ex-situ tests that can be performed on the membrane, none of these tests irrefutably point to the optimum MEA construction. Therefore, membrane and MEA developments go hand-in-hand. This is an iterative process where the optimum parameters are taken forward to the next set of MEAs. At various times in the project, new and optimized membrane materials were fed into the MEA optimization process.

[7] J. Rozière and D. J. Jones, *Ann Rev. Mats. Res*. **33**, (2003), pp. 503-555
[8] M. Aoki, H. Uchida and M. Watanabe, *Electrochem. Comm*., **7**, (2005), pp. 1434-1438
[9] H. Liu, H. A. Gasteiger, A. B. LaConti and J. Zhang, *ECS Transactions*, **1**, (2006), pp. 283-293

Task 2.2.1: Effect of Cell Operating Conditions

Effect of Cell Humidity

Figure 2.3a shows the polarization data obtained from 50cm^2 MEAs fabricated using Arkema's M31 membrane and a commercial PFSA membrane for reference; all other components of the two MEAs are equivalent. Polarization curves were measured at a cell temperature of 80°C, H_2/O_2 and H_2/Air and using both 100% relative humidity and 75% relative humidity at the cathode. The corresponding resistance measurements are shown in Figure 2.3b. It can be seen that the performance of the M31 containing MEA decreases with reduced relative humidity. This reduced performance is consistent with the increased resistance at 75% relative humidity, although the performance at 75% is still lower than at 100% relative humidity after correcting for IR losses - Figure 2.4.

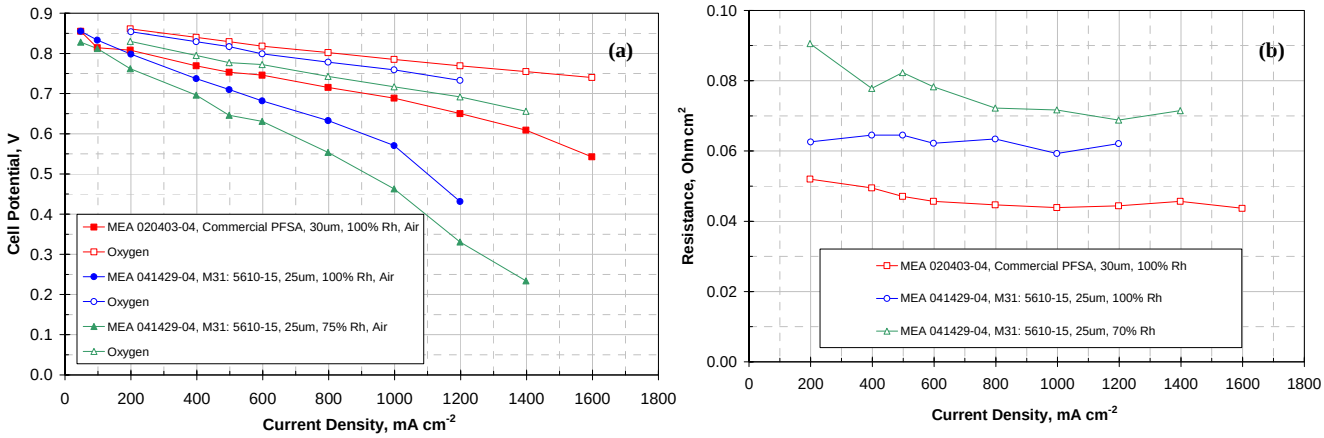

50cm^2 MEA, Test Cell 80°C, H_2 / O_2, Air at 100 / 100 KPa Gauge, 1.5 / 10, 2 Stoich, 100%Rh_{anode} / 100%, 75% $Rh_{cathode}$

Figure 2.3: Effect of Cathode Humidity: (a) Polarisation Data – Comparing M31 with Commercial PFSA Membrane (b) Corresponding membrane resistance measurements (H_2/O_2) obtained using current interrupt method

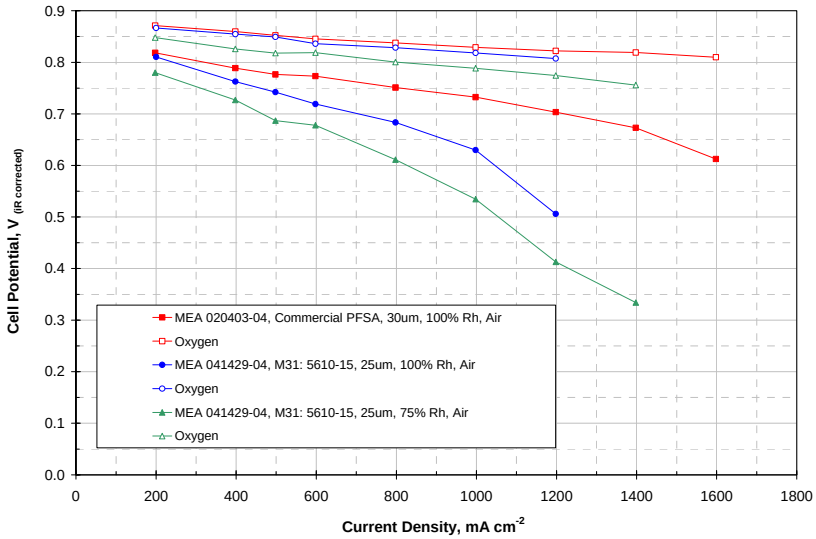

Figure 2.4 : Effect of Cathode Humidity: IR Corrected Polarisation Data – M31 vs. Commercial PFSA Membrane

Effect of Operating Temperature

An alternative approach to manage the water within the MEA fabricated with the M31 membrane was to decrease the cell operating temperature such that 100% $Rh_{cathode}$ could be maintained but that the total level of cell hydration was reduced.

Figure 2.5 shows the cell conditioning data for MEAs of M31 and commercial PFSA membranes at both 80°C and 60°C. For both MEA types, an increase in conditioning time is required before the cell voltage measured at 60°C rises to that obtained at 80°C. However, the additional time required to condition the M31 MEA at the reduced cell temperature relative to the PFSA MEA case is evident.

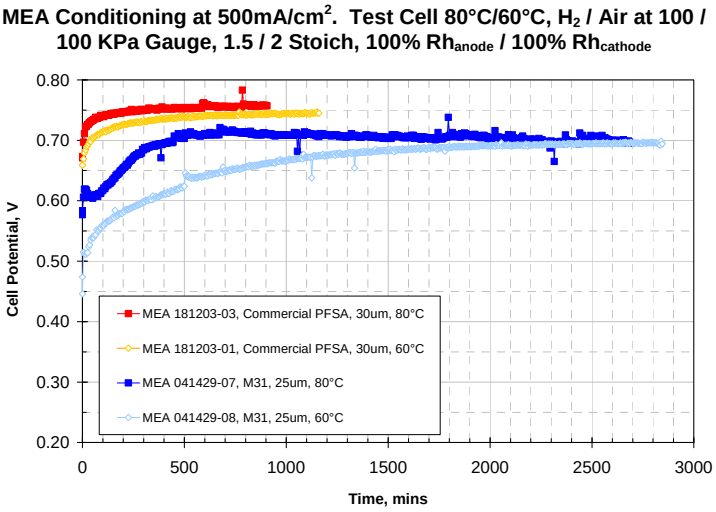

Figure 2.5: Effect of temperature on cell conditioning for MEAs containing M31 and commercial PFSA membrane

The corresponding cell resistance and polarization data for these MEAs are shown in Figures 2.6a and 2.6b. As expected, an increase in membrane resistance is observed for both M31 and the commercial PFSA material when reducing the cell temperature from 80°C to 60°C owing to the decreased level of hydration within the MEA and the effect of temperature on proton conductivity. It is also noteworthy that

the resistance of the M31 membrane is higher than that of the commercial reference at both operating temperatures despite the reduced membrane thickness; M31~ 25 microns, PFSA material ~ 30 microns.

50cm^2 MEA, Test cell at 80°C/60°C, H_2/Air, O_2 at 100/100 kPa gauge, 1.5/2.0,10.0 Stoich., 100%Rh_{anode}/100%$Rh_{cathode}$

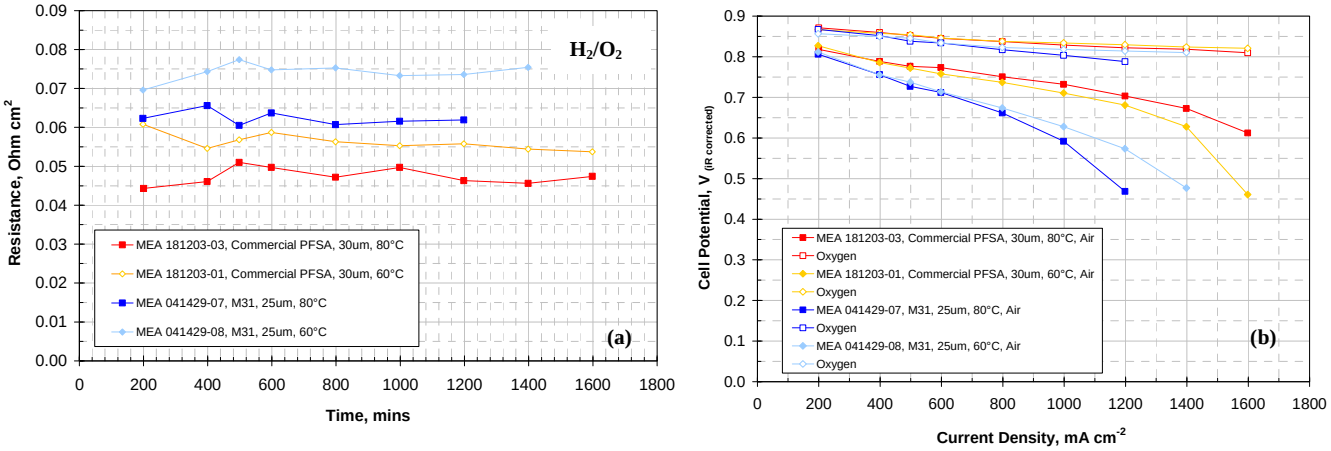

Figure 2.6: Effect of temperature on cell performance for MEAs with M31 and commercial PFSA membranes

From the IR corrected polarization data of Figure 2.6b, the MEA performance of the M31 membrane, once fully conditioned, under oxygen at 60°C is comparable with that obtained from the commercial PFSA membrane across the entire current density range, and shows that from the kinetic perspective at least, the lower cost Arkema materials could match the performance of the more costly PFSA state of the art materials.

Despite the excellent oxygen performance of the M31 material, a marked decrease in performance is observed on air operation compared to the reference sample. At 80°C, 1000mA/cm^2 the performance of the M31 containing MEA is ~140mV lower than that from the PFSA based MEA. However, on lowering the cell operating temperature from 80°C to 60°C, a clear improvement is observed in the performance of the M31 MEA at current densities in excess of 800mA/cm^2. This data suggests that, when coupled with the M31 membrane, the cathode electrode is very susceptible to flooding. Reduction of the cell temperature and correspondingly, dew point, resulted in an MEA that operated under a drier condition – and enabled improved cell performance at higher current densities relative to the 80°C case. From this result, it was also proposed that the water back diffusion properties of the M31 membrane was having an over-riding influence on cell performance. A reduced ability of the membrane to transport water from the cathode to the anode side would result in both cathode flooding (observed) and also a high membrane resistance. It is shown in Figure 2.6a that the membrane resistance of the M31 is higher than that of the PFSA material at both operating temperatures, supporting the theory that the anode electrode is running dry.

Task 2.2.2: Effect of Cathode Layer

M31 Membrane

Having obtained some understanding of the inherent properties of the M31 membrane, particularly its water handling characteristics, it was anticipated that the cell performance could be further improved by modification of the MEA cathode layer. In accordance with Task 2.2.3, a number of cathode variations were fabricated specifically for utlilisation with the M31 membrane such that the water management of the overall MEA could be more successfully controlled. Figure 2.7 shows polarization data from 50cm^2 MEAs fabricated with a standard anode layer, M31 membrane and a variety of cathode electrodes. Owing to the improvement in performance previously obtained upon reduction of the cell operating temperature, these optimized MEAs were also assessed at 60°C. Data from the commercial PFSA MEAs and MEA 041429-08 (M31, 60°C) discussed previously are repeated here for reference.

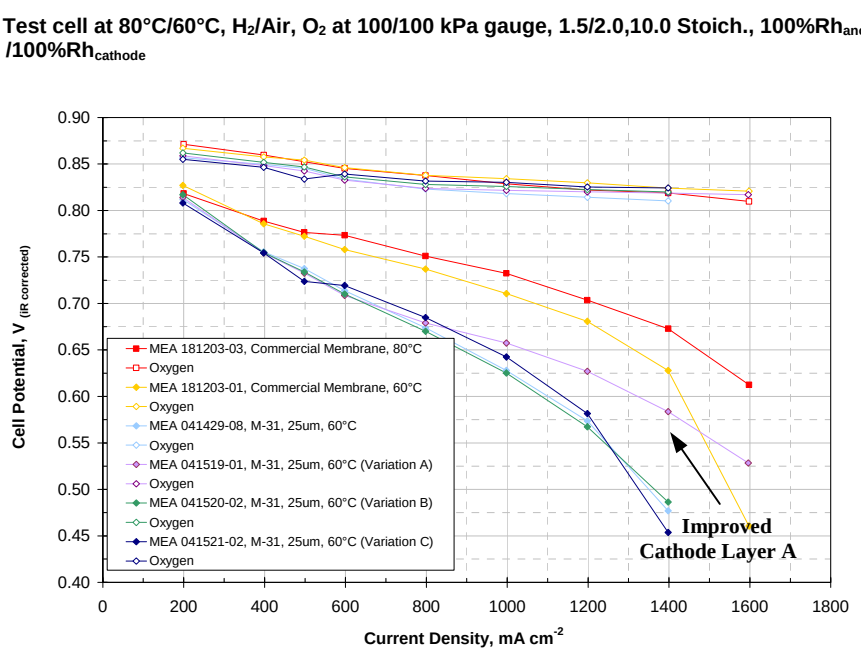

Figure 2.7: Effect of cathode electrode optimization on M31 MEA performance. Variant A shows significantly less flooding induced performance decay at high current density

Polarization data for M31 MEAs constructed with a standard cathode layer (MEA 041429-08 – light blue) and cathode "Variation B" (MEA 041520-02 – green) show equivalent performance under both oxygen and air.

Cathode "Variation C" results in some improvement in the air performance of the MEA over current densities 600-1200 mA/cm^2 yet shows more severe flooding than the standard layer as the current density exceeds 1250 mA/cm^2. A significant improvement in the H_2/air performance was observed, however, for the M31 MEA fabricated with cathode Variation A. Increased voltage is seen at all current densities above 800mA/cm^2 relative to the M31 MEA with a conventional cathode layer. The improvement yielded by the altered cathode layer is such that a 50mV increase in performance is observed at 1200mA/cm^2 which rises to 100mV gain at 1400mA/cm^2. The modified electrode architecture of Variation A clearly enables more successful removal of water from the cathode layer, leading to a significant reduction in layer flooding.

Whilst the absolute performance of the M31 containing MEAs was still lower than that obtained from the PFSA layers at 60°C, these results showed that optimization of the properties of fuel cell electrodes in accordance with those of the fuel cell membrane could yield significant improvements in MEA performance.

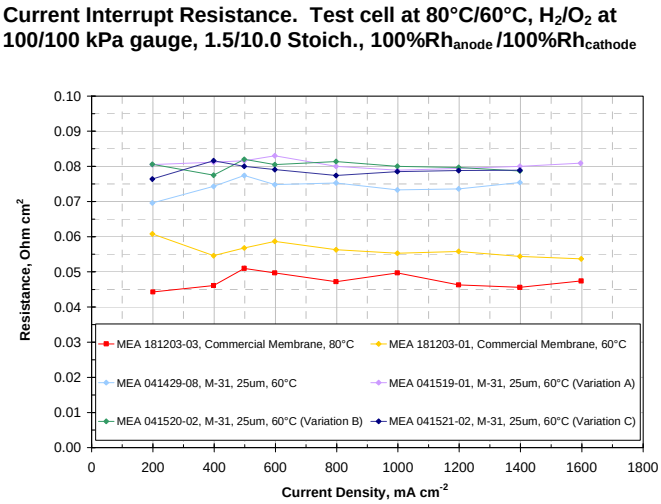

Figure 2.8: Effect of cathode electrode optimization on M31 MEA Resistance measure by current interrupt method

The corresponding resistance data for the MEAs of Figure 2.7 are shown in Figure 2.8. The measured resistance of all of MEAs containing the M31 membrane is much higher than from the PFSA MEAs. The reduced cathode flooding of cathode Variation A led to an MEA with a slightly higher overall cell resistance than the standard cathode layer of MEA 041429-08. This supports the hypothesis that Variation A provides for increased removal of water from the cathode into the air flow stream, but further reduces the ability of the M31 to back diffuse water to the anode side of the membrane, causing the membrane to run overly dry in this MEA configuration. Thus, a further increase in MEA resistance was observed, despite the overall improved performance on air operation

Thoughout Year 2 of the program, modifications to the cathode layer and the overall MEA construction were continued around the M31 membrane. Select performance results from these trials are shown in Figure 2.9. Test data from the MEA fabricated with a commercial PFSA membrane with standard cathode (MEA 181203-01), M31 and standard cathode (MEA 041429-08) and M31 with optimized cathode Variation A (MEA 041519-01) are repeated for reference.

To improve the contact between membrane and catalyst layer, a catalyst coated membrane (CCM) using a standard cathode was prepared and tested both with Toray and an alternate gas diffusion layer (GDL) (MEA 041829-01 and 041829-04 respectively). The H_2/air performance of both of these MEAs is considerably lower than was obtained from M31-MEA 041429-08 in which the catalyst layer was applied directly to the GDL. The poor performance of these MEAs is mainly the result of flooding, presumably due to poor contact between the GDL and the CCM.

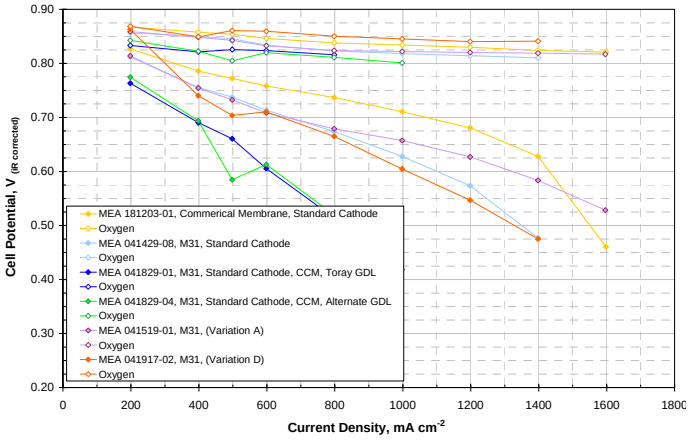

Figure 2.9: CI corrected polarization data for alternative MEAs utilizing M31 membrane

The cathode layer Variation D was selected for further studies with the M31 membrane as ex-situ electrochemical testing showed this catalyst to have increased activity and corrosion resistance compared to that used in cathode Variation A. The improved catalyst used in Layer D showed 20-25mV higher performance (CI

corrected) for H_2/O_2 operation compared to the M31/standard catalyst layer (HiSPEC® 4000) and the previously optimized M31/cathode Variation A. However, this higher catalytic activity was not readily observed for this MEA for H_2/air operation, as the layer again exhibiting flooding at higher current densities. Further optimization was necessary to obtain better catalyst utilization in an MEA under H_2/air operation.

Optimization of MEA Fabrication Conditions

To further improve the performance of the M31 MEA a series of MEAs was generated, using a standard JMFC cathode (equivalent to that of MEA 041429-08, Figure 2.7) and a range of fabrication parameters. The variables modified in the MEA lamination process included pressure, temperature, lamination time and membrane pre-treatment. However, no alteration in initial MEA performance was observed.

M40 Membrane

In Project Year 3, MEAs incorporating M40 membrane and JMFC standard electrodes were fabricated and preliminary testing was conducted in a 50cm^2 test cell. Figure 2.10 shows the conditioning curve for the M40 MEA W14002-001. Despite exhibiting a high OCV of 0.93V, the MEA performance is quite poor, yielding only 0.40V at 500mA/cm^2 after 2000 minutes of conditioning. This compares with values of 0.70-0.75V @ 500mA/cm^2 for MEAs fabricated with M31 membrane / JMFC standard electrodes.

Figure 2.10 also shows the resistance measurement of the M40 MEA, which at 0.13 – 0.15 ohm·cm^2 is much higher than that obtained from the M31 MEAs (0.07 and 0.085 ohm·cm^2 from earlier figures). This indicates that the properties of the M40 membrane are significantly different than the M31, perhaps with further reduced water handling characteristics. Alternatively, the results of Figure 2.10 could also have been indicative of a poorly bonded MEA despite the use of laminating conditions that had proved effective for the M31 membrane.

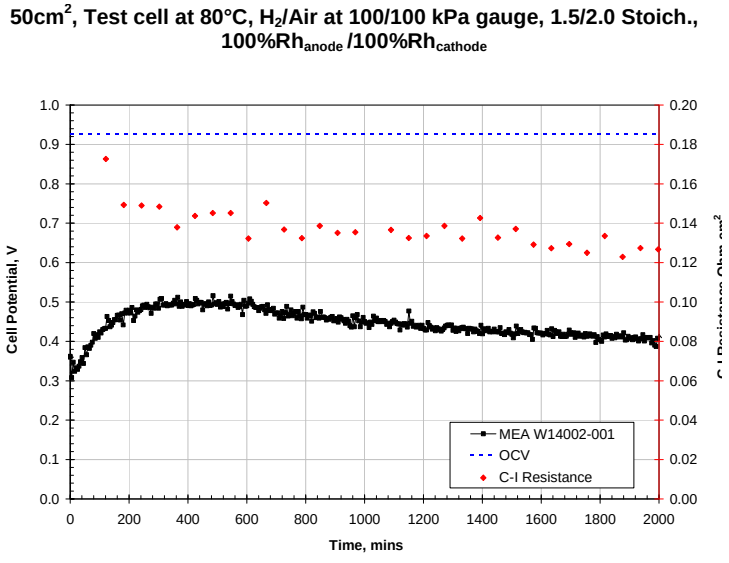

Figure 2.10: MEA Conditioning 500mA/cm^2 MEA W14002-001; M40 membrane/Standard cathode

To assess the appropriateness of the M31 optimized laminating conditions for the M40 membrane, 5 MEA samples were fabricated using a range of temperatures and pressures and their performance assessed on a minicell test station (active sample area = 3.14cm^2 from 1cm diameter disk). The performance obtained was either equivalent or significantly worse than was given by the M40 containing sample generated with the initial fabrication parameters. It was also found that any increase in temperature or pressure relative to the standard conditions employed led to a decrease in MEA performance across the polarization curve, including at current densities typically associated

with catalyst kinetic activity. This suggests that some penetration of the membrane into the catalyst layer was occurring, resulting in decreased utilization, and thus performance, of the catalyst. Owing to the poor performance characteristics of this membrane, no additional effort was given to MEA development with this material.

M41 Membrane

MEAs incorporating Arkema's M41 membrane and JM standard electrodes were fabricated and preliminary testing of a M41 50cm^2 MEA was performed at 60°C.

Figure 2.11 shows the CI corrected performance curve for the M41 MEA (W14761-002) which is compared to the standard MEAs based on commercial 30µm PFSA membrane and those fabricated with Arkema M31. The initial performance of the M41 containing MEA is generally equivalent to that produced by the M31 containing MEA and yields slightly better performance at higher current densities when standard cathode electrodes are used (MEAs W14761-002 and 041429-08 respectively). However, despite good performances on oxygen, the H_2/air performance of the M41 MEA is again lower than obtained from the reference sample containing the PFSA membrane. Since the IR corrected oxygen data is very similar for the three MEA types, the lower air performance of the M41 MEA is again attributed principally to mass transport losses. The reduced proton conductivity of the M41 membrane relative the PFSA materials may be seen in Figure 2.12 in which the membrane resistances for the MEAs of Figure 2.11 are shown. Here it is shown that the resistance of the M41 MEA is considerably higher than from the PFSA sample and slightly higher than obtained from previous M31 MEAs. The mass transport losses are again thought to be a result of over-wetting of the cathode catalyst layer due to the lower level of water back diffusion (i.e. diffusion of water from cathode to anode) compared to conventional PFSA materials. The reduced water permeability of the M41 was subsequently confirmed with ex-situ membrane tests and is discussed later in this report.

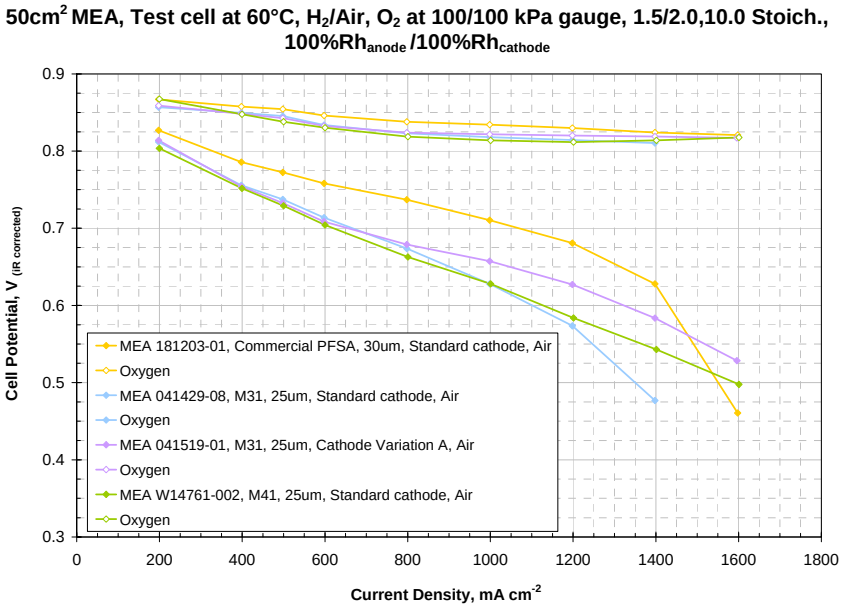

Figure 2.11: Resistance Corrected polarization curves for M-41 MEAs versus previous M-31 and commercial PFSA containing MEAs at 60 °C

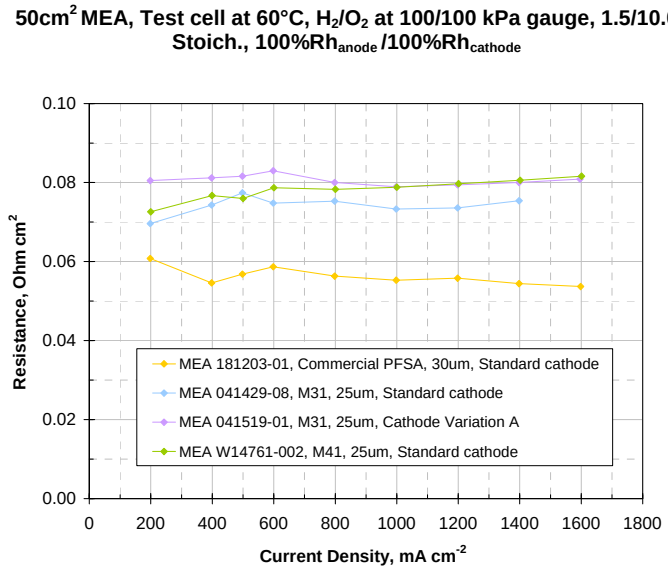

Figure 2.12: CI resistance plot for the M41 MEA *vs*. M31 and commercial PFSA containing MEAs at 60 °C

This back diffusion property resulting in mass transport losses was also observed for the M31 membrane and was partially resolved by modifying the cathode catalyst layer, thus improving performance at higher current densities. Aiming to replicate this improvement with the new membrane material, MEAs were fabricated with M41 with a more hydrophobic catalyst layer and/or alternate catalyst layer structures to determine whether it was possible to remove excess water more effectively from the cathode layer and thus, improve air performance.

Testing was performed using the 50cm^2 screener cell at 80°C under fully humidified conditions. Figure 2.13 shows the CI corrected performance curve at 80°C for five M41 MEAs; one sample contains a standard cathode electrode (MEA W14761-003) and four MEAs with variations in the cathode layer are also shown. Each of the modified electrodes provides some degree of performance improvement over the M41 MEA with a standard cathode. MEA W15109-001 (shown in light blue) was generated by modifying the typical layer properties of the HiSPEC® 4000 catalyst (used in the standard layer). This change in layer architecture results in ~ 40mV improvement in performance at 800mA/cm^2 and an additional 80mV at 1000mA/cm^2. The use of an alternative fabrication to route to create a catalyst layer with the same properties as that in MEA W15109-001 (yielding MEA W15931-01) resulted in a small improvement in H_2/air performance at current densities less than 800mA/cm^2, but which exhibited more pronounced flooding at higher current densities. Further attempts to improve the catalyst layer using HiSPEC® 4000 (MEA W15959-01) led to a substantial reduction in H_2/air performance relative to the previous two cases such that the polarization data obtained was similar to that from the M41 MEA with standard electrodes.

In a continued effort to use the cathode layer to manage the water distribution within the MEA, an additional sample using an alternative catalyst was prepared. It was expected that the intrinsic properties of the catalyst would facilitate water removal from the cathode side. The polarization data from this MEA (W15467-003) is also given in Figure 2.13 and showed the highest H_2/air performance from this sequence of samples.

To try to improve the 80°C M41 MEA performance further, an additional MEA was fabricated using a HiSPEC® 9100 catalyst (twice the active metal area of HiSPEC® 4000) and incorporating the same modification as proved successful in MEA W15109-001. H_2/O_2 and H_2/air data for this MEA (W15930-01) is given in Figure 2.14; reference data for this type of catalyst layer with a conventional PFSA membrane is also provided.

For this set of test conditions the modified HiSPEC® 9100 layer, when used with a PFSA membrane, provides an additional 20-25mV in performance across the polarization curve when operating under oxygen but this improvement is not realized under H_2/air. Conversely, for the case

in which when the modified HiSPEC® 9100 is used with the M41 membrane, little improvement is seen in the CI corrected H_2/O_2 data (except at current densities greater than 1600mA/cm^2) compared to the previous highest performing M41 containing MEA. (The M41/HiSPEC® 4200 data of MEA W15647-003 is also repeated in Figure 2.14). However, a 30mV improvement in performance was obtained under H_2/air for the modified HiSPEC® 9100 – the higher catalyst surface area providing a kinetic benefit at low current densities and layer properties enabling a reduction in flooding and thus mass transport limitations at higher current densities.

50cm^2, Test cell at 80°C, H_2/Air, O_2 at 100/100 kPa gauge, 1.5/2.0,10.0 Stoich., 100%Rh$_{anode}$ /100%Rh$_{cathode}$

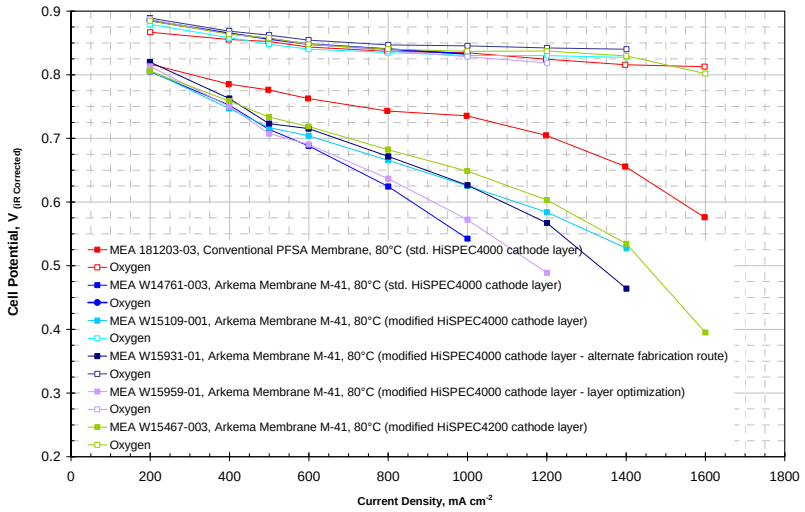

Figure 2.13: CI Corrected Polarization curves for M41 MEAs versus conventional PFSA at 80 °C

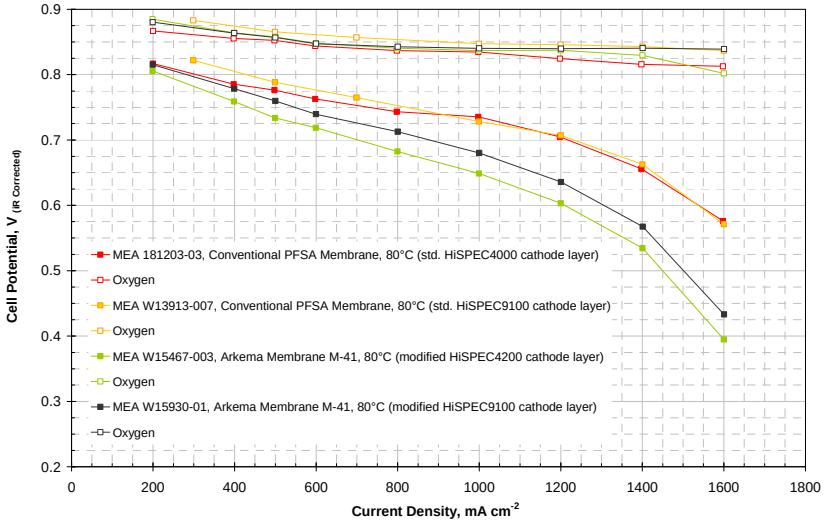

Figure 2.14: CI Corrected Polarization curves for M41 MEAs compared versus PFSA at 80 °C

Although a significant gain in performance is observed for the M41 MEA with the new catalyst layer, and performances much closer to a PFSA based MEAs were now being obtained, the performance is still around 20mV lower @ 500mA/cm^2 compared to the conventional PFSA membrane. The lower performance for the M41 MEA continues to be attributable to both mass transport losses (due to the poor back diffusion property of the membrane and thus cathode flooding) and conductivity losses. The CI resistance data for all of the MEAs of Figures 2.13 and 2.14 are given in Figure 2.15, where it is shown that the membrane resistance of the M41-MEAs continues to be significantly higher than from commercial PFSA material. With the exception of the case in which the HiSPEC® 4200 was employed, the membrane resistance does not vary with the properties of the cathode layer.

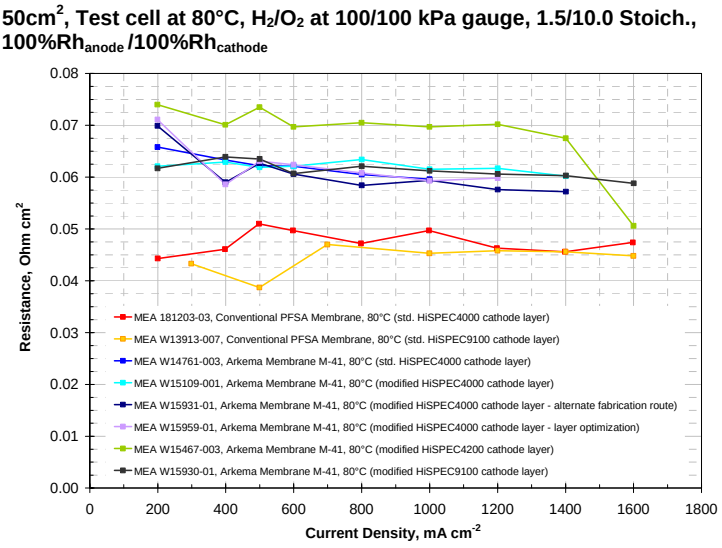

Figure 2.15: CI Resistance of M41 Containing MEAs

Both the MEA fabrication optimization and the continued improvements afforded by both the catalyst layer architecture and intrinsic catalyst properties enabled significant improvements to be made in the performance of PEM MEAs containing the Arkema membranes. However, the results obtained strongly indicated that further significant improvements in MEA performance would not be attained by electrode optimization alone. The intrinsic properties of the membrane dominate the MEA performance and further modifications to the proton conduction and water handling characteristics would be required to more closely match conventional PFSA membrane performance.

Significant progress in the performance of MEAs utilizing Arkema's membranes has been made over the course of the three year project. Figure 2.16 shows a comparison of early polarization data, obtained during 80°C testing of an M31 MEA (previously shown in Figure 2.6) with that from the optimized MEA using M41 membrane. Clear improvements in both the H_2/O_2 and H_2/air data are visible.

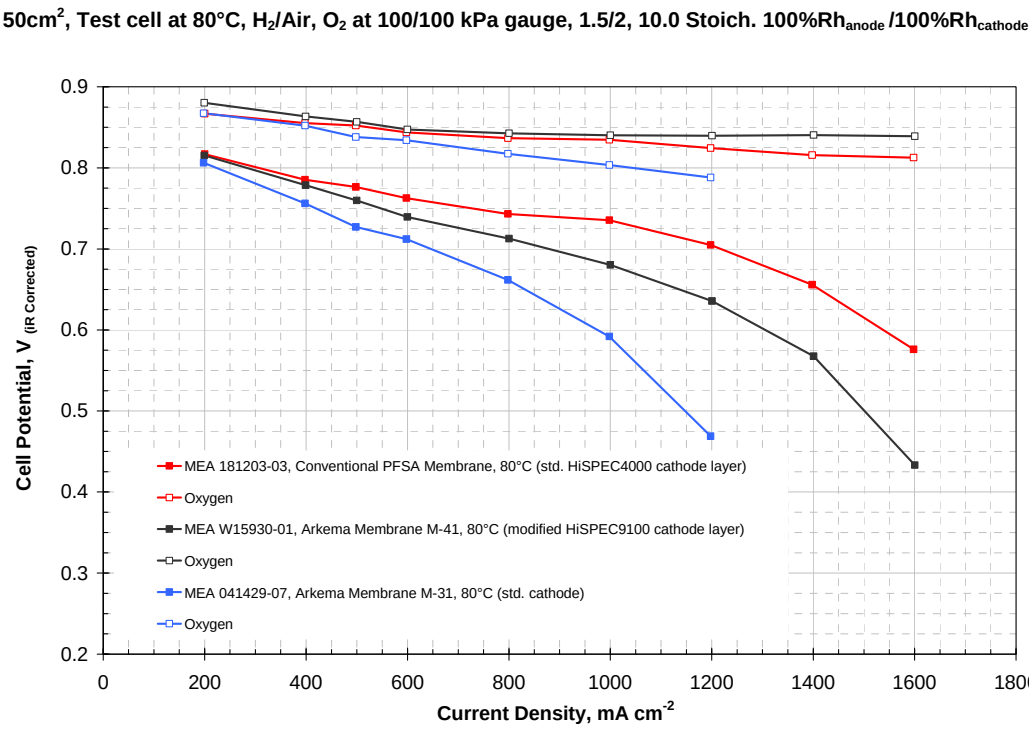

Figure 2.16: Comparison of polarization data obtained from M31 MEA at project start and optimized M41 MEA at project end

Task 2.2.3: In-Situ Membrane Stability Testing

In addition to testing PEM MEA performance using the novel SIPN membranes, JMFC also conducted in-situ membrane durability testing using both steady state and an accelerated OCV durability test for the most promising membrane materials.

M31 Membrane

Steady State Durability

The steady state durability test protocol comprised the following key steps:

- MEA conditioned overnight/until stable voltage @ 500 mA/cm^2 with full humidification at 80 °C, stoic. 1.5/2.0 H_2/air, 100kpag pressure
- Hold at 500 mA/cm^2, 80 °C, H_2/air at 100/100 kPa, 100/100 %Rh A/C, 1.5/2.0 stoichiometry.
- BOL performance testing under H_2/air, oxygen
- Membrane failure detected by voltage decay rate and OCV decay rate

Using an MEA of Type 041519-01 (Standard anode, Cathode Variant A, Figure 2.7), the stability of an MEA with M31 membrane was assessed using a 500 hour, constant current density test – Figure 2.17.

Test cell at 60°C/60°C, H_2/Air at 100/100 kPa gauge, 1.5/2.0 Stoich., 100%Rh_{anode} /100%$Rh_{cathode}$

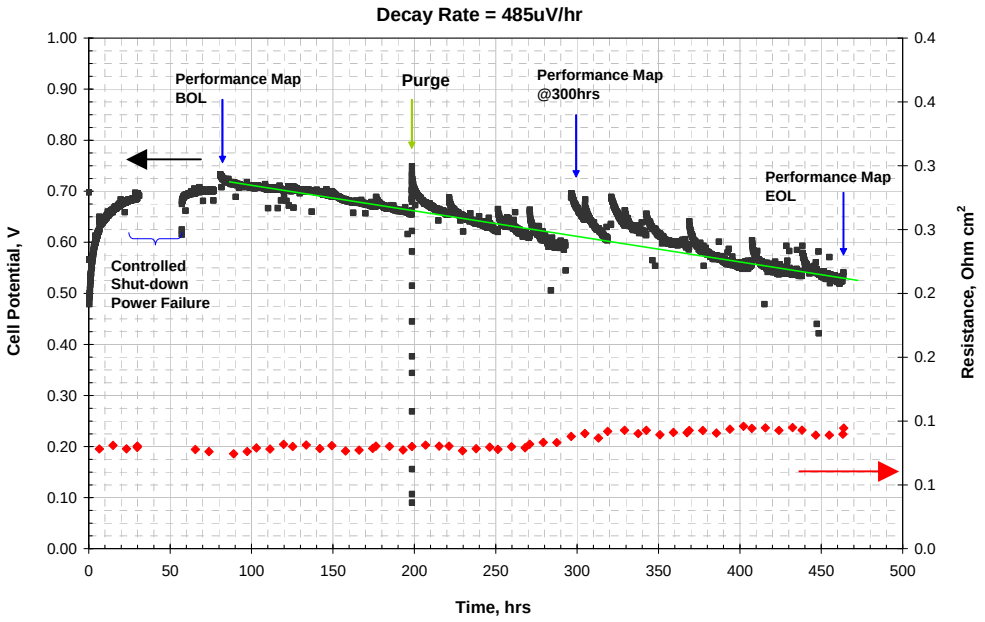

Figure 2.17: 500 hour stability testing of M31 membrane using optimized cathode from Figure 2.7. Tested under constant current density of 500mA/cm^2.

The M31 MEA shows a steady decrease in performance with time and after approximately 500 hours, a voltage decay of ~ 485 µV/hr is observed. A component of the cell voltage decay can be attributed to an increase in mass transport resistance with time - induced by MEA flooding at this current density despite the modified electrode architecture.

Whilst this voltage decay is considered high, this result shows a significant improvement in membrane development over version M27 – the data for which is not shown here but for which the cell voltage repeatedly oscillated between 0.7V and 0.3V during the course of an equivalent test. Figure 2.18 shows the MEA OCV decay rate with time; during the 500 hour test, the M31 MEA exhibited an OCV decay of 54µV/hr. The decay in OCV can be caused by H_2 leakage through the membrane to the cathode or by shorting of the anode and cathode electrodes through the membrane. From the data gathered it is not possible to tell which of these mechanisms is dominant, but previous work has shown that shorting was very common with this type of membrane. This conclusion is also supported by the long-term OCV test data reported below.

Test cell at 60°C/60°C, H_2/Air at 100/100 kPa gauge, 1.5/2.0 Stoich., 100%Rh_{anode} /100%$Rh_{cathode}$

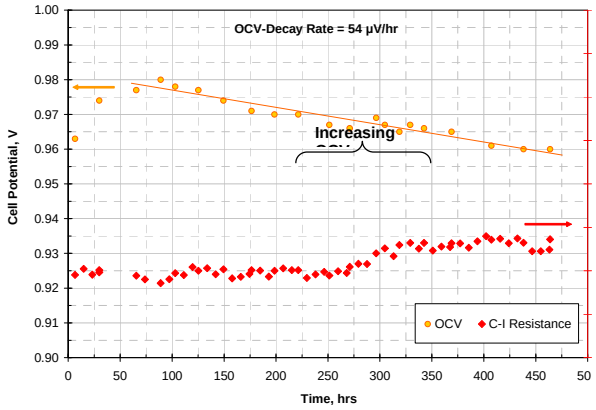

Figure 2.18: OCV decay rate and membrane resistance of

It is also notable that the membrane CI resistance began to increase after approximately 250 hours, a trend which continued thoughout the next 150 hours (Figure 2.18). This suggests that some property of the membrane was altering during the course of the test protocol leading to a reduction in the water handling abilities of the membrane and hence, an increase in membrane resistance.

Figure 2.19 shows the resistance corrected polarization data of MEA 04-1519-02 at Beginning of Life (BOL), after 300 hours and after 500 hrs = End of Life (EOL). The largest component of MEA performance loss occurred during the first 300 hours of operation with a much smaller performance decay observed between 300 and 500 hours.

Test cell at 60°C, H_2/Air, O_2 at 100/100 kPa gauge, 1.5/2.0,10.0 Stoich., 100%Rh_{anode} /100%$Rh_{cathode}$ (durability protocol = hold 500mA/cm^2)

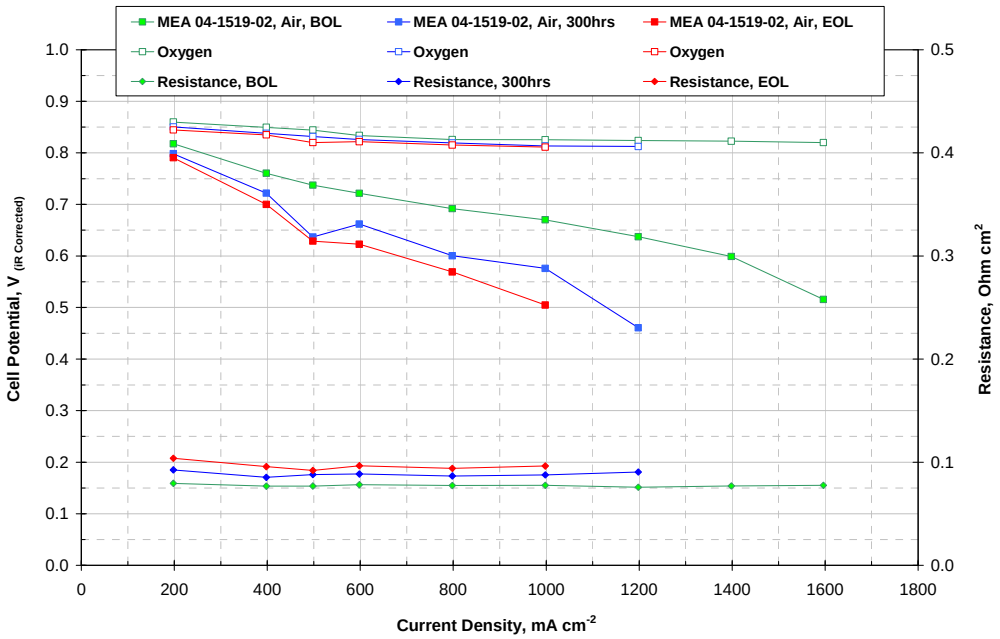

Figure 2.19: Resistance Corrected Polarization Data of M31 MEA with Optimized Cathode Variation A at Beginning of Life, 300 hours and End of Life during constant current density durability testing

M41 Membrane

Steady State Durability

Using the application of a constant current density according to the test protocol given above, the durability of an M41 containing MEA (W15467-1, cathode = HiSPEC® 4200) was also assessed. Due to an obvious increase in the stability of the M41 membrane relative to M31, the steady state durability test was extended from 500 hours to 950 hours. In addition, as an excellent improvement in MEA performance of this membrane was observed, the durability protocol was conducted at the more conventional PEM operating temperature of 80°C rather than the reduced 60°C employed for the M31 material. The results of the application of this test protocol to M41 MEA W15467-1 are shown in Figure 2.20.

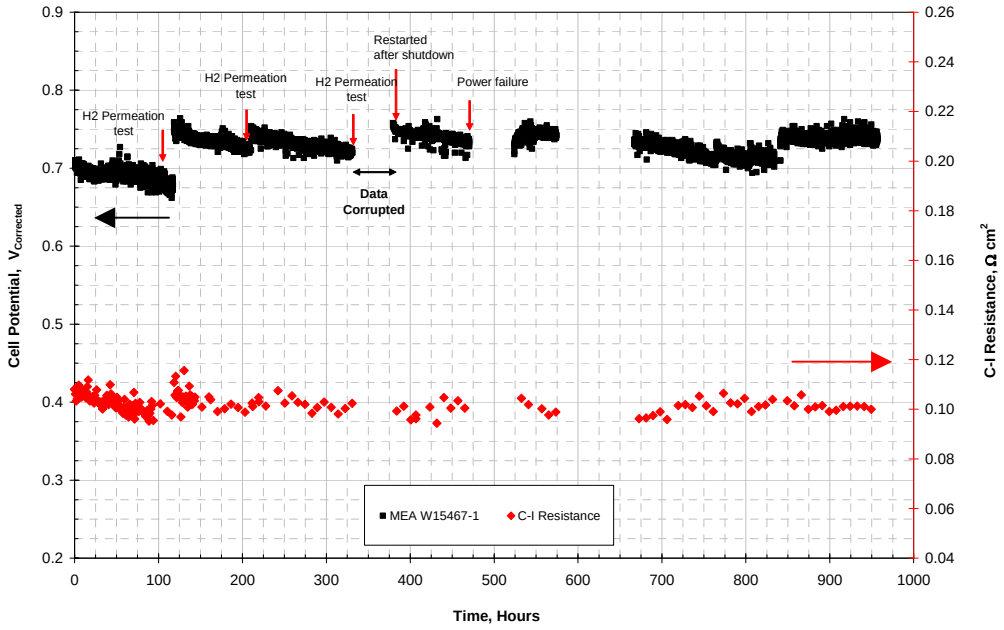

Figure 2.20: Steady state durability testing for the M41 MEA W15467-1 with modified HiSPEC® 4200 layer

Test cell at 80°C/80°C, H_2/Air at 100/100 kPa gauge, 1.5/2.0 Stoich., 100%Rh_{anode} /100%$Rh_{cathode}$

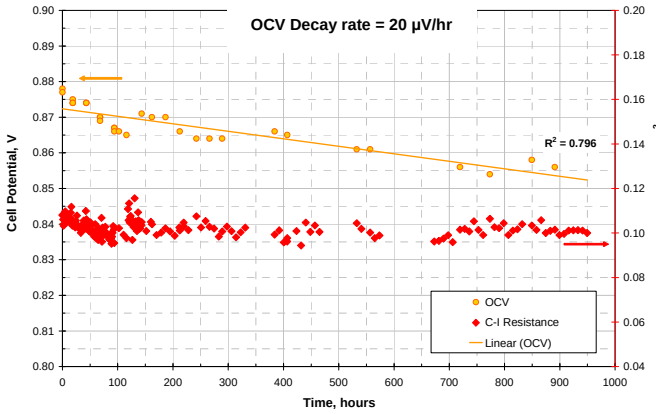

Figure 2.21: OCV decay rate and membrane resistance of M41 MEA (W15467-1) with modified HiSPEC 4200 cathode

No measurable decay in cell potential occurs over the test period for the MEA containing the M41 membrane. This positive result marks a clear improvement in the M41 membrane relative to the M31 material – for which a decay rate of approximately 485µV/hr was measured when tested under the same durability protocol.

The OCV of the MEA was again periodically assessed during the hold test; the results are shown in Figure 2.21. (The high CI resistance shown in both Figures 2.20 and 2.21 below are attributable to MEA test stand issues.)

Over the 950 hour test time, a decrease in the OCV was observed with a much lower, average decay rate of 20µV/hr. For PFSA membranes, such a decrease in OCV is indicative of shorting or increased H_2 crossover as mentioned above. However, it should be noted that the effect of the ~ 20mV in (1000 hours) loss on the operating MEA i.e. when a current is drawn, would be sufficiently small that no change in performance would be detected in the experimental noise of the data of Figure 2.20.

OCV Hold Durability

The durability of the M41 membrane was probed using an in-situ accelerated OCV hold test on a 50cm^2 MEA. Key features of this test were as follows:

- Accelerated OCV hold test utilising aggressive cell conditions
- MEA conditioned overnight / until stable voltage obtained at 500 mA/cm^2, full humidification, 85 °C
- Hold OCV, 85 °C, H_2/air at 100/100 kPa abs., 13/13 % Rh A/C, 1.5/2.0 stoichiometry at 200mA/cm^2
- Periodic assessment of MEA (typically every 24hrs) by gas cross-over and electrical resistance measurements
- Membrane failure detected by OCV decay rate and nitrogen/hydrogen cross-over leak rate
- Post-mortem analysis of the MEA to determine cause of membrane failure e.g. locate tears, assess membrane thinning

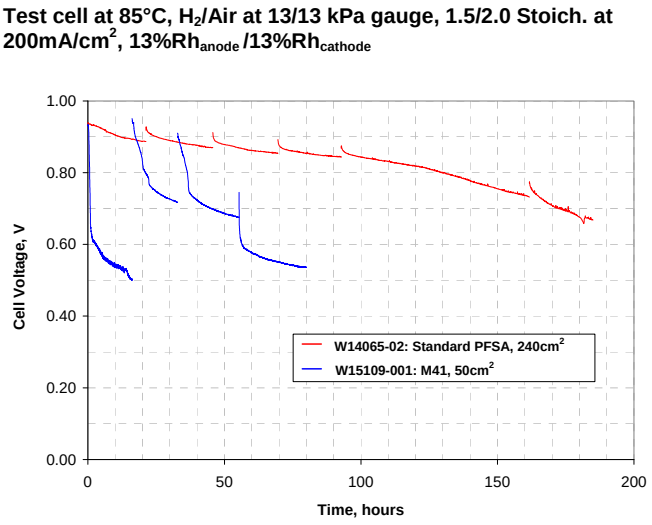

Figure 2.22: OCV hold data for MEA W15109-001; M41 with modified HiSPEC® 4200 cathode vs. Standard PFSA

As outlined above, the OCV test was periodically interrupted (approximately every 24 hours) for the completion of membrane diagnostics, after which, the OCV test recommenced. The performance data for MEA W15109-001 (cathode = modified HiSPEC® 4000, membrane = M41) are shown in Figure 2.22. This data has been plotted such that it is shown as total time spent at OCV (hours) with disconnects in the data-set occurring as gas cross-over and electrical short tests were conducted. The presentation of the OCV hold data in this format shows more clearly that there is no obvious trend observable in the OCV with time. It is also apparent that within any one OCV hold (4 separate 'OCV holds' shown), the voltage measured drops unexpectedly quickly.

Test cell at 85°C, H_2/Air at 13/13 kPa gauge, 1.5/2.0 Stoich. at 200mA/cm^2, 13%Rh_{anode} /13%$Rh_{cathode}$

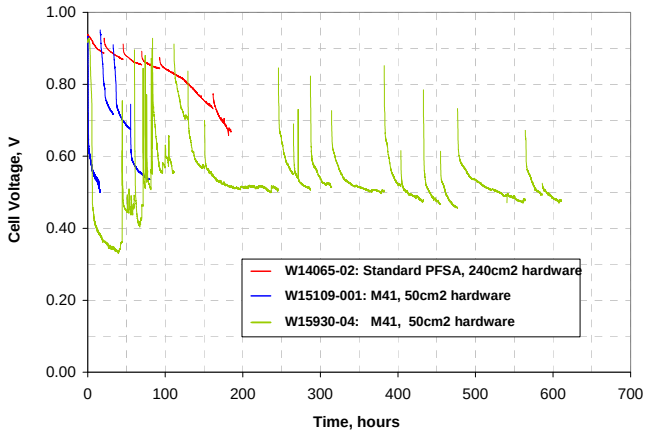

Figure 2.23: OCV hold data for MEA W15930-04; M41 with modified HiSPEC® 4000 cathode vs. Standard PFSA

For comparison, OCV data obtained from a more conventional PFSA membrane is also shown in Figure 2.22 (data in red; MEA W14065-02). It should be noted that this data was collected from a significantly larger MEA in entirely different cell hardware than the M41 sample, but serves to show the data trend expected in this OCV test. In the six 'OCV holds' shown (again with MEA diagnostics in-between) a steady decrease in the OCV was measured with time. Unlike the case for MEA 15109-001 (M41 membrane), the PFSA reference sample does not exhibit significant variations in OCV following each stop/start cycle.

Owing to both the low electrical resistance of 66 Ohm·cm^2 obtained (BOL = 4674 Ohm·cm^2), the low OCV but yet no leak in the MEA detectable by gas-crossover measurements, the durability test was aborted after 80 hours of testing. An additional 50cm^2 MEA utilizing M41 membrane (MEA W15930-04) was fabricated and subjected to the same OCV test protocol. This test was conducted for 610 hours and the results are shown in Figure 2.23. For reference, data from the PFSA containing MEA and previous M41 MEA are also shown.

The OCV data obtained from the second M41 containing MEA also does not exhibit any obvious trend with time (i.e. voltage decay). Following each set of diagnostic tests, the OCV is typically 0.7V – 0.85V, yet quickly falls to 0.45V – 0.55V. This behaviour is atypical and not representative of historical observations when MEAs containing non-Arkema membranes are subject to this test. It is not currently well understood why a large percentage of the OCV loss is recovered between sequential 'OCV holds' or why the voltage falls so quickly in any one test period.

Test cell at 85°C, H_2/Air at 13/13 kPa gauge, 1.5/2.0 Stoich. at 200mA/cm^2, 13%Rh_{anode} /13%$Rh_{cathode}$

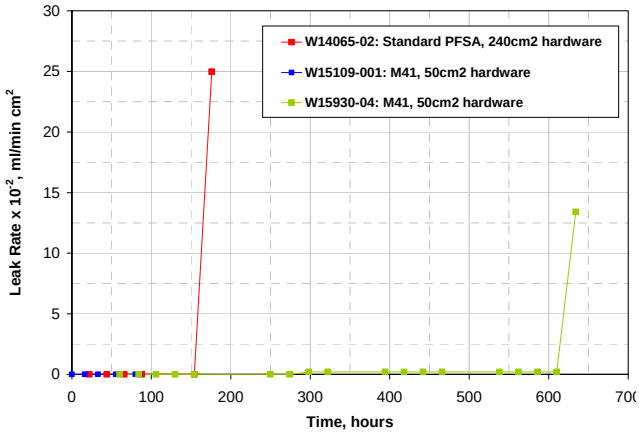

Figure 2.24: Leak Rate detected using N_2 Cross-Over

Ultimately, the final series of MEA diagnostics were aimed at showing signs of mechanical damage to the membrane, detected by the flow of nitrogen through the M41 using a gas cross-over test. These data are shown in Figure 2.24. For MEA W15930-04, the flow of N_2 detected upon application of pressurized gas rose from a negligible value to ~ 13.5 ml/min·cm^2 at 634 hours. An equivalent data-set for the M41 MEA previously tested using this OCV protocol (MEA W15109-001) are also included, in which no cross-over was reported after the total 80 hours test time. For comparison, data from the reference sample W14065-02 containing a conventional PFSA membrane shows substantial nitrogen cross-over at 176 hours of testing. However, it is again stressed that the tests upon the PFSA

membrane were completed in 240cm^2 hardware that could induce different mechanical stresses within the MEA. Therefore, caution should be exercised when making a direct comparison of the two membranes. (Comparison 50cm^2 PFSA data under 13% RH conditions are not available.) It should also be noted that the leak data have been normalized per unit area of MEA (240cm^2 PFSA, 50cm^2 M41) leading to leak rate units of ml/min·cm^2.

On completion of the OCV durability test, MEA W15930-04 was sectioned and assessed by optical microscopy in an attempt to ascertain the point of failure within the membrane. Of the sections imaged, no obvious defect was found although thinning of the M41 membrane was observed throughout. Figure 2.25 shows a representative micrograph. The thickness of the membrane has been measured at 7 points within this sample, (shown within Figure 2.25) and the measurements are given in Table 2.5. The average width of this section of membrane was only 15.6µm, the membrane having lost ~ 38% of its thickness. Assessment of other sections of the MEA showed average membrane thicknesses of 17.9µm, 17.3µm 17.0µm and 16.7µm. It is not known whether this reduction in the *xy* membrane dimension was caused by chemical attack or by leaching of the polyelectrolyte component of the membrane into the catalyst layer.

MEA W15930-004, Section 4	
X Position (Left to Right)	**XY Length, microns**
1	18.25
2	17.06
3	19.91
4	15.17
5	14.22
6	16.35
7	11.14
Average Thickness	**15.64**
STDEV Thickness	**2.68**

Table 2.5: Membrane dimensions measured for MEA section shown in Figure 2.26

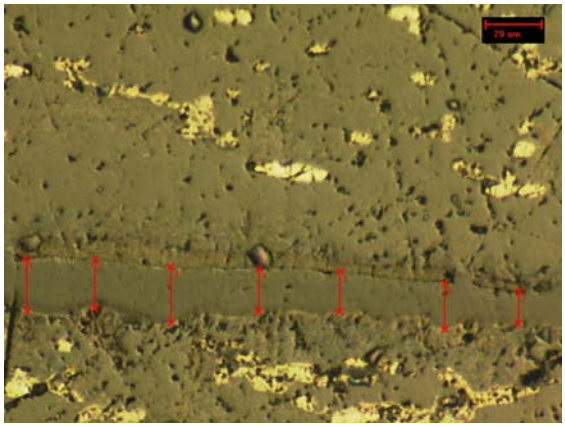

Figure 2.25: Optical Microscopy Image of MEA W15930-04 Section. Membrane runs through the image and points of thickness measurements are marked

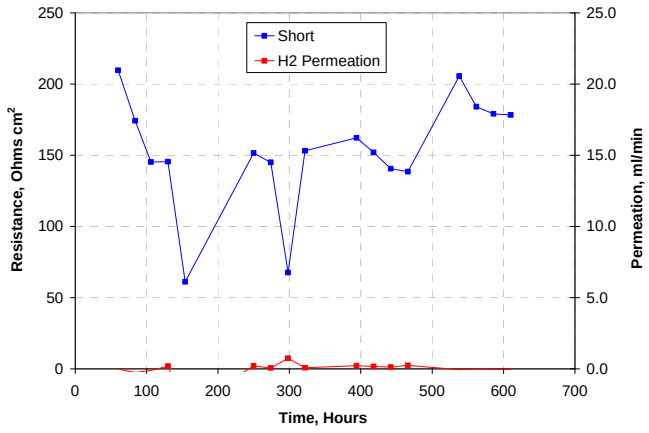

Figure 2.26: Hydrogen Permeation and MEA resistance measurements for MEA W15930-04 obtained during the course of the OCV hold test protocol

It would be expected that the thinning of the membrane could be followed via the membrane diagnostics that are run throughout the OCV test. In particular, it would be anticipated that an increase in hydrogen cross-over would be observed in proportion to the thinning of the membrane. The results of the hydrogen permeation and resistance measurements for MEA W15930-04 are shown in Figure 2.26.

It may be seen from the permeation data that, contrary to expectation, no significant variation in hydrogen cross-over was observed in the course of the MEA diagnostics despite the reduction in membrane thickness. Further, there is no trend apparent in the MEA resistance data which may be expected to decrease with the changing dimensions of the membrane. Note, no hydrogen permeation and electrical resistance measurements were conducted at 634 hours - at which time the nitrogen permeation test showed mechanical failure of the membrane.

Whilst the results of the OCV test are not internally consistent (recoverable OCV but with dramatic loss despite no obvious leak or electrical short within the membrane) or comparable with those from more conventional PFSA materials, they do support the observations of M41 membrane behaviour reported previously. These results show that further testing, both experimental repeats and use of different cell hardware, are required to obtain a more comprehensive understanding of the OCV test data for the M41 case and enable more direct comparison with PFSA membranes.

Task 2.2.4: Understanding In-Situ Membrane Performance

Membrane Gas Permeability

PFSA type membranes suffer from chemical degradation as a result of peroxide formation during cell operation. One of the mechanisms proposed for hydrogen peroxide radical formation is from hydrogen radicals [H•] formed at the anode reacting with O_2 molecules that have diffused from the cathode side into the membrane. This results in the formation of hydrogen peroxide radicals [HO_2•] which attack PFSA membrane materials. Therefore, it is important to ascertain whether O_2 diffuses through the membrane. Alternatively, H_2 can diffuse from the anode resulting in peroxide formation at the cathode electrode and thus, the rate of H_2 diffusion through the membrane is also important.

The H_2 and O_2 permeability of the membranes were assessed in a fully conditioned MEA. The test cell was then disconnected and for the case of determining H_2 permeation, H_2 was fed to the anodes and N_2 was fed to the cathode. Using a GC, the cathode exhaust was then analysed for H_2. For the determination of O_2 permeability, oxygen was fed to the cathode, H_2 to the anode and the anode exhaust was assessed for O_2.

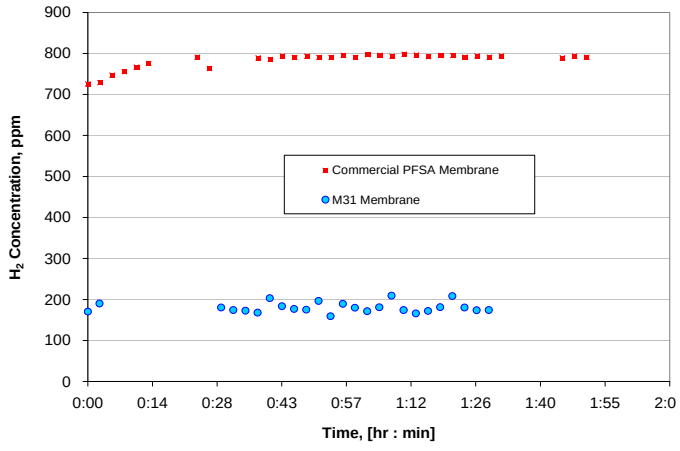

Figure 2.27: H_2 permeability of M31 and PFSA membranes by GC measurement

Figure 2.27 shows the H_2 measured on the cathode side for both a PFSA membrane and M31. It can be seen that the H_2 permeation through the commercial (30µm) membrane is 4 times higher than through the M31 (25µm) membrane. This trend correlated with electrochemical measurements, where a H_2 permeation of 0.2-0.4 ml/min for the M31 membrane compared to 1.4-1.5 ml/min for the commercial membrane was measured (see Table 2.6). The actual values of H_2 permeation measured are about a factor of 2 higher for the electrochemical measurement compared

to the GC case. In the GC experiment, based on a dry N_2 flow of 0.8 L/min and 200 ppm H_2, the H_2 permeation rate was calculated to be 0.16 ml/min vs. the 0.2-0.4 ml/min measured electrochemically. The GC measurement for the H_2 permeability could be lower due to the fact that some of the H_2 dissolves in the liquid water phase and does not get measured in GC experiment.

Table 2.6: H_2 Permeability of M31, M41 and PFSA Membranes

Membrane	H_2 Permeation (Electrochemical) ml/min	H_2 Permeation (GC Gas Phase) ml/min
Commercial PFSA	1.44	0.64
Arkema M-31 (MEA 041429-08)	0.27	0.16
Arkema M-41 (MEA W14765-005)	0.25	--

Table 2.6 also compares the H_2 permeation measured in-situ electrochemical test for the M41 membrane compared to both M31 and a commercial PFSA material. The Arkema M41 membrane provides a factor of 6 reduction in cross-over compared to the commercial 30μm PFSA membrane.

Similarly the oxygen permeation of the M31, M41 and PFSA membranes were measured. First the cell was fully conditioned (500 mA/cm^2, fully humidified, 60 °C, H_2/air, cell pressure at 100 kPa) after which the H_2 was switched to N_2. Oxygen was measured by a GC (Agilent). Using the GC approach, no O_2 could be detected passing through the M31 and M41 membranes; however the detection limit of the GC was around 20 ppm. Consequently, the anode exhaust was assessed using a mass spectrometer with a ppb measuring capability.

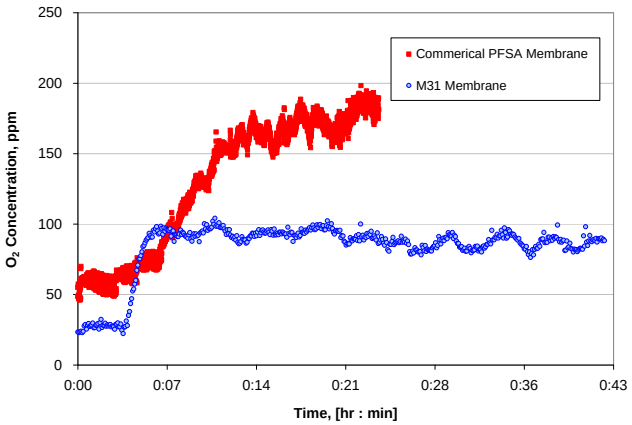

Figure 2.28: O_2 permeability of M31 and PFSA membranes by GC measurement

Figure 2.28 and Table 2.7 provides the O_2 permeability measurements for the commercial PFSA, M31 and M41 containing MEAs. It can be seen that the O_2 permeability for the commercial membrane is considerably higher than for the Arkema materials. A reduced O_2 permeability should be beneficial to overall durability of the M31/M41 since the opportunity for peroxide radical formation is reduced.

Table 2.7: O_2 Permeability of M31, M41 and PFSA Membranes

Membrane	Concentration, ppm	Rate, ml/min
Conventional PFSA (30 μm)	107	0.062
M31 (25 μm)	60	0.035
M41 (25 μm)	85	0.049

Membrane Water Permeability

JMFC has set-up a system to measure water permeability (ex-situ) of fuel cell components, and the technique has been applied in this program to test the water permeability of the M-41 membrane and the data compared with conventional PFSA membranes. As stated previously, based on the in-cell test data it was proposed that mass transport losses in the polarization data of Arkema M31 and M41 containing MEAs were due to over wetting of the cathode catalyst layer caused by lower level of water back diffusion for the Arkema membranes compared to conventional PFSA types (i.e. diffusion of water from cathode to the anode). To confirm this hypothesis, the set-up in Figure 2.29 was used to measure the water permeability of the Arkema M-41 membrane.

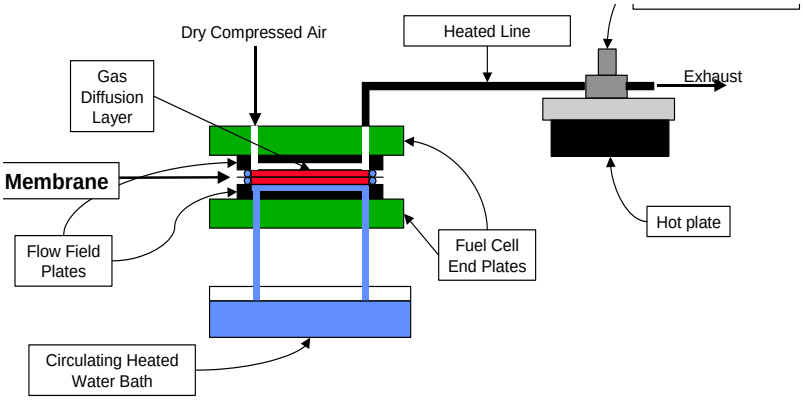

Figure 2.29: Apparatus for measuring membrane water permeability

In this apparatus, the sample is held in a miniature fuel cell with heated water flowing one side and dry gas (air) flowing the other. The water content of the exiting gas stream is measured using a humidity probe and expressed as partial pressure of water (accounts for temperature variations).

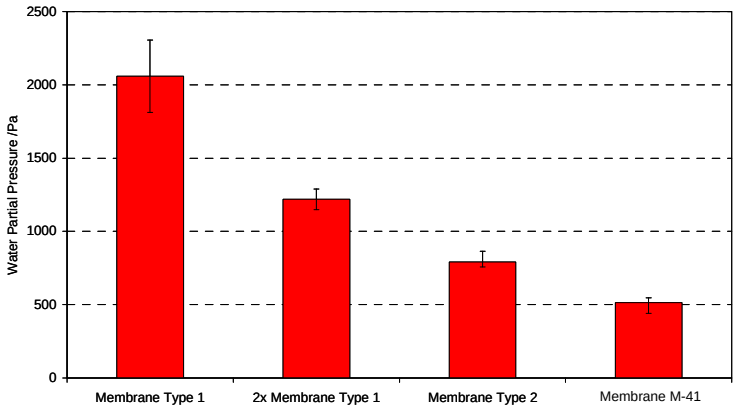

Figure 2.30: Membrane water permeability for M-41 membranes compared versus conventional PFSA membrane (Type 1)

Figure 2.30 shows that the M41 membrane has substantially lower water permeability compared to the conventional PFSA membrane (Type 1) despite the reduced membrane thickness (PFSA = 30 microns, M41 = 25 microns). The water transportation properties of the M41 membrane are restricted to such an extent that a higher

quantity of water passes through a 2 x 30micron PFSA test sample. This reduced ability to transport water is firmly believed to account for the low gas permeability of the Arkema membranes since some H_2/O_2 diffusion occurs via transport of dissolved gases in the water phase of the operating membrane. It is also not expected that the water permeance of the new membranes needs to be equivalent to that of PFSA materials in order to produce an MEA capable of high performance. However, in the series of MEA test data presented in this report, it is clear that some improvement to the water handling characteristics of the M41 membrane is required to alleviate cathode flooding.

Using the apparatus for ex-situ measurements of membrane water permeance JMFC has completed assessment of M41 membranes produced at a number of different thicknesses - see Figure 2.31. The data is plotted as 1/water permeance against the wet membrane thickness and is compared against an equivalent data-set from a range of Nafion membranes.

The intercept of the extrapolated data with the y-axis indicates the resistance to the passage of water from a film of zero thickness i.e. it shows the contribution of the surfaces to the overall resistance to permeation. The M41 membrane surface contribution is similar/slightly lower than from Nafion. The slope in the M41 data-set is much steeper than for Nafion showing that the M41 membranes are less permeable to water. This data strongly supports the inference from earlier MEA cell performance data, that lower back diffusion of water from the cathode to anode side of the MEA limits high current density performance on air operation. From extrapolation of the both datasets to thickness = 0, the Arkema M41 membrane is predicted to be more permeable than Nafion only at very low film thickness (<5 microns). Typically, the M41 membrane is about 2.5 times less permeable than a Nafion film of the same thickness.

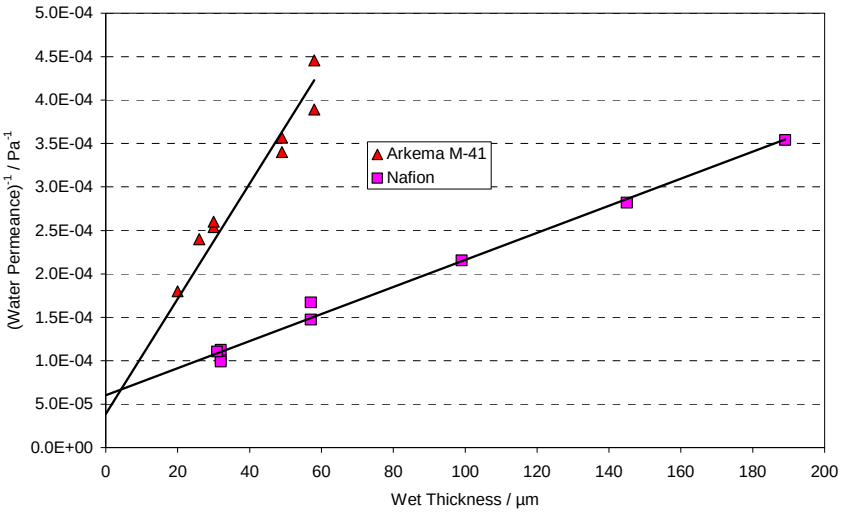

Figure 2.31: Water permeance of M41 membranes of varying thicknesses relative to Nafion membranes

Conclusions

At 60°C, the H_2/O_2 performance of an MEA containing M31 membrane is comparable with that obtained from an MEA containing a commercial PFSA material. Thus, from a kinetic perspective, the lower cost materials can match the performance of a more costly, state-of-the-art PFSA membranes.

Optimisation of the cathode layer (Variation A) such that the properties of M31 membrane and electrode layers were more suitably matched yielded a 50mV increase in performance at 1200 mA/cm^2, rising to a 100mV gain at 1400 mA/cm^2 for H_2/air, 60°C, relative to the case in which standard electrodes were used.

Despite this improvement in performance, the H_2/air M31 MEA result was still significantly below that obtained from the PFSA reference samples at 60°C, with a reduction in cell voltage of 40mV at $500mA/cm^2$ and 75mV at $1200mA/cm^2$. This main reason for this loss in performance was thought to be due to membrane and anode layer drying owing to the reduced ability of M31 to transport water relative to more conventional membranes.

When combined with membrane M31 a novel cathode catalyst, which showed increased electrochemical activity and stability in half-cell electrochemical testing, resulted in a 20-25mV improvement under H_2/O_2. Unfortunately, this improved performance was not observed under H_2/air.

M41 MEA / standard electrodes showed comparable performance to M31 / standard electrodes under H_2/O_2, 60°C with a slight increase in voltage at high current densities. Again, mass transport losses associated with the reduced water handling properties of the SIPN membrane meant that H_2/air performance was less than that for an MEA containing PFSA membrane.

The continuation of electrode optimization work yielded a significant improvement in the H_2/air performance of M41 containing MEAs such that at 80°C, 500 mA/cm^2, only a 20mV loss in performance is seen relative to the PFSA case. This result is in clear contrast with the 75mV loss observed for the M31 membrane tested under the same conditions at the start of this funded project. The stability of the M41 material was found to be sufficiently improved such that cell testing could be conducted at 80°C rather than the 60°C required by M31.

Steady state testing showed significant improvements in the durability of the M41 relative to M31. Initial testing conducted with M31 showed a 485 μV/hr decrease in performance at 500 mA/cm^2 over a 500 hour test for the M31 material with a corresponding drop of 54 μV/hr in OCV (60°C). When a similar test was conducted using the M41 material, no significant loss in performance was detected at 500 mA/cm^2 and the OCV loss was reduced to 20 μV/hr (80°C, 950 hours).

Both M31 and M41 membranes show substantial reduction in hydrogen and oxygen crossover compared to conventional PFSA materials. This reduction in gas crossover prevents localized mixed potentials from occurring e.g. if H_2 diffused to the cathode, thereby minimizing cell performance losses. In addition, the reduced gas crossover minimizes the opportunity for peroxide formation and thus, chemical attack of the membrane.

Ex-situ water permeance testing showed that the M41 membrane has substantially lower water permeability than conventional PFSA membranes, despite the reduced thickness of the membrane (25 microns *cf* 30 microns). This behaviour is thought to account for the low gas permeability since

some H_2/O_2 diffusion occurs via transport of dissolved gases in water and thus, is in part, advantageous. However, some improvement in the water transport properties of the SIPN membranes is required to enable back diffusion of water from the cathode to the anode in an operating MEA, alleviating mass transport issues associated with cathode flooding.